



LUND
UNIVERSITY



THE EFFECT OF MATRIC SUCTION ON TOTAL STABILITY EVALUATIONS IN CLAY

ROBIN TVRDEK

Geotechnical
Engineering

Master's Dissertation

DEPARTMENT OF CONSTRUCTION SCIENCES

GEOTECHNICAL ENGINEERING

ISRN LUTVDG/TVGT--15/5053--SE (1-91) | ISSN 0349-4977

MASTER'S DISSERTATION

**THE EFFECT OF
MATRIC SUCTION ON TOTAL
STABILITY EVALUATIONS
IN CLAY**

ROBIN TVRDEK

Supervisors: Professor **OLA DAHLBLOM**, Dept. of Construction Sciences, LTH, Lund
and **HÅKAN LINDGREN**, MSc, Sweco Civil AB.

Examiner: Professor **KENT PERSSON**, Dept. of Construction Sciences, LTH, Lund.

Copyright © 2015 Geotechnical Engineering,
Dept. of Construction Sciences, Faculty of Engineering (LTH), Lund University, Sweden.

Printed by Media-Tryck LU, Lund, Sweden, June 2015 (*PI*).

For information, address:

Geotechnical Engineering, Dept. of Construction Sciences,
Faculty of Engineering (LTH), Lund University, Box 118, SE-221 00 Lund, Sweden.

Homepage: <http://www.geoteknik.lth.se>

Abstract

In this master's dissertation I investigated if it is possible to increase the total stability for excavations in clay, if suction is taken into account during the calculations. The work has been performed at, and in cooperation with, *Sweco Civil AB* as well as the *Dept. of Construction Sciences* at *Faculty of Engineering LTH, Lund University*.

The objective of this master's dissertation is to assess if it is reasonable to evaluate suction using the finite element method, if it is possible to use this to obtain a higher value of the total stability and if it is reasonable doing so. In order to do so, this work has been divided into three parts.

- Two idealized excavations, one sloped and one excavation pit with a reinforced retaining structure was investigated. The objective was to evaluate how suction varies with changes in parameters as, precipitation, evapotranspiration, location of the phreatic level and the appearance of the soil water retention curve.
- These two cases are then compared to evaluate how boundary conditions affect the factor of safety for the two excavation pits.
- After evaluating the results from the idealized cases, these are applied to an actual case, the excavation for the Target building at the ESS-site. The goal is to see if similar results are obtained for a "real life" case.

In order to evaluate this, numerical calculations have been performed in *Plaxis 2D*. It is based on the finite element method and one of the most commonly used software for geotechnical engineering. To be able to evaluate the effect of suction, every calculation phase where suction was allowed has been compared to an identical phase where the suction effect was ignored.

The results clearly indicate that a higher value of the factor of safety is obtained in all but one of the cases when suction is taken into account. Both of the idealized excavation pits show the same pattern: if a higher value of the factor of safety is obtained for one case a higher value is also obtained for the other case. However, an evident difference is visualized; the amplitude for the sloped case is much larger, which means that the factor of safety fluctuates more than the factor of safety for the sheet-piled excavation pit. In addition it is evident that the level of the phreatic surface has a large impact on the total stability, as it increases when the groundwater level is located further from the ground surface.

Keywords: capillary rise, clay, excavation, factor of safety, finite element method, matric suction, Plaxis, sheet pile, soil water retention curve, total stability evaluation, unsaturated soil

Acknowledgements

This master's dissertation was conducted at the Dept. of Construction Sciences at Faculty of Engineering LTH, Lund University in cooperation with Sweco Civil AB during the period, December 2014 till May 2015.

I would like to thank my supervisors, Håkan Lindgren (Geotechnical engineer, Sweco Civil AB) who has guided and answered my questions during the composition of this project and Prof. Ola Dahlblom (Dept. of Construction Sciences, LTH) for his knowledge and interest in this project. Furthermore, I would also like to express my sincere appreciation to Stefan Jarl Wellershaus (Geotechnical engineer, Sweco Civil AB) for his help with the finite element analysis and interest in the project. Additionally I would like to acknowledge Bo Malmberg (PhD in Soil Mechanics, Sweco Civil AB) and thank him for his helpful insight regarding this topic.

Furthermore Mattis Johansson, (Hydro geologist, Sweco Environment AB) and Prof. Magnus Persson, (Dept. of Building and Environmental Technology) assisted me with input and knowledge about precipitation and evapotranspiration.

Additionally I would like to thank my friend, Felix Carlsson for his support and interest in this project. Without the support and help from others this project would not be possible to conduct. To all my friends and family whom have made my time in Lund a remarkable journey, I would like to extend my appreciation and gratitude.

Lund May, 2015



Robin Tvrdek

Notations

Latin upper case letters

ΔA	Incremental area
A	Area
E	Youngs Modulus
E_{steel}	Elasticity Modulus for steel
EA	Axial stiffness
EI	Bending stiffness
I	Moment of inertia
\bar{I}	Invariant
\bar{J}	Invariant
K_0	Coefficient of initial earth-pressure
$L_{spacing}$	Anchor spacing
M_{sf}	Incremental strength reduction
R_1, R_2	Radii of curvature in orthogonal planes
S_{eff}	Effective saturation
S_{sat}	Full saturation
S_{res}	Residual saturation
T_s	Surface Tension
V_w	Volume of pore water
V_p	Total pore volume
V_{tot}	Total volume

Latin lower case letters

c	Cohesion
c'	Effective cohesion
e_{void}	Initial void ratio
g	Gravitational acceleration
g_a	Air-entry value (fitting parameter)
g_n	Rate of water extraction (fitting parameter)
g_c	Fitting parameter for the van Genuchten function
g_l	Fitting parameter for the van Genuchten function
h_e	Height of excavation
h_r	Height of retaining structure
h_s	Height of slope
h_c	Height of the capillary rise
h_{ref}	Reference value of head
k_{rel}	Relative permeability
k_{sat}	Saturated permeability
l	Lateral length of slope

\mathbf{m}	Unit vector
\mathbf{n}	Unit vector
\mathbf{n}	Eigenvector
p_{active}	Active pore pressure
p_{excess}	Excess pore pressure
p_{steady}	Steady state pore pressure
p_w	Suction pore stress
p_{water}	Pore water pressure
q	Rate of infiltration or evapotranspiration
r	Radii of pores
t	Thickness
t	Traction vector
Δu	Pressure difference
u_a	Air pressure
u_w	Water Pressure
u_x, u_y, u_z	Deformation in the general directions
v	Possions ratio

Greek upper case letters

Θ	Normalized volumetric water content
Φ	Volumetric Water content

Greek lower case letters

γ_{sat}	Saturated unit weight of soil
γ_{unsat}	Unsaturated unit weight of soil
γ_{steel}	Unit weight of steel
γ_w	Unit weight of water
δ_{ij}	Kroneckers Delta
ε	Strain
θ_r	Residual water content
θ_s	Saturated water content
λ	Eigenvalue
ρ_w	Density of water
σ	Total stresses
σ'	Effective stresses
σ'_h	Horizontal effective stress
σ_{ij}	Stress tensor
σ_n	Normal stress
σ'_v	Vertical effective stress
τ	Shear stress
φ	Internal friction angle

ϕ_p	Pressure head
ψ	Dilatancy angle
ψ_b	Air-entry pressure (desorption curve)
ψ_{min}	minimum pore pressure head
ψ_{max}	maximum pore pressure head
ψ_{matric}	Matric Suction
$\psi_{osmotic}$	Osmotic Suction
ψ_{total}	Total Suction

Abbreviations

2D	Two-dimensional
3D	Three-dimensional
AS	Allow Suction
ESS	European Spallation Source
FCFD	Fully coupled flow-deformation
FE	Finite Element
FEM	Finite element method
FS	factor of safety
IS	Ignore Suction
SMHI	The Swedish Meteorological Hydrological Institute
SWCC	Soil Water Characteristic Curve
SWRC	Soil Water Retention Curve

Table of Contents

1.	Introduction.....	1
	1.1 Background.....	1
	1.2 Objective.....	1
	1.3 Limitations.....	2
	1.4 Method.....	3
	1.5 Disposition.....	3
2.	Unsaturated soil	5
	2.1 The unsaturated soil profile	5
	2.2 Water in Unsaturated soil	6
	2.3 Pore pressure	7
	2.4 Capillary rise	7
	2.5 Suction.....	8
	2.5.1 Environmental changes	9
	2.5.2 Effects on total stability.....	12
	2.5.3 Suction and the SWRC.....	12
	2.6 Surface Tension	12
	2.7 Soil Water Retention Curve (SWRC).....	14
	2.7.1 Modelling the soil water retention curve.....	16
	2.8 The van Genuchten Model	16
3.	Constitutive Modelling	19
	3.1 Strain	19
	3.2 Strain invariants.....	20
	3.3 Stress	22
	3.4 Stress invariants	24
	3.5 Plasticity	24
	3.6 Hardening and softening.....	25
	3.7 Yield Criteria	26
	3.8 The Mohr-Coulomb Model.....	27
	3.9 Symmetry properties.....	29
	3.10 Plane strain.....	31
4.	Plaxis.....	33
	4.1 Mesh.....	33
	4.2 Elements.....	33

4.3 Plate elements.....	35
4.4 Interfaces and interface elements	36
4.5 Fixed-end anchors	36
4.6 Boundary Conditions	36
4.7 Drainage	38
4.8 Initial stress generation	39
4.9 Safety Calculations	39
4.10 Fully coupled flow-deformation	40
4.11 Pore pressures.....	40
4.12 Predefined Data sets	41
4.13 Suction.....	41
4.13.1 Ignore suction.....	41
4.13.2 Allow suction	42
4.14 Material models	42
4.14.1 Mohr-Coulombs material model – Linear elastic perfectly plastic	42
4.14.2 Groundwater flow – transient flow.....	44
4.14.3 Hydraulic Models – van Genuchten	45
5. Idealized cases.....	47
5.1 Idealized geometries	47
5.2 Hydraulic conditions.....	48
5.3 Parameters	50
5.4 Mesh.....	50
5.5 Variables.....	51
5.6 Results	52
5.6.1 Precipitation	52
5.6.2 Groundwater	58
5.6.3 Soil water retention curve.....	59
5.6.4 Failure mechanism	61
6. Case study - ESS.....	62
6.1 Idealized Geometry	62
6.2 Hydraulic conditions.....	63
6.3 Parameters	63
6.4 Mesh.....	65
6.5 Results	66

7. Discussion and conclusions	68
7.1 Discussion and conclusions	68
7.2 Future work	71
8. Bibliography.....	72
Appendix.....	

1. Introduction

1.1 Background

During erection of structures, excavations in soil are often needed in order to provide a stable foundation. Sweco Civil AB is conducting geotechnical investigations in several projects around the country and this has raised a series of questions on how suction affects the loadbearing capacity in unsaturated soil.

Unsaturated soil is the stage between a fully saturated and a completely dry soil and unlike saturated soil three phases, the water-, air- and soil solid phase interact. The additional air phase makes the soil mechanics of unsaturated soil more complicated than for saturated soil. The matric suction phenomenon only exists in unsaturated soil and is strongly linked to the water content in the pores, where a low water content is connected to a high suction value and vice versa.

Traditionally suction and negative pore water pressures are ignored in stability assessments of excavations in unsaturated soils. This is usually both due to lack of necessary soil parameters and conservatism in the profession. Frydman, S and Baker, R (2014), Fredlund, D., & Rahardjo, H. (1993) among others suggest the importance of suction or loss of, for stability evaluations.

A correct analysis of suction is problematic due to environmental effects like evapotranspiration, infiltration, precipitation, variations of the phreatic level, and soil properties as hydraulic conductivity, which have an impact on the water content in the soil profile. Several of these properties and elements are very hard to predict and causes time dependent variations of suction, and has therefore generally been neglected during geotechnical calculations.

However, at present time there are several finite element software that are able to take suction into account. In this master's dissertation, numerical analyses of excavations in clayey soil, suction and its effect on the factor of safety for total stability are made using *Plaxis 2D*.

In order to do this, the results from two idealized excavation pits will be compared to a "real life" case. This "real life" case is based on an excavation at The European Spallation Source (ESS AB); a massive research facility which is being built at the outskirts of Lund. The comparison is made in order to investigate if the results from this case correlate with the results from the idealized cases.

1.2 Objective

The intention of this master's dissertation is to establish if it is reasonable to use suction to more accurately evaluate the factor of safety for excavations made in clay and possibly use it to obtain a higher value of the factor of safety at certain times during the year.

The objective of this master's dissertation is divided into several questions.

- Is it reasonable to use suction to obtain a higher value of the factor of safety during excavations in clay when compared to the same case when suction is ignored?
- Is this a good approximation with satisfying accuracy? Is it, with considerable accuracy, possible to determine and use suction to obtain a higher value of the factor of safety for sloped and sheet-piled excavation pits?
- Over a period of one year, when is it best to open an excavation?
- How does an alteration in parameters as, the position of the phreatic level, different soil water retention curves and, a variation in precipitation and evapotranspiration affect the total stability?

Since there are many parameters that affect suction and the factor of safety, the work has been split in to three parts. This is done to evaluate the significance of these parameters.

- Part one consists of an evaluation of a general case, with an excavation without supporting structures. The first step is to evaluate how precipitation, evapotranspiration, the position of the phreatic level and a varied SWRC affect the factor of safety when suction is considered. The second step consists of a comparison of the same calculations but neglecting suction.
- Part two consists of the same evaluation as for part one but for an idealized excavation pit with a supporting structure. This will be an excavation pit supported by sheet-pile and reinforced with a shoring.
- Part three will use the same approach as for the two previous parts, but for a “real life” case at the ESS-site.

The main goal is not to answer how big the contribution from suction to the factor of safety is, merely to determine if it is possible to use suction to obtain a higher value of the factor of safety and indicate how this varies over the year. It is also of interest to see if loss of suction can lead to a lower value of the factor of safety, compared to traditional evaluation of total stability.

1.3 Limitations

All cases in *Plaxis* are modelled in two-dimensions. The benefit of modelling in two instead of three-dimensions is faster calculations. This is not considered to be a major limitation when the suction phenomenon is modelled due to the fact this master's dissertation does not consider structural effects, ergo effects that are taken into account in three-dimensional modelling but not in two-dimensional modelling.

The work is limited to cohesion material as clay or clayey soil and friction materials will therefore not be considered in this master's dissertation. *The Mohr-Coulomb model* is used to model the soil behaviour and *the van Genuchten function* is used to model the transient groundwater flow. There are several other models available but these are not considered here.

In this master's dissertation the work is also limited to performing analytical calculations, to ensure that the sheet-pile is able to endure the active earth pressure and numerical calculations in *Plaxis 2D*, to evaluate the total stability.

1.4 Method

The method used in this master's dissertation consists of four different parts. First an extensive literature study was performed to gain knowledge about unsaturated soils, constitutive modelling, soil suction and previous work concerning suction.

After the literature study a general modelling phase began. Two different, idealized geometries were modelled in *Plaxis 2D*, these consist of one sloped and one sheet-piled excavation pit. Identical soil- and material properties were used for both cases.

The results from the idealized study were then evaluated and used as a guide to model the "real life" excavation at the ESS-site.

The fourth and last step consisted of an evaluation and discussion of the modelling results.

1.5 Disposition

A short summary of the chapters in this work follows below:

Chapter 2 – Contains theory about unsaturated soil, suction, theory about hydraulic models and different approaches to determine the volumetric water content in soils.

Chapter 3 – Contains the main theory needed to understand the finite element theory in *Plaxis 2D*.

Chapter 4 – Includes a short introduction to the finite element software, *Plaxis 2D*, that was used in this master's dissertation and also a short introduction to calculation and modelling methods utilized in *Plaxis*.

Chapter 5 – The material models used in *Plaxis 2D* are explained and reviewed.

Chapter 6 – Modelling of the simplified idealized cases, with and without the supporting structure is presented. This chapter describes the geometry, assessment of the parameters that are used and presents the results from the numerical calculations.

Chapter 7 – The real-life case, ESS-excavation is treated in this chapter. In analogy with Chapter 6, the geometry, parameters and results are presented here.

Chapter 8 – This section contains discussion, conclusions, observed problems and suggested further work.

Chapter 9 – Bibliography.

2. Unsaturated soil

Unsaturated soil, also referred to as partially saturated soil, is the state between an absolutely dry and a totally saturated soil. The relatively simple case of saturated soil only has two phases, the soil solid phase and the water phase. However, the case with partially saturated soil introduces an additional phase, the air phase, which can be seen in the simplified phase diagram, Figure 2.1. These three phases interact with one another and the additional air phase has a huge impact on the mechanical properties of the unsaturated soil (Fredlund & Rahardjo, 1993).

As mentioned in the previous section, soil mechanics is divided into two characteristic parts, saturated and unsaturated soil mechanics. In the field of geotechnical engineering there is a perception that the mechanical properties of unsaturated soil are much more complicated than those for saturated soil (Lu & Likos, 2004). This chapter will present some of the mechanics, which is important for this master's dissertation.

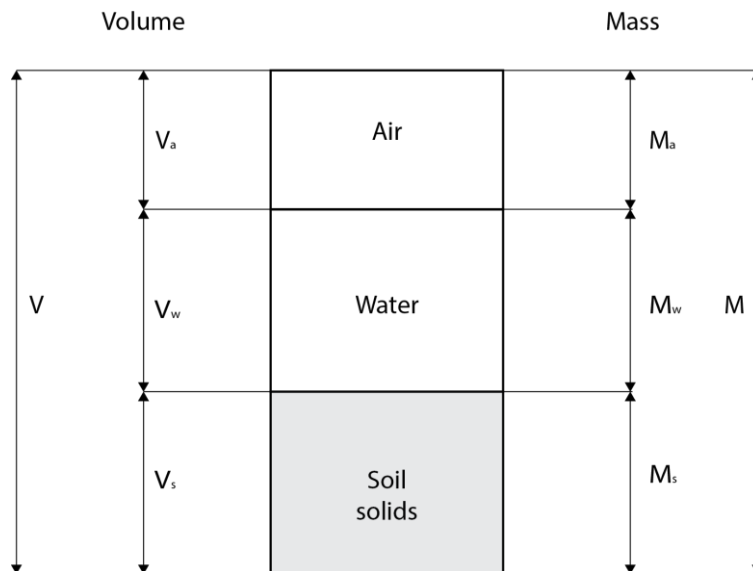


Figure 2.1 - Phase diagram for unsaturated soil after Fredlund & Rahardjo (1993).

2.1 The unsaturated soil profile

The soil profile can be divided into two components, the saturated and the unsaturated zone. Where the saturated zone extends up to the groundwater table, defined as the pressure surface where the pressure from the water is equal to the atmospheric pressure. The saturated zone includes the area where the soil is saturated by capillary rise of water (the capillary fringe) and the unsaturated zone begins where the capillary rise is no longer able to saturate the soil.

The unsaturated zone is in-turn divided into the surface water zone and the intermediate zone, seen in Figure 2.2, where the intermediate zone only exists if the groundwater table is located at a considerable depth. In the surface water zone the water content mostly depends on infiltration from precipitation and evaporation and therefore this zone can momentarily be fully saturated. In the intermediate zone, water is transported from the surface zone down to the ground water level by gravity. Due to the influence of external

factors the groundwater state above the groundwater surface is seldom stationary (Hultén, et al., 2005).

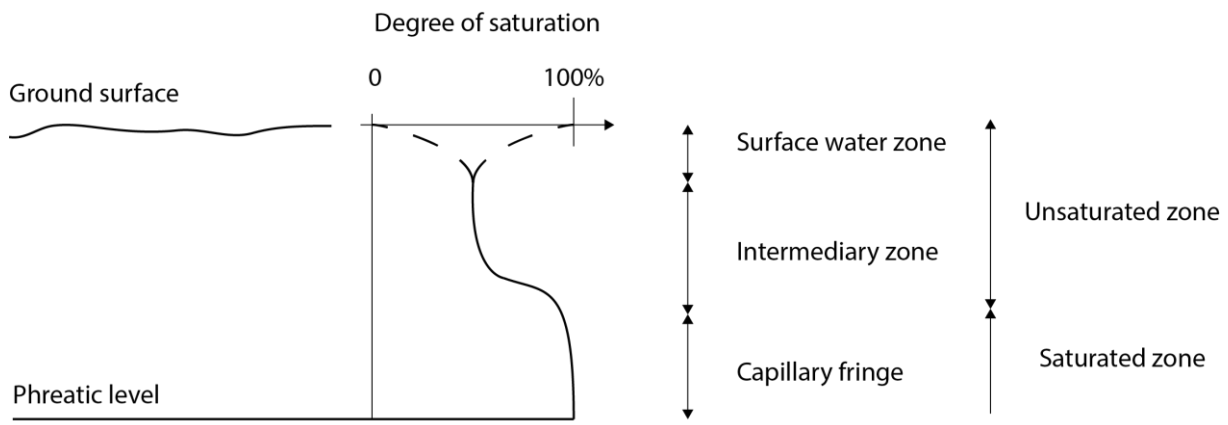


Figure 2.2 - Typology of the unsaturated zone, with the surface water zone, intermediate zone and the capillary fringe after Hultén et al.

2.2 Water in unsaturated soil

In partially saturated soil the three phases, solid, water and air, are all active and influence the properties of the soil. The relationship between air and water in the unsaturated zone can primarily be described by three stages (Lu & Likos, 2004).

- Under situations where the water content is low, the air phase is continuous. During this stage the water is bound as a thin skin around the soil particles and is therefore not continuous.
- When the water content increases to a certain value the water phase becomes continuous and now both phases are continuous.
- Close to saturation of the soil, the water phase stays continuous and the air occurs in form of small, occluded air bubbles in the water. The air phase is not continuous.

There are multiple ways to describe water in soil, in this master's dissertation volumetric water content and degree of saturation is used and can be described as

- Volumetric water content, Φ – Ratio between the volume of pore water, V_w and total volume of soil and water V_{tot} . This is denoted $\Phi = \frac{V_w}{V_{tot}}$.
- Degree of Saturation, S – Ratio between volume of the pore water, V_w and total pore volume V_p . The degree of saturation is denoted $S = \frac{V_w}{V_p}$.

In modelling application it can be useful to define a normalized volumetric water content variable, Θ (dimensionless). It can be seen below and is constructed of the residual, θ_r and saturated, θ_s values for the water content.

- $\Theta = \frac{\theta - \theta_r}{\theta_s - \theta_r}$

2.3 Pore pressure

Pore pressure is defined in relation to the atmospheric pressure. The total pressure in the soil pores is the sum of the air pressure, the capillary pressure and the osmotic pressure. In normal cases the air pressure inside the pores can be assumed to be equal to the atmospheric pressure and the osmotic pressure is normally neglected. At the water table the pore pressure is equal to zero and under hydrostatic conditions the pore water pressure increases linearly below and decreases linearly above the water table. Negative pore pressures are therefore a result of capillary rise. In reality the water profile is more complex than the conceptualized case explained here and is dependent on the soil profile and the water content in the soil etc. (Fredlund & Rahardjo, 1993). Capillary rise is explained in more detail in Section 2.4.

2.4 Capillary rise

Capillary rise in soil can be conceptualized by the following model, where small tubes, as seen in Figure 2.3, are used to simulate the pores in soil. The pore size distribution, surface tension and its contact angle (the tendency to wet the surface) towards the minerals are the parameters which control the height of the capillary rise, h_c and can be expressed as

$$h_c = \frac{2T_s}{\rho_w g r} \tag{2.1}$$

where

- T_s = Surface tension
- r = Radius of the pores
- ρ_w = Density of water
- g = Acceleration caused by gravity

Since this is a conceptualized model, the capillary tube system in soil would have tubes with variable sizes and lengths (Lu & Likos, 2004).

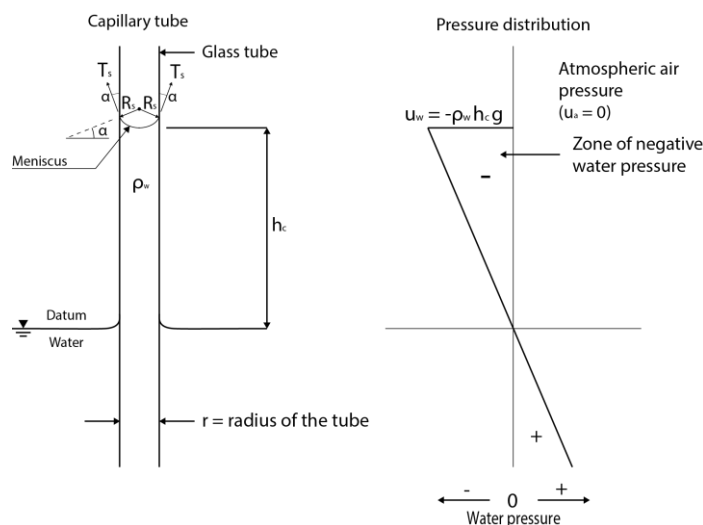


Figure 2.3 - The capillary rise and its connection to the negative pore pressures after Fredlund & Rahardjo (1993).

It is worth noticing that the capillary phenomenon is associated with matric suction, explained in Section 2.5. The radius of curvature and the height of the capillary rise directly influence the relationship between matric suction and water content also known as the soil water retention curve (SWRC). This model, which is explained further in Chapter 2.7, exhibits a difference for the drying and the wetting process. The capillary model provides an explanation for this behaviour; during wetting the height of the capillary rise is dependent on the largest pore radius in the soil profile but for situations when the capillary water decreases, for example when the water table is lowered, the smallest pore radius is decisive. This results in a capillary rise that is higher for the drying process than the corresponding wetting process, seen in Figure 2.4 (Fredlund & Rahardjo, 1993).

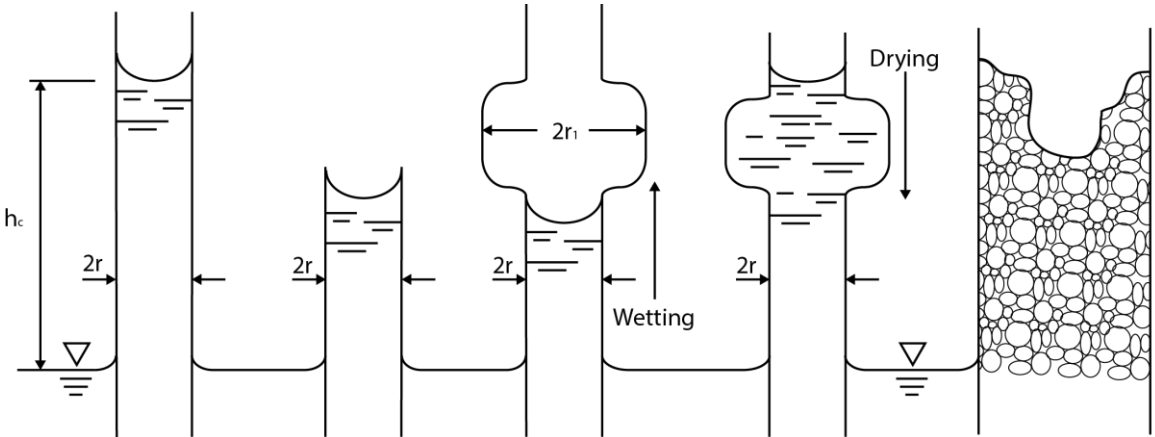


Figure 2.4 - The pore size significance for the hysteresis in capillary rise after Fredlund & Rahardjo (1993).

2.5 Suction

Total suction is a phenomenon in unsaturated soil which, when present, significantly increases the shear strength in the soil. Despite the additional shear strength suction is not a stress but a potential. Total suction is the relation between the soil water potential and the potential of free water. Water without dissolved solutes, affected only by the gravitational force and no interaction with the other two phases is defined as free water. Short-range adsorption, capillary and osmotic effects are the mechanisms that generally act to decrease the potential of the pore water. The effects of gravity, temperature and inertial effects are generally ignored (Lu & Likos, 2004).

The total suction phenomenon can be fragmented into matric and osmotic suction, where matric suction, ψ_{matric} is unique for unsaturated soil. Matric suction is the effect from both capillary rise and short range adsorption. Osmotic suction, $\psi_{osmotic}$ on the other hand is a component that is a result of dissolved solutes in the soil water. The total suction can be written as (Lu & Likos, 2004)

$$\psi_{total} = \psi_{matric} + \psi_{osmotic} \tag{2.2}$$

It is important to once again point out that suction is a potential (or soil water energy) and not a stress state. The reader might note that matric suction consists of one part due to capillary rise, an interaction between the air and water phase in the macroscopic soil pores which is a stress defined as the difference between the air, u_a and the water pressure, u_w . However, the interaction between clay mineral and water, i.e. the adsorption effect is not to be considered as a stress (Frydman & Baker, 2014). Frydman and Baker both point to the fact that magnitude of matric suction can reach up to 1000 MPa while the tensile strength of pure water only is in the order, 150 MPa. Therefore it is concluded that matric suction can not be treated as a stress in constitutive modelling.

Adsorption effects

Adsorption effects are created by van der Waals and electrical fields that act in the soil solid-liquid interface. These effects are most important for soil with a small grain-size distribution and decrease with the distance to the soil particles. The adsorption effects are most significant at a low degree of saturation, when water is mainly located as thin films surrounding the soil particles (Lu & Likos, 2004).

Osmotic effects

As mentioned previously osmotic effects arise due to dissolved solutes in the soil pore water. These solutes can both be naturally occurring or externally introduced and these will reduce the chemical potential of the pore water (Lu & Likos, 2004).

2.5.1 Environmental changes

The matric suction is highly dependent on the water content in the soil and is therefore linked to several environmental mechanisms. In this section these important mechanisms are explained to gain an understanding of the complex nature of suction.

During dry seasons matric suction increases due to the net loss of water and in contrast the soil has a net gain of water during the wet season and therefore the matric suction decreases. These changes are also connected to the depth in the soil profile and normally the largest changes occur close to the surface (Fredlund & Rahardjo, 1993).

The soils ability to transmit and drain water is associated with the property, permeability, and therefore this will furthermore indicate alterations in matric suction caused by environmental events. Unlike for saturated soil where the permeability is constant the permeability of the unsaturated soil varies with the water content (Fredlund & Rahardjo, 1993).

Environmental mechanisms as precipitation, evaporation and transpiration all influence the depth of the unsaturated zone and the water content in the soil profile. The natural hydrological cycle and the above mentioned mechanisms are shown in Figure 2.5 (Lu & Likos, 2004).

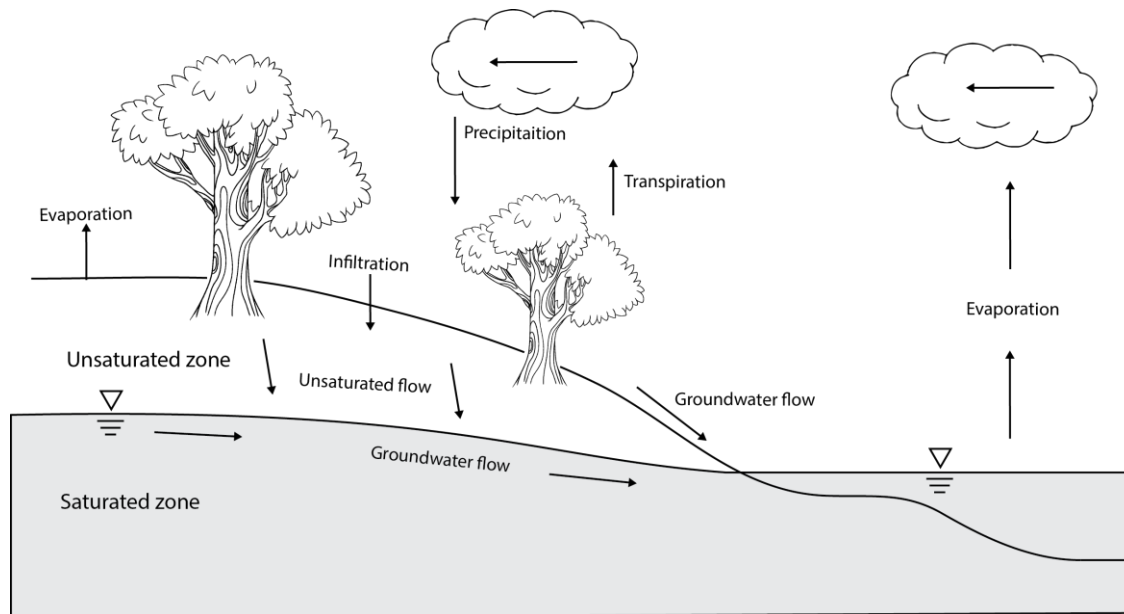


Figure 2.5 –The natural hydrological cycle and the role of the unsaturated zone after Fredlund &Rahardjo (1993).

There are different ways of approaching the unsaturated zone, but Lu & Likos (2004) suggest that it can be pictured as two different zones, one seasonal steady and one seasonal unsteady zone. In the unsteady zone, near the surface, various time-dependent factors as relative humidity, temperature, precipitation, evaporation among others cause the soil suction to fluctuate. The steady zone is situated below this zone and is relatively time independent. Properties as the steady recharge rate, surface topography, soil type and the ground water table strongly influence the suction profile in this zone.

It is of importance to understand how the flow of fluids, influence the suction profile. It is possible to show the influence by considering two general cases, one steady upward flow and one steady downward flow, seen in Figure 2.6 (Lu & Likos, 2004).

As seen in Figure 2.6 the suction head is distributed linearly only under hydrostatic conditions (no flow), which is a result of the fact that the total head is constant across the entire profile. As mentioned before the value of the water content for every suction profile can be seen in a corresponding soil water retention curve (SWRC) (Lu & Likos, 2004). The corresponding SWRC (for the no-flux situation) can be seen in the middle of Figure 2.6b and a further explanation to the SWRC is given in Chapter 2.7.

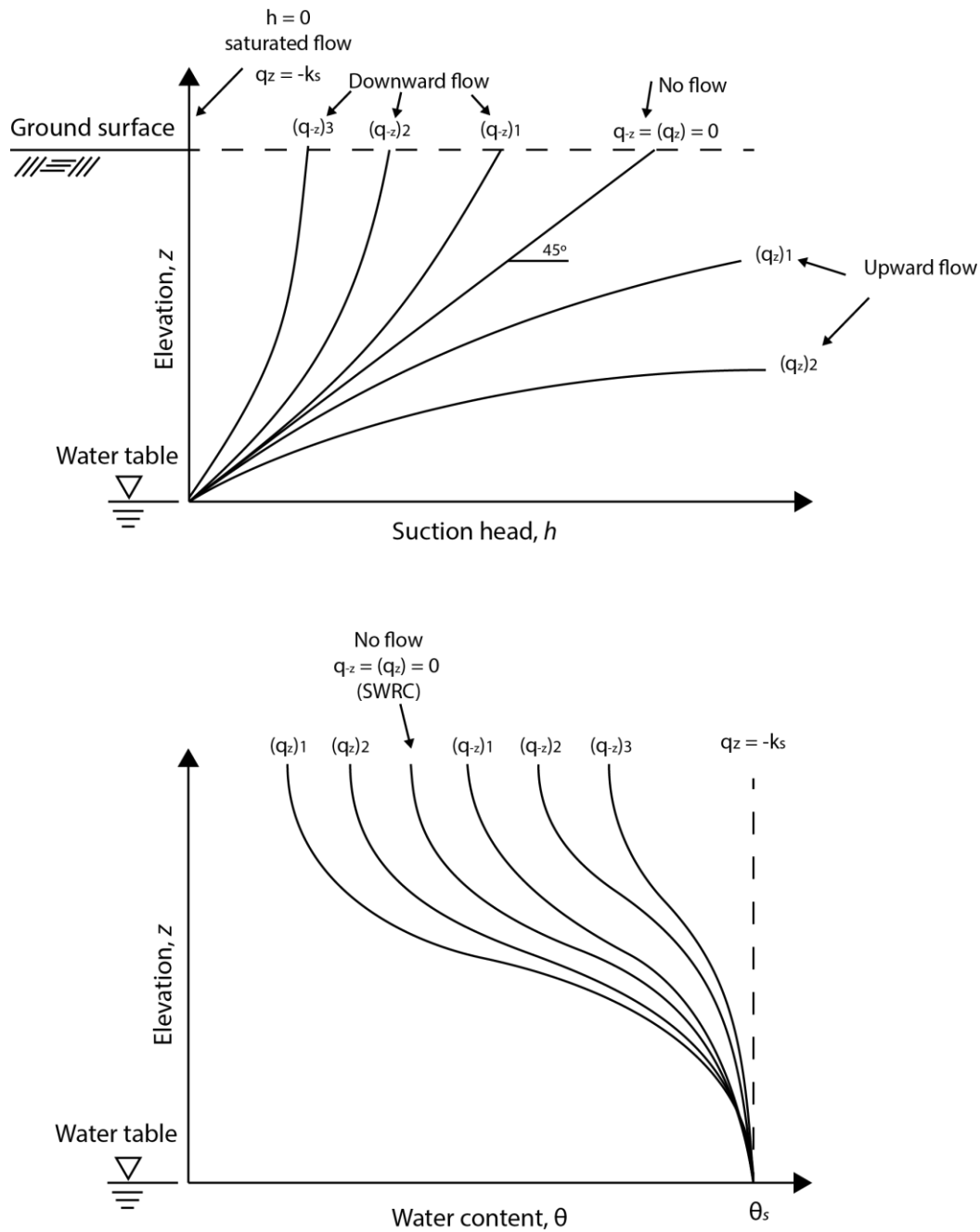


Figure 2.6 - Conceptual pressure head (a) and water content (b) in a homogeneous layer of unsaturated soil under steady vertical drawdown and steady vertically upward flow after Lu and Likos (2004).

Precipitation and evapotranspiration both affect the suction head along the soil profile. An increase in infiltration is connected to a decrease in suction. This is associated with precipitation and can distinctly be seen in the profiles for downward flow in Figure 2.6. Equivalently, an increase in upward flow caused by evapotranspiration leads to a decrease in water content and consequently an increase in suction. The rate of infiltration or evaporation, q regulates to what extent the suction profile is moved from the hydrostatic case (Lu & Likos, 2004).

2.5.2 Effects on total stability

These environmental mechanisms are the reasons why prediction of matric suction is so complicated. There are numerous cases when natural slopes have failed due to the occurrence of extra heavy rainfalls, as the articles by Zhou, et al. (2010) and Blatz, et al (2004) show. In both cases the water content increases sufficiently so that the matric suction is highly reduced. This extra-large (in comparison with the one occurring in connection to regular seasonal rainfalls) reduction of matric suction results in slope failures.

2.5.3 Suction and the SWRC

In the previous section it was stated that the vertical distribution of matric suction in a natural deposit of unsaturated soil depends on several factors, where the hydrological properties is of most importance. These properties are given by the soil water retention curve (SWRC) and the hydraulic conductivity function as a result from the SWRC. Factors that control infiltration and evaporative fluxes caused by the environment, geometric boundary or drainage conditions such as ground water level are also of importance (Lu & Likos, 2004).

These profiles have been studied for an extensive period of time and Lu & Likos (2004) suggests an analytical calculation approach to determine the matric suction for the steady zone in an unsaturated soil. However the matric suction profile in the unsteady zone is of importance for understanding the behaviour of expansive soils and stability of shallow geotechnical structures (Lu & Likos, 2004). To be able to evaluate this transient unsaturated flow has to be considered and to this usage of the finite element method (FEM) is needed.

2.6 Surface tension

Surface tension is an important property of unsaturated soils and is connected to the air-water interface (contractile skin). The cohesive forces acting on the water molecules in the contractile skin are at first unbalanced, unlike the case when the water molecules are surrounded by water where it is subjected to equal forces on all sides of the molecule. This unbalanced force in the air-water interface is directed towards the water and to achieve mechanical equilibrium, a resultant force, surface tension, T_s is generated in the contractile skin (Fredlund & Rahardjo, 1993). The surface tension of the air-phase does exist, but is not of significant value and can therefore be ignored (Lu & Likos, 2004).

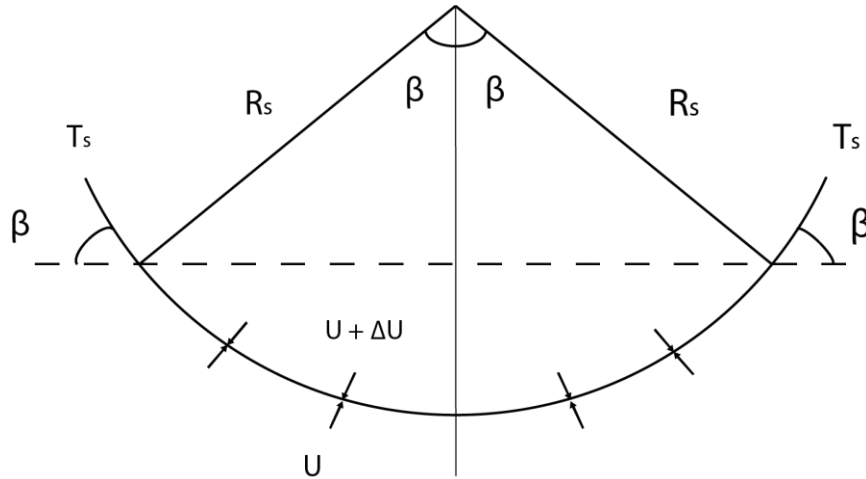


Figure 2.7 - Pressures and surface tension for a two-dimensional surface. Tensile force, T_s and the radius of curvature, R_s after Fredlund and Rahardjo (1993).

The water pressure, u_w in the soil pores of unsaturated soil is lower than the air pressure u_a , and therefore the contractile skin is subjected to a pressure difference. This pressure difference results in that the interface takes a concave shape, directed towards the higher pressure. Considering, Figure 2.7, the pressure difference can be expressed in surface tension and the radius of curvature (Fredlund & Rahardjo, 1993).

As stated above it is easy to see that the horizontal forces are balanced but the vertical forces need to uphold the following criterion for equilibrium

$$2T_s \sin \beta = 2\Delta u R_s \sin \beta \quad (2.3)$$

where

T_s	Surface tension measured in tensile force per unit length
R_s	Radius of curvature
Δu	Pressure difference
$2R_s \sin \beta$	Membrane length projected on to the horizontal plane

For a three-dimensional case, Equation 2.3, can be expressed in pressure difference using Laplace equation, as (Fredlund & Rahardjo, 1993):

$$\Delta u = T_s \left(\frac{1}{R_1} + \frac{1}{R_2} \right) \quad (2.4)$$

where R_1 and R_2 expresses the radii of curvature in two orthogonal principal planes.

For the case where water rises in a capillary tube the radius of curvature is equal in all directions, $R_1 = R_2 = R_s$ (Lu & Likos, 2004). Since the air pressure is greater than the water pressure in an unsaturated soil, the pressure difference can be expressed as (Fredlund & Rahardjo, 1993)

$$u_a - u_w = \frac{2T_s}{R_s} \quad (2.5)$$

where

u_a Is the air pressure, $u_a \geq 0$

u_w is the water pressure, $u_w < 0$

In connection with unsaturated soil mechanics this pressure difference $u_a - u_w$ is normally referred to as the matric suction (Fredlund & Rahardjo, 1993) (Lu & Likos, 2004). Upon further inspection on Equation 2.5, it is obvious that the radii must decrease to result in an increase in matric suction. In analogy the radii goes to infinity when the pressure difference goes toward zero and when the matric suction goes toward zero a flat air-water interface is created (Fredlund & Rahardjo, 1993).

In reality there are other factors that affect the surface tension, as for example the temperature, when the temperature increases the surface tension decreases. (Fredlund & Rahardjo, 1993). However this is not taken into consideration in this master's dissertation.

2.7 Soil water retention curve (SWRC)

As mentioned previously the constitutive relation between soil suction and water content is described by the soil water retention curve (SWRC). It relates the pore water potential to that of free water as a function of the absorbed water (Lu & Likos, 2004). Characteristic curves for different soils are shown in Figure 2.8.

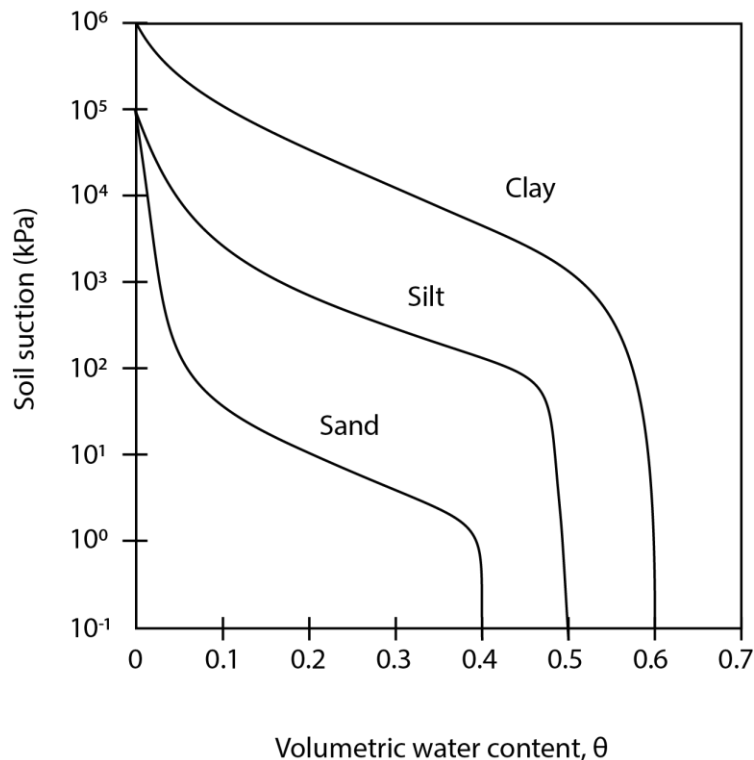


Figure 2.8 - Representative soil water retention curves for sand, silt and clay after Lu & Likos (2004).

The suction value is high for relatively low water content since the pore water potential is low compared with the free water potential. In correspondence the suction is equal to zero when the potential of free water and pore water have the same value and in other words

suction values of zero are approached when the soil approaches a fully saturated state (Lu & Likos, 2004).

The soil water characteristic curve (SWCC) describes both the adsorption and desorption curve. In general more water is retained during the drying process than the soil absorbs during the wetting process (for the same value of suction). The desorption-curve is generally used in geotechnical practice, since it is easier to measure and this is known as the soil water retention curve (Lu & Likos, 2004).

Properties as pore size distribution, grain size distribution, mineralogy, density, content of organic material among others strongly influence the shape of the soil water retention curve (Lu & Likos, 2004).

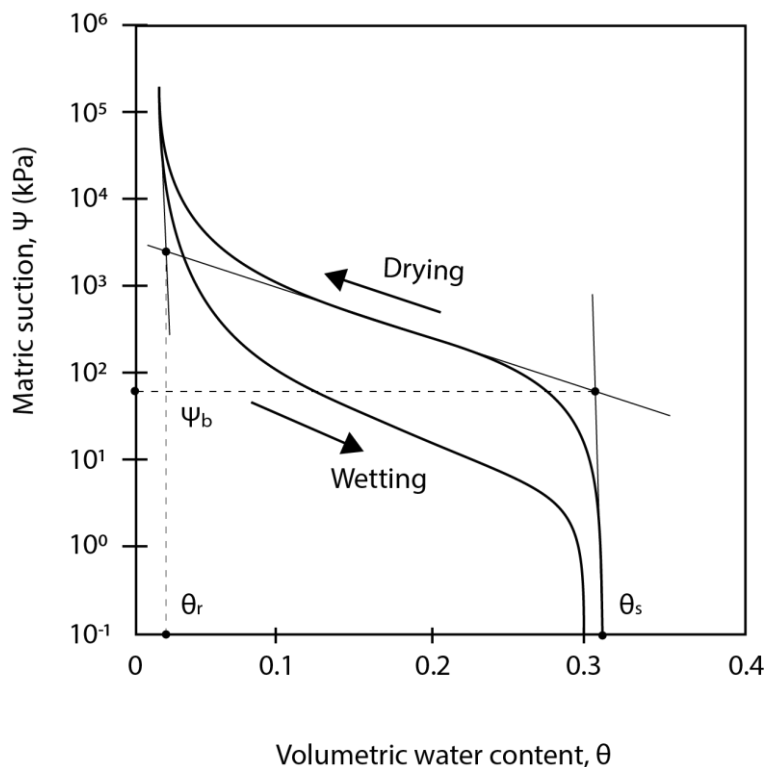


Figure 2.9 - Typical soil water characteristic curve, for matric suction and water content after Lu and Likos (2004).

When desaturation in the soil commences, air begins to enter the largest pores of the soil (air-entry level). The air-entry pressure ψ_b depicts the suction on the desorption curve of the SWCC and is equal to the height of the capillary fringe, seen in Figure 2.9. In Figure 2.9 both the saturated, θ_s and residual water content, θ_r can be seen. When the pores in the soil matrix are 100 % filled with water, the soil has reached its saturated water content. This value is normally reached on the desorption curve. In contrast, the residual water content has been reached when pore water mainly exists as menisci in the soil matrix. Exceptionally large changes in suction are needed to remove more water from the soil. Both the water content and air-entry pressure can be shown in the SWCC by constructing pairs of tangents as seen in Figure 2.9 (Lu & Likos, 2004).

It is possible to obtain several discrete data points to describe the SWRC by experimental techniques. However this creates a problem since continuous mathematical relations are usually needed to foreseeing stress, deformation and flow problems. Therefore several mathematical suggestions have been made in order to model the SWRC. In describing geotechnical problems there are basically three different models, the model by Brooks and Corey (1964), *The van Genuchten model* (1980) and the model by Fredlund and Xing (1994) (Lu & Likos, 2004). In this master's dissertation *the van Genuchten model* is treated, and the reader is suggested to go elsewhere for more information about the other models.

2.7.1 Modelling the soil water retention curve

The soil water characteristic curve can basically be approximated in two ways (Lu & Likos, 2004)

- Using a database with general soil water characteristic curves, selected by the grain size distribution of the specific soil.
- Fitting a mathematical model to the SWRC by determine soil properties in a laboratory.

In this master's dissertation only the mathematical models are considered. Common for these models is that they have two or three fitting parameters that will approximate the soil water retention curve. There are both positive and negative aspects of choosing a model with three fitting parameters. As any other mathematical approximation, an additional parameter can implicate that the simplicity of the model is sacrificed. However, this also means that the model more accurately describes the SWRC for an extensive range of suction. To be able to optimize the parameters to the curve usually a non-linear regression algorithm is used (Lu & Likos, 2004)

The soil water retention curve is used to estimate the hydraulic conductivity in the soil (van Genuchten, 1980). The different models generally have problems with describing the curve in its ends, where the highest and lowest pressures occur (Fredlund, 2006). Hereon after *the van Genuchten model* will be used throughout this master's dissertation. This is an equation that has a continuous slope and therefore the unsaturated hydraulic conductivity can be derived from *the van Genuchten function* (van Genuchten, 1980).

2.8 The van Genuchten model

The van Genuchten (VG) model is one of the models most commonly used to approximate the soil water retention curve and from the SWRC the unsaturated hydraulic conductivity can be determined. In this model, three fitting parameters, α , n and m are incorporated into the equation for normalized volumetric water content, $\Theta = \frac{\theta - \theta_r}{\theta_s - \theta_r}$ (van Genuchten, 1980).

The relative hydraulic conductivity K_r can be evaluated from the SWRC and is given by

$$K_r = \Theta^{0.5} \left[\frac{\int_0^\Theta \frac{1}{h(x)} dx}{\int_0^1 \frac{1}{h(x)} dx} \right] \quad (2.6)$$

where h is the pressure head given as a function of the normalized water content and can be expressed by the equation (van Genuchten, 1980)

$$\Theta = S_{eff} = \left[\frac{1}{1+(ah)^n} \right]^m \quad (2.7)$$

where a approximates the air-entry height of the capillary fringe [m^{-1}], n is connected to the pore size distribution and m is connected to the symmetry of the SWRC.

Compared to *the Brooks and Corey model*, the VG model shows the sigmoidal shape and the inflection point of the SWRC in a better way. Therefore, as mentioned before, this model is valid for a wider range of suction. This model also gives smooth changes when suction approaches residual conditions and at air-entry values of the SWRC. In the VG-model the suction term can be expressed both in units of pressure ψ : [kPa] and in head h : [m] and since *Plaxis* uses head, this will be used in the rest of this chapter (Lu & Likos, 2004).

It is possible to simplify the VG model to a model with only two fitting parameters. However this restricts the precision and flexibility of the model. This simplification also gives a better stability when calculating the parameters and offers the solution to the hydraulic conductivity in closed form. By introducing a function which relates the m parameter to the n parameter, the VG model is turned into a two parameter model, as (Lu & Likos, 2004)

$$m = 1 - \frac{1}{n} \quad (2.8)$$

A flatter soil water retention curve is simulated by larger values of the parameter n and lesser values of the parameter a and reflects soils with a higher air-entry pressure (Lu and Likos 2004).

Van Genuchten (1980) shows that the relative hydraulic conductivity can be expressed in pressure head as

$$K_r(\Theta) = \frac{\{1-(ah)^{n-1}[1+(ah)^n]^{-m}\}^2}{[1+(ah)^n]^{\frac{m}{2}}} \quad (2.9)$$

where m is given by Equation 2.8. The relation between the saturated conductivity and the relative conductivity is formulated as

$$K = K_S K_r \quad (2.10)$$

The equation for the soil-water diffusivity, $D(\Theta)$ expressed in the hydraulic conductivity is given by (van Genuchten, 1980)

$$D(\Theta) = \frac{(1-m)K_s}{\alpha m(\theta_s - \theta_r)} \Theta^{\left(\frac{1}{2} - \frac{1}{m}\right)} \left[\left(1 - \Theta^{\frac{1}{m}}\right)^{-m} + \left(1 - \Theta^{\frac{1}{m}}\right)^m - 2 \right] \quad (2.11)$$

3. Constitutive modelling

The relation between stresses and strains is normally referred to as a constitutive model. The focus in this chapter will be to explain different constitutive models that will be used in the numerical calculations in *Plaxis 2D*. Underlying finite element theory will not be explained here and the reader is suggested to go elsewhere, for example *Introduction to the finite element method* by Ottosen and Petersson (1992).

3.1 Strain

During finite element calculations the deformation of the body needs to be described. This is done with the strain tensor, \mathbf{E}_{ij} , a quantity that is not affected by any rigid-body motions and therefore only describes the deformation of the body. In this chapter only situations where the displacement gradient is small will be considered, i.e. the strain tensor can be described by the symmetric small strain tensor ε_{ij} given by (Ottosen & Ristinmaa, 2005)

$$\varepsilon = \begin{bmatrix} \varepsilon_{11} & \varepsilon_{12} & \varepsilon_{13} \\ \varepsilon_{21} & \varepsilon_{22} & \varepsilon_{23} \\ \varepsilon_{31} & \varepsilon_{32} & \varepsilon_{33} \end{bmatrix} = \begin{bmatrix} \varepsilon_{11} & \varepsilon_{12} & \varepsilon_{13} \\ \varepsilon_{12} & \varepsilon_{22} & \varepsilon_{23} \\ \varepsilon_{13} & \varepsilon_{23} & \varepsilon_{33} \end{bmatrix} \quad (3.1)$$

The principal strains describe the maximum and minimum values for strain of the elements, which occur when the shear strains ε_{12} , ε_{13} and ε_{23} are equal to zero.

For a specific choice of coordinate system the strain tensor takes a simple form. For this reason look at a direction given by the unit vector \mathbf{n} , then a vector \mathbf{q} can be defined as (Ottosen & Ristinmaa, 2005)

$$\mathbf{q} = \varepsilon_i \mathbf{n}_i \quad (3.2)$$

Figure 3.1 illustrates that the unit vector \mathbf{m} is orthogonal to the unit vector \mathbf{n} and the normal strain ε_{nn} in the direction of the unit vector \mathbf{n} is given by

$$\varepsilon_{nn} = n_i \varepsilon_{ij} n_j \text{ or } \varepsilon = \mathbf{n}^T \boldsymbol{\varepsilon} \mathbf{n} \quad (3.3)$$

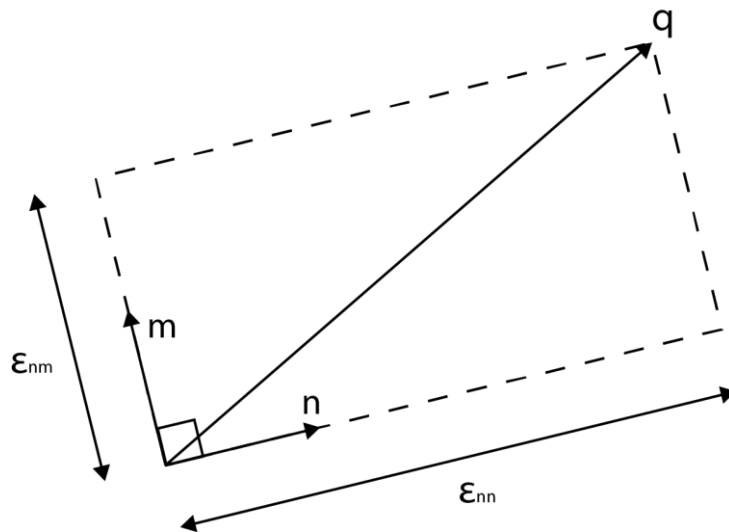


Figure 3.1 - The vector $\mathbf{q} = \boldsymbol{\varepsilon} \mathbf{n}$ and its components after direction \mathbf{n} and \mathbf{m} after Ottosen & Ristinmaa (2005).

In analogy with the above stated approach the normal strain ϵ_{nm} in the direction of the unit vector \mathbf{m} can be expressed as

$$\epsilon_{nm} = m_i \epsilon_{ij} n_j \text{ or } \boldsymbol{\epsilon} = \mathbf{m}^T \boldsymbol{\epsilon} \mathbf{n} \quad (3.4)$$

where ϵ_{nm} is the shear strain in the direction of \mathbf{m} . According to Ottosen and Ristinmaa (2005) the principal strains are found when the direction of \mathbf{n} is chosen in a way where the shear strain, ϵ_{nm} is equal to zero. In order to do this the vector \mathbf{q} must be collinear with \mathbf{n} , therefore \mathbf{q} is defined as

$$q_i = \lambda n_i \quad (3.5)$$

Equations 3.3 and 3.5 requires that $\epsilon_{nm} = \lambda$. Additionally Equation 3.2 and 3.5 gives the following expression for the renowned eigenvalue problem (Ottosen & Ristinmaa, 2005)

$$(\boldsymbol{\epsilon} - \lambda \mathbf{I}) \mathbf{n} = \mathbf{0} \text{ or } (\epsilon_{ij} - \lambda \delta_{ij}) n_j = 0 \quad (3.6)$$

where $\mathbf{0}$ is given by $\mathbf{0}^T = [0 \ 0 \ 0]$. For a non-trivial answer \mathbf{n} to be possible the following statement must be true

$$\det(\boldsymbol{\epsilon} - \lambda \mathbf{I}) = 0 \quad (3.7)$$

Equation 3.7 provides the cubic equation for determination of λ and is known as the characteristic equation. When the eigenvalues, λ_i have been determined they provide the principal strains and the \mathbf{n} -vector is known as the direction of the principal strains. The strain tensor can therefore be expressed as (Ottosen & Ristinmaa, 2005)

$$\boldsymbol{\epsilon}' = \mathbf{A} \boldsymbol{\epsilon} \mathbf{A}^T = \begin{bmatrix} \lambda_1 & 0 & 0 \\ 0 & \lambda_2 & 0 \\ 0 & 0 & \lambda_3 \end{bmatrix} = \begin{bmatrix} \epsilon_1 & 0 & 0 \\ 0 & \epsilon_2 & 0 \\ 0 & 0 & \epsilon_3 \end{bmatrix} \quad (3.8)$$

where $\mathbf{A}^T = [\mathbf{n}_1 \ \mathbf{n}_2 \ \mathbf{n}_3]$

3.2 Strain invariants

In this section the strain invariants are presented. The importance of invariants is that they have an identical value in all coordinate systems. Ottosen and Ristinmaa (2005) prove that the principal strains are invariants. The Cauchy strain invariants can be defined from the characteristic equation and be seen in Equations 3.10, 3.11 and 3.12 (Ottosen & Ristinmaa, 2005).

Equation 3.7 provides the following

$$-\lambda^3 + \theta_1 \lambda^2 - \theta_2 \lambda + \theta_3 = 0 \quad (3.9)$$

With the Cauchy strain invariants $\theta_1, \theta_2, \theta_3$ equal to

$$\theta_1 = \epsilon_{11} + \epsilon_{22} + \epsilon_{33} = \epsilon_{ii} \quad (3.10)$$

$$\theta_2 = \epsilon_{11} \epsilon_{22} + \epsilon_{22} \epsilon_{33} + \epsilon_{11} \epsilon_{33} - \epsilon_{23}^2 - \epsilon_{12}^2 - \epsilon_{13}^2 = \frac{1}{2} \theta_1^2 - \frac{1}{2} \epsilon_{ij} \epsilon_{ji} \quad (3.11)$$

$$\theta_3 = \varepsilon_{11}\varepsilon_{22}\varepsilon_{33} - \varepsilon_{11}\varepsilon_{23}^2 - \varepsilon_{22}\varepsilon_{13}^2 - \varepsilon_{33}\varepsilon_{12}^2 + 2\varepsilon_{12}\varepsilon_{13}\varepsilon_{23} = \det(\varepsilon_{ij}) \quad (3.12)$$

The generic invariants are characterized by their systematic definition and have an exclusive connection to the Cauchy invariants. The generic invariants follow a systematic way in their definition and can be stated as (Ottosen & Ristinmaa, 2005)

$$\tilde{I}_1 = \varepsilon_{ii} = \varepsilon_1 + \varepsilon_2 + \varepsilon_3 \quad (3.13)$$

$$\tilde{I}_2 = \frac{1}{2}\varepsilon_{ij}\varepsilon_{ji} = \frac{1}{2}(\varepsilon_1^2 + \varepsilon_2^2 + \varepsilon_3^2) \quad (3.14)$$

$$\tilde{I}_3 = \frac{1}{3}\varepsilon_{ij}\varepsilon_{jk}\varepsilon_{kl} = \frac{1}{3}(\varepsilon_1^3 + \varepsilon_2^3 + \varepsilon_3^3) \quad (3.15)$$

This relationship between the generic and Cauchy invariants is defined as (Ottosen & Ristinmaa, 2005)

$$\tilde{I}_1 = \theta_1$$

$$\tilde{I}_2 = \frac{1}{2}\theta_1^2 - \theta_2$$

$$\tilde{I}_3 = \frac{1}{3}\theta_1^3 - \theta_1\theta_2 + \theta_3$$

The invariants for the deviatoric strain tensor can be described in the same manner as the invariants were described previously in this chapter. The deviatoric strain tensor, e_{ij} can be defined as:

$$e_{ij} = \varepsilon_{ij} - \frac{1}{3}\varepsilon_{kk}\delta_{ij} \quad (3.16)$$

From this it can be seen that the deviatoric strain tensor and the strain tensor have the same principal directions. An exclusive relationship exists between $\theta_1, \theta_2, \theta_3$ and $\tilde{I}_1, \tilde{I}_2, \tilde{I}_3$ and in analogy with the strain tensor the generic invariants for the deviatoric strain tensor can be described as

$$\tilde{J}_1 = e_{ii} = \text{tr } \mathbf{e} = e_1 + e_2 + e_3 = 0 \quad (3.17)$$

$$\tilde{J}_2 = \frac{1}{2}e_{ij}e_{ji} = \frac{1}{2}\text{tr } (\mathbf{e}^2) = \frac{1}{2}(e_1^2 + e_2^2 + e_3^2) \quad (3.18)$$

$$\tilde{J}_3 = \frac{1}{3}e_{ij}e_{jk}e_{kl} = \frac{1}{3}\text{tr } (\mathbf{e}^3) = \frac{1}{3}(e_1^3 + e_2^3 + e_3^3) = e_1e_2e_3 \quad (3.19)$$

where tr is the trace of a 3x3 matrix. A plane where the normal to the plane makes equal angles to the three principal strain directions is referred to as an octahedral plane and there are eight planes that exist. From the equations above the octahedral normal strain ε_0 and octahedral shear strain γ_0 are then defined as (Ottosen & Ristinmaa, 2005)

$$\varepsilon_0 = \frac{1}{3} \tilde{I}_1 \quad (3.20)$$

$$\gamma_0 = 2 \sqrt{\frac{2}{3} \tilde{J}_2} \quad (3.21)$$

3.3 Stress

In the previous section the deformation of the body i.e. the strain tensor was described and in this section the loading of the body in an arbitrary point also known as the stress tensor, will be described.

The traction vector, \mathbf{t} is given by

$$\mathbf{t} = \begin{bmatrix} t_1 \\ t_2 \\ t_3 \end{bmatrix} = \boldsymbol{\sigma} \mathbf{n} \quad (3.23)$$

where \mathbf{n} is the unit normal vector and $\boldsymbol{\sigma}$ is the stress tensor. The traction vector for an arbitrary surface, t can also be described as

$$t_i = \lim_{\Delta A \rightarrow 0} \left(\frac{\Delta P_i}{\Delta A} \right) \quad (3.24)$$

where ΔP_i is the incremental force vector that acts on the incremental surface area ΔA . When ΔA approaches zero the ratio between the force vector and the incremental surface approaches the value of t (Ottosen & Ristinmaa, 2005).

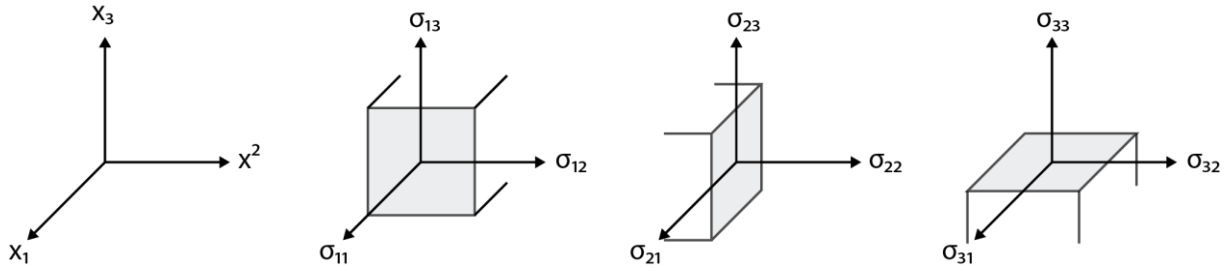


Figure 3.2 - Illustrations of stress components after Ottosen and Ristinmaa (2005).

Now, sections perpendicular to the main coordinate axes are considered, i.e. the outer unit normal vector, \mathbf{n} is taken in the direction of the different coordinate axis to form the corresponding traction vectors. The symmetric stress tensor can then be defined as (Ottosen & Ristinmaa, 2005)

$$[\sigma_{ij}] = \begin{bmatrix} \mathbf{t}_1^T \\ \mathbf{t}_2^T \\ \mathbf{t}_3^T \end{bmatrix} = \begin{bmatrix} \sigma_{11} & \sigma_{12} & \sigma_{13} \\ \sigma_{21} & \sigma_{22} & \sigma_{23} \\ \sigma_{31} & \sigma_{32} & \sigma_{33} \end{bmatrix} = \begin{bmatrix} \sigma_{11} & \sigma_{12} & \sigma_{13} \\ \sigma_{12} & \sigma_{22} & \sigma_{23} \\ \sigma_{13} & \sigma_{23} & \sigma_{33} \end{bmatrix} \quad (3.25)$$

This results in two different kinds of stress components in the stress tensor σ_{ij} , normal stresses i.e. $\sigma_{11}, \sigma_{22}, \sigma_{33}$ and shear stresses i.e. $\sigma_{12}, \sigma_{13}, \sigma_{23}$, seen in Figure 3.2 (Ottosen & Ristinmaa, 2005).

For the stress tensor the components of the traction vector parallel to \mathbf{n} is called the normal stress, σ_n and can be described as (Ottosen & Ristinmaa, 2005)

$$\sigma_n = n_i t_i = n_i \sigma_{ij} n_j \text{ or } \sigma_n = \mathbf{n}^T \mathbf{t} = \mathbf{n}^T \boldsymbol{\sigma} \mathbf{n} \quad (3.26)$$

The component of the traction vector perpendicular to \mathbf{n} is called the shear stress and is therefore the component in the direction of \mathbf{m} , seen in Figure 3.1. This can be formulated as (Ottosen & Ristinmaa, 2005)

$$\tau_n = m_i t_i = m_i \sigma_{ij} n_j \text{ or } \tau_n = \mathbf{m}^T \mathbf{t} = \mathbf{m}^T \boldsymbol{\sigma} \mathbf{n} \quad (3.27)$$

Equation 3.26 and 3.27 provides a physical interpretation of the eigenvalue problem for the stress tensor. In the same way stated in Section 3.1 the solution of this problem gives the stress invariants and in analogy at a simple case is achieved when the traction vector \mathbf{t} is collinear with the unit vector \mathbf{n} . The direction of the unit vector \mathbf{n} should be chosen in such a way that it provides (3.28)

$$t_i = \lambda n_i \quad (3.28)$$

where Equation 3.26 indicates that λ is equal to σ_n . As stated earlier \mathbf{m} and \mathbf{n} are orthogonal, in analogy with the reasoning for the strain tensor the use of Equation 3.23 and 3.28 will result in the eigenvalue problem of the stress tensor. This is formulated as (Ottosen & Ristinmaa, 2005)

$$(\boldsymbol{\sigma} - \lambda \mathbf{I}) \mathbf{n} = \mathbf{0} \text{ or } (\sigma_{ij} - \lambda \delta_{ij}) n_j = 0 \quad (3.29)$$

Likewise Equation 3.30 is called the characteristic equation of the stress tensor. Since the solution to the eigenvalue problem between the stress tensor and strain tensor is equivalent, the same derivation for the stress invariants can be used (Ottosen & Ristinmaa, 2005)

$$\det(\boldsymbol{\sigma} - \lambda \mathbf{I}) = 0 \quad (3.30)$$

The characteristic equation provides the three principal stresses and the principal directions correspond to a λ -value. In analogy with the reasoning for the strain tensor this provides a solution for the stress tensor: (Ottosen & Ristinmaa, 2005)

$$\boldsymbol{\sigma}' = \mathbf{A} \boldsymbol{\sigma} \mathbf{A}^T = \begin{bmatrix} \sigma_1 & 0 & 0 \\ 0 & \sigma_2 & 0 \\ 0 & 0 & \sigma_3 \end{bmatrix} \quad (3.31)$$

where $\mathbf{A}^T = [\mathbf{n}_1 \ \mathbf{n}_2 \ \mathbf{n}_3]$

3.4 Stress invariants

The stress tensor also satisfy the *Cayley-Hamilton theorem* and therefore the same equations used for the strain tensor applies. The Cauchy stress invariants are therefore given by the coefficients in the characteristic equation and in similarity with the generic strain invariants, the generic stress invariants can be expressed as (Ottosen & Ristinmaa, 2005)

$$I_1 = \sigma_{ii} \quad (3.32)$$

$$I_2 = \frac{1}{2} \sigma_{ij} \sigma_{ji} \quad (3.33)$$

$$I_3 = \sigma_{ij} \sigma_{jk} \sigma_{kl} \quad (3.34)$$

The deviatoric stress tensor is defined as

$$s_{ij} = \sigma_{ij} - \frac{\sigma_{kk}}{3} \delta_{ij} \quad (3.35)$$

where the term $\frac{\sigma_{kk}}{3}$ is referred to as the hydrostatic stress. The hydrostatic stress is important for material such as soils and rocks since this severely affects the calculations and therefore needs to be included into the numerical calculations. Since σ_{ij} and s_{ij} have the same principal direction the generic invariants for the deviatoric stress tensor can be expressed as (Ottosen & Ristinmaa, 2005)

$$J_1 = s_{ii} = 0 \quad (3.36)$$

$$J_2 = \frac{1}{2} s_{ij} s_{ji} \quad (3.37)$$

$$J_3 = \frac{1}{3} s_{ij} s_{jk} s_{ki} \quad (3.38)$$

From the equations above the octahedral normal stress σ_0 and the octahedral shear stress τ_0 are described as (Ottosen & Ristinmaa, 2005)

$$\sigma_0 = \frac{1}{3} I_1 \quad (3.39)$$

$$\tau_0 = \sqrt{\frac{2}{3} J_2} \quad (3.40)$$

3.5 Plasticity

Materials which are loaded and unloaded may be subjected to plastic deformations. The following chapter explains the basic constitutive modelling theory for plasticity. In accordance with the uniaxial stress-strain curve in Figure 3.3, the material behaves linear elastic when the stress is below the initial yield stress σ_{y0} . In this situation the stiffness is given by Young's modulus, E and no plastic deformations occur when the material is unloaded (Ottosen & Ristinmaa, 2005).

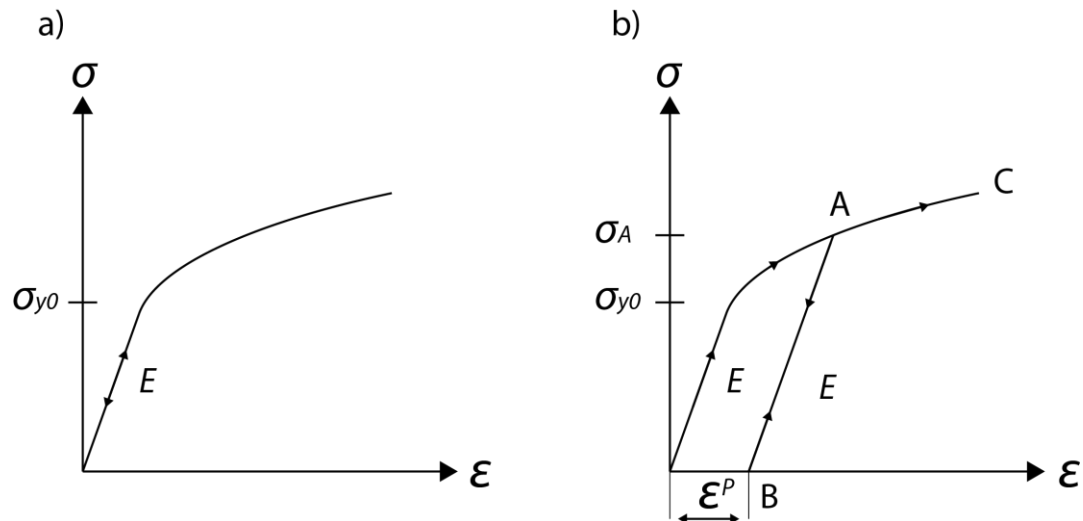


Figure 3.3 – Loading below the initial yield stress and loading above the initial yield stress after (Ottosen & Ristinmaa, 2005).

If the material is reloaded to the stress σ_A yielding occurs, and at unloading a plastic strain, ϵ^p will still be present. If the material is reloaded the strain will then again follow the linear elasticity curve to point A if the material is reloaded, reaching point A yielding is then initiated once more and the strain will follow the curve AC as unloading never occurred (Ottosen & Ristinmaa, 2005).

3.6 Hardening and softening

The plasticity theory has two different important effects, the hardening and softening effect. In Figure 3.3 the stress σ_A which is required to activate further plastic deformations will increase when the material is subjected to reloading. This is known as the hardening effect.

When the strain is increased sufficiently the material will reach a maximum stress, also known as the failure stress σ_f . After the failure stress has been reached the stress decreases when the strain is increased, as seen in Figure 3.4b. This is referred to as the softening effect and is distinctive for materials like concrete, soils and rocks (Ottosen & Ristinmaa, 2005).

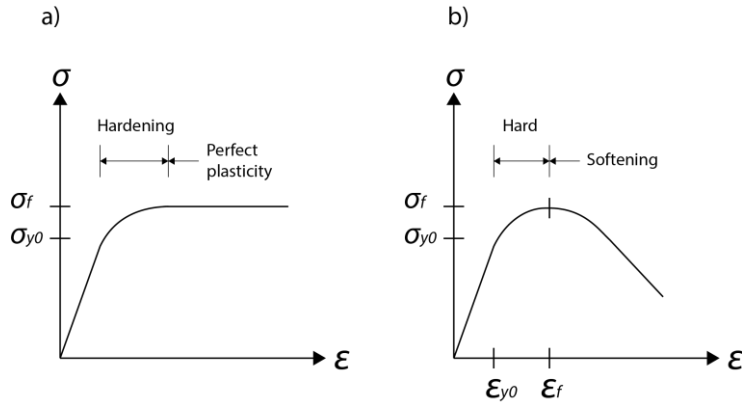


Figure 3.4 - Hardening and perfect plasticity, Hardening and softening plasticity (Ottosen & Ristinmaa, 2005).

3.7 Yield criteria

In the section above the initial yield was described for a uniaxial state of stress. In reality the yield criterion is more complex and is defined using the stress tensor.

When a homogenous material loaded in a homogenous stress state the failure criterion, F can be considered to only depend on the stress tensor σ_{ij} , considering proportional loading (Ottosen & Ristinmaa, 2005). This will result in a function, F with the following requirements

$$F(\sigma_{ij}) = \sigma - \sigma_{y0} \quad (3.41)$$

$$F(\sigma_{ij}) < 0 \quad \text{Elastic} \quad (3.42)$$

$$F(\sigma_{ij}) = 0 \quad \text{Yielding starts} \quad (3.43)$$

$$F(\sigma_{ij}) > 0 \quad \text{Above yield} \quad (3.44)$$

F is an invariant and considering the isotropic situation (a material that has no directional properties) this generates the following (Ottosen & Ristinmaa, 2005)

$$F(\sigma_1, \sigma_2, \sigma_3) = 0 \quad (3.45)$$

Where it is provided that the relation $\sigma_1 \geq \sigma_2 \geq \sigma_3$ is true and tensile stresses are considered positive. Equation 3.45 can be written with stress invariants, stated previously in this master's dissertation. The original eigenvalue problem is linked to the determination of the principal stresses and when this expression is reformulated with invariants this is avoided. The stress invariants are obtained from the stress tensor and the failure criterion can then be expressed as (Ottosen & Ristinmaa, 2005).

$$F(I_1, J_2, \cos 3\theta) = 0 \quad (3.46)$$

$$J_2 = \frac{1}{2} s_{ij} s_{ji} \quad (3.47)$$

$$\cos 3\theta = \frac{3\sqrt{3}}{2} \frac{J_3}{J_2^{3/2}} \quad (3.48)$$

$$J_3 = \frac{1}{3} s_{ij} s_{jk} s_{kl} \quad (3.49)$$

Where I_1 is the influence of the hydrostatic stress, and deviatoric stresses are expressed with J_2 and J_3 . $\cos 3\theta$ is referred to as the direction of the deviatoric stress. The J_2 -term contains information about the magnitude of the deviatoric stresses and the $\cos 3\theta$ -term about direction of these stresses. Multiple symmetry properties of the initial yield criterion can be derived from the $\cos 3\theta$ -term (Ottosen & Ristinmaa, 2005).

To further explain the geometric interpretation of the stress invariants an arbitrary point P in the coordinate system in Figure 3.5 is studied. Since the axis are $\sigma_1, \sigma_2, \sigma_3$ this is called *Haigh-Westergaards* coordinate system. The unit vector can be viewed as the space diagonal and can be described by (Ottosen & Ristinmaa, 2005)

$$\mathbf{n} = \frac{1}{\sqrt{3}}(1, 1, 1) \quad (3.50)$$

Along this axis all principal stresses are equal and therefore this axis is considered as the hydrostatic axis. The deviatoric plane is located perpendicular to the hydrostatic axis and contains the line NP, as seen in Figure 3.5.

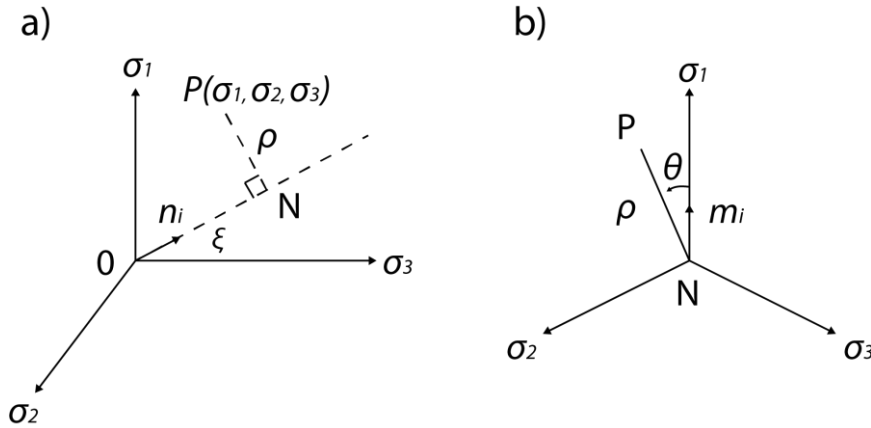


Figure 10.5 - Haigh-Westergaard coordinate system and deviatoric plane perpendicular to the hydrostatic axis containing line NP (Ottosen & Ristinmaa, 2005).

3.8 The Mohr-Coulomb model

The *Mohr-Coulomb* failure criterion can be stated as (Labuz & Zang, 2012)

$$|\tau| = c - \sigma_n \tan \phi \quad (3.51)$$

where c is the cohesion, σ_n is the normal stress and $\tan \phi$ is the coefficient of internal friction (ϕ is the angle of internal friction). By using the failure criterion and trigonometric relations, which can be seen in Figure 3.6, the above yield function can be rewritten as a function of the principal stresses (Labuz & Zang, 2012):

$$\sigma_1 - \sigma_3 = (\sigma_1 + \sigma_3) \sin \phi + 2c \cos \phi \quad (3.52)$$

This is consistent with a linear failure envelope. In the *Mohr-Coulomb model*, the mean stress $(\sigma_1 - \sigma_3)/2$ is considered, which is of significance for materials as soil and rocks.

The model also permits a curved failure envelope, which is a behaviour (non-linear) that conforms with the behaviour of several rock types (Labuz & Zang, 2012).

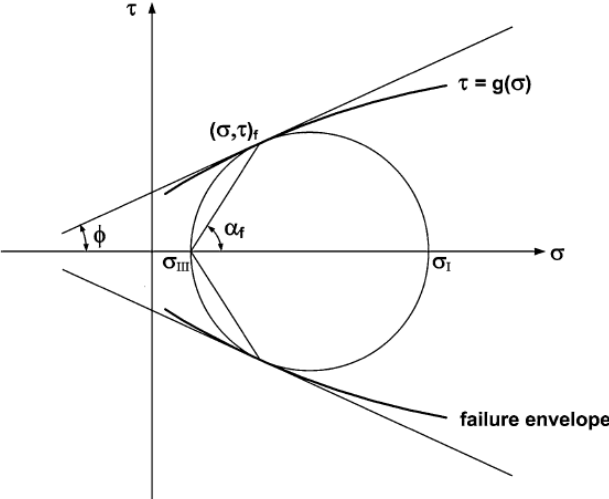


Figure 3.6 - The failure envelope in a Mohr-Diagram (Labuz & Zang, 2012).

Tension cut-offs

The theoretical tensile capacity according to *Mohr-Coulomb* differs from the measured one during experiments where the tensile capacity of soil is much lower and measured as $\sigma_1 = 0, \sigma_3 = -T$. Experiments show that for tensile values of the minor principal stress, the failure plane is perpendicular to $\sigma_3 = -T$. Paul Burton introduced a modified MC model (requiring three material constants) and the concept of tension cut-offs to account for tensile failure. For the case with principal stresses the hexagonal cone is cut off by a pyramid which has three planes perpendicular with the stress axes. This is shown in Figure 3.7. (Labuz & Zang, 2012).

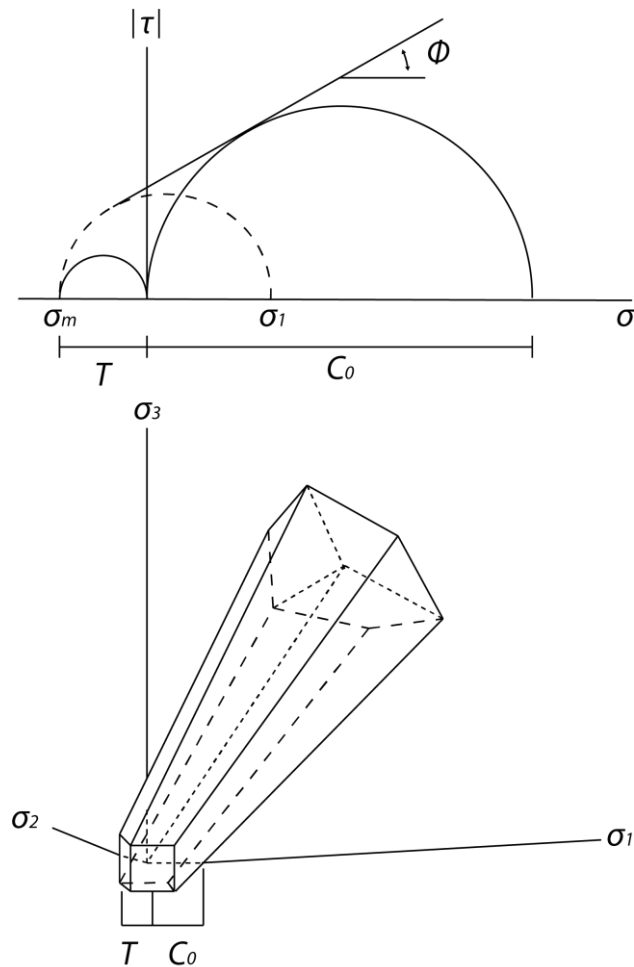


Figure 3.7 - Tension-cut-offs for the modified Mohr-Coulomb failure criterion, (a) failure envelope in the Mohr-diagram, (b) representation in principal stress space (Labuz & Zang, 2012).

3.9 Symmetry properties

The cosine function concludes the yield curve in the deviatoric plane, where the former is periodic with a period of 360° and the latter is periodic with a period of 120° . Due to this the function in the deviatoric plane can be shown to be symmetric with $\cos x = 60^\circ, 180^\circ$ and 300° . If the relation $0^\circ \leq \theta \leq 60^\circ$ is determined, it provides that all states of stress in the deviatoric space is known. The possible failure mode in the deviatoric space is illustrated in Figure 3.8. Experimental evidence rather than mathematics has provided this interpretation of the initial yield curve in the deviatoric plane (Ottosen & Ristinmaa, 2005).

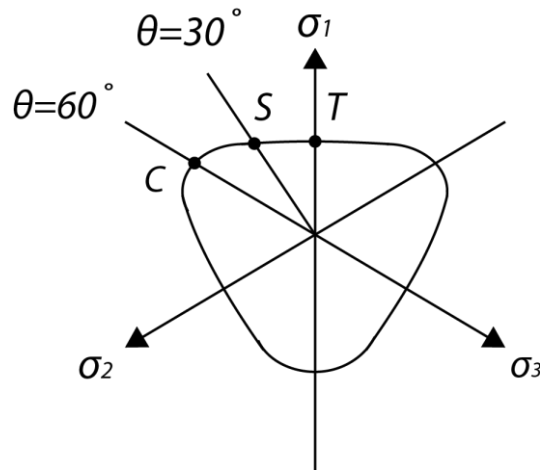


Figure 3.8 - Possible shape of failure or initial yield curve in the deviatoric plane. T=tensile meridian, C=compressive meridian and S=shear meridian (Ottosen & Ristinmaa, 2005).

A meridian is the curve where the initial yield surface and a plane containing the hydrostatic axis intersect each other, while $\theta = \text{constant}$ applies. The meridians are drawn in a coordinate system which is referred to as the meridian plane, where the axes depend

on $\frac{I_1}{\sqrt{3}}$ and $\sqrt{2J_2}$, illustrated in Figure 3.9.

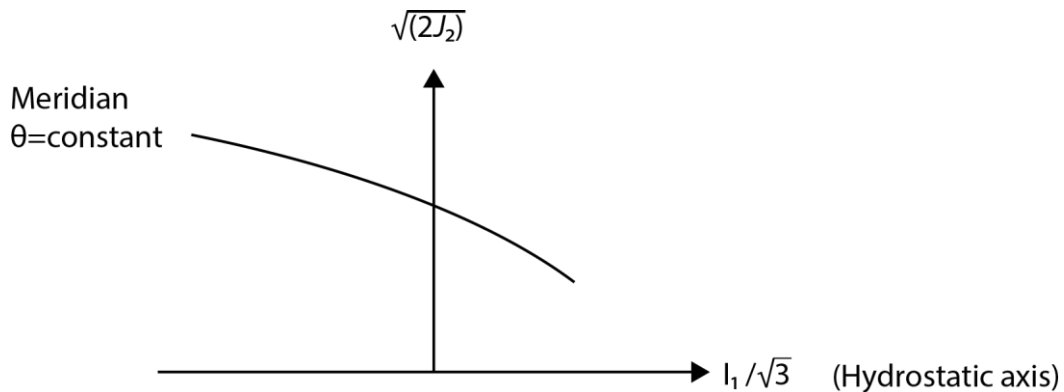


Figure 3.9 - Meridian plane obtained by the intersection of the failure or initial yield surface with a plane containing the hydrostatic axis (Ottosen & Ristinmaa, 2005).

There are three different kinds of meridians that are of special interest, the tensile-, compressive- and shear meridian, illustrated in Figure 3.8. The tensile meridian is defined as the stress ratio $\sigma_1 > \sigma_2 = \sigma_3$ i.e. $\theta = 0^\circ$. This coincides with uniaxial tensile stress states and biaxial compressive stress states when the principal stresses are equal. A geometric interpretation of this is when a hydrostatic stress state is intersected by a tensile stress directed in the σ_1 -direction (Ottosen & Ristinmaa, 2005).

If the stress ratio is reversed, $\sigma_1 = \sigma_2 > \sigma_3$ the compressive meridian is achieved. This holds for $\theta = 60^\circ$. Likewise this relates to a hydrostatic stress state intersected by a compressive stress in the σ_3 -direction. Uniaxial compressive stress states are therefore located on this meridian (Ottosen & Ristinmaa, 2005).

The third and final meridian, the shear meridian is equal to $\sigma_1 > \sigma_2 = \frac{\sigma_1 + \sigma_3}{2} > \sigma_3$ i.e. $\theta = 30^\circ$. It is equal to a hydrostatic stress state intersected by a positive stress τ in the σ_1 -direction or a negative stress $-\tau$ in the σ_3 - direction (Ottosen & Ristinmaa, 2005).

Materials like soils, rocks and concrete have no well-defined initial yield stress and this is visualized as a smooth appearance of the stress-strain curve. Experimental proof regarding the failure of these materials can be summed in: (Ottosen & Ristinmaa, 2005)

- The term $\cos 3\theta$ is important
- The failure surface is convex
- The hydrostatic stress has a strong influence.

For materials as rocks, concrete and soil all terms in Equation 3.46 are of primary importance. Further treatment of the material models used in this master's dissertation is presented in Chapter 4.

3.10 Plane strain

If no deformation occurs in the x_3 -direction i.e out-of-plane, then it is talked about plane strain. The displacement vector u_i for the case x_1x_2 -plane is given by (Ottosen & Ristinmaa, 2005)

$$[u_i] = \begin{bmatrix} u_1(x_1, x_2) \\ u_2(x_1, x_2) \\ 0 \end{bmatrix} \quad (3.53)$$

For plane strain it is assumed that the body is unable to move in the length direction. It is also important to point out that the cross-sections are in the same state as one another. The plane strain is a special state of strain that is used in *Plaxis 2D*. The strain tensor can hereby be simplified into (Ottosen & Ristinmaa, 2005)

$$[\varepsilon_{ij}] = \begin{bmatrix} \varepsilon_{11} & \varepsilon_{12} & 0 \\ \varepsilon_{21} & \varepsilon_{22} & 0 \\ 0 & 0 & 0 \end{bmatrix} \quad (3.54)$$

In two-dimensional modelling there can be a certain loss of information compared to the three-dimensional modelling. Even though this might occur there can be a lot of advantages using 2D, quicker calculations and a result which is more easily interpreted. Since the offset in the x_3 -direction is equal to zero this can be simplified into (Ottosen & Ristinmaa, 2005)

$$du_1 = \frac{\partial u_1}{\partial x_1} dx_1 + \frac{\partial u_1}{\partial x_2} dx_2 \quad (3.55)$$

$$du_2 = \frac{\partial u_2}{\partial x_1} dx_1 + \frac{\partial u_2}{\partial x_2} dx_2 \quad (3.56)$$

This will result in the following plane elastic relations derived from the kinematic equation, where $\varepsilon_i = \tilde{\nabla} u_i$ (Ottosen & Petersson, 1992)

$$\varepsilon = \begin{bmatrix} \varepsilon_{11} \\ \varepsilon_{22} \\ \gamma_{12} \end{bmatrix} \quad (3.57)$$

$$\tilde{\nabla} = \begin{bmatrix} \frac{\partial}{\partial x} & 0 \\ 0 & \frac{\partial}{\partial y} \\ \frac{\partial}{\partial y} & \frac{\partial}{\partial x} \end{bmatrix} \quad (3.58)$$

$$u = \begin{bmatrix} u_1 \\ u_2 \end{bmatrix} \quad (3.59)$$

Hooke's generalized law can be defined as

$$\sigma = D\varepsilon \quad (3.60)$$

Hooke's generalized law, seen in Equation 3.29 is used for linear elasticity and therefore Equation 3.61, 3.62 and 3.63 will apply for an isotropic material (Ottosen & Ristinmaa, 2005)

$$\begin{bmatrix} \sigma_{11} \\ \sigma_{22} \\ \sigma_{12} \end{bmatrix} = \frac{E}{(1+\nu)(1-2\nu)} \begin{bmatrix} 1-\nu & \nu & 0 \\ \nu & 1-\nu & 0 \\ 0 & 0 & \frac{1}{2}(1-2\nu) \end{bmatrix} \begin{bmatrix} \varepsilon_{11} \\ \varepsilon_{22} \\ \gamma_{12} \end{bmatrix} \quad (3.61)$$

$$\sigma_{33} = \frac{E\nu}{(1+\nu)(1-2\nu)} (\varepsilon_{11} + \varepsilon_{22}) \quad (3.62)$$

$$\sigma_{13} = \sigma_{23} = 0 \quad (3.63)$$

4. Plaxis

Plaxis is a software that uses the finite element method to perform numerical calculations of geotechnical problems as deformation, consolidation, stability and flow analyses etc. *Plaxis* provides the user with the ability to simulate excavations, adding structures, loading and unloading of the soil in different phases in a similar manner with real projects. These features in *Plaxis* enable for a well suited modelling process.

Plaxis 2D is used in this master's dissertation; it provides methods to perform initial stress generation, plastic calculations, *Fully coupled flow-deformation analysis* and safety calculations among others. The software is used to model the groundwater flow and total stability of excavation pits in unsaturated clay. The goal is to evaluate the factor of safety for geometries where suction is considered or not.

In this section, the necessary features of *Plaxis 2D* are presented, aspects which are necessary to enable as good numerical calculations as possible.

4.1 Mesh

In order to perform the calculations the mesh in *Plaxis* has to be generated. When *Plaxis* creates the mesh, it automatically divides the geometries into finite elements. It is important to generate a sufficiently fine mesh in order to get accurate results from *Plaxis*. In this case this means that a finer mesh should not generate any differences in the factor of safety compared to the previously used mesh. It is important to notice that the finer the mesh, the longer the calculation will take to perform. Hereby an unnecessarily fine mesh should be avoided due to long calculation times. This is however, a relatively small problem in *Plaxis 2D* and of much more concern in *Plaxis 3D*. *Plaxis* generates the elements in the mesh by using a triangulation procedure (PRM, 2015).

4.2 Elements

In this section the different ways to model soil elements are presented, later on in this work the possible structural and interface elements are described. In *Plaxis* it is possible to use 6-nodal or 15-nodal triangular elements for the soil, as seen in Figure 4.1 and 4.2. It is important to point out that the default mode is 15-node elements, this provides a fourth order integration for displacements and the numerical integration uses 12 gauss points. The 15-node elements result in a finer distribution of nodes and therefore more accurate calculations in comparison to the 6-nodal elements. This is more time consuming, but is assessed as necessary to get accurate results and used in this master's dissertation (PRM, 2015).

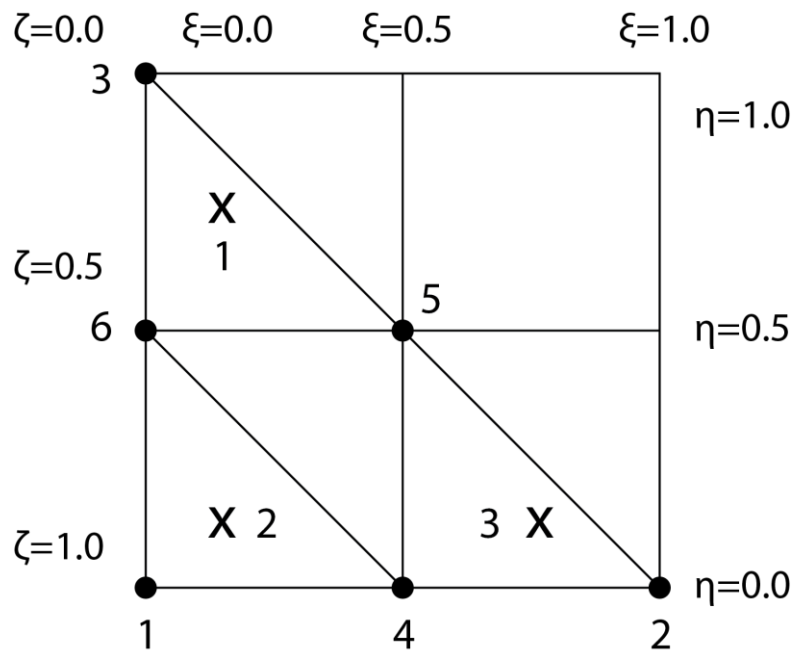


Figure 4.1 – Local numbering and positioning of nodes and integration points (x) of a 6 node triangular element (PSM, 2015).

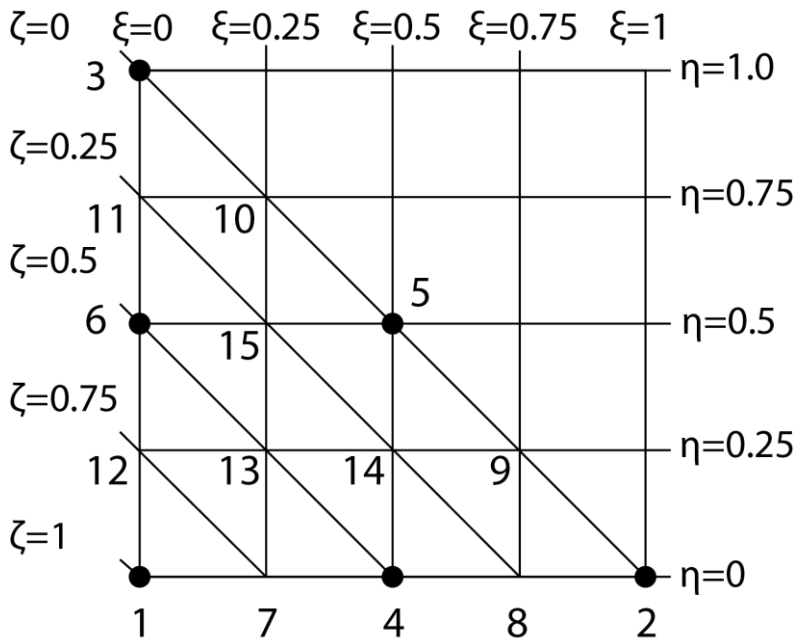


Figure 4.2 – Local numbering and positioning of nodes of a 15-node 34triangular element (PSM, 2015).

Plaxis automatically generates a mesh depending on the target element size, l_e which is a global entity generated by the dimension of the outer geometry and the element distribution factor selected in *Plaxis*. The element distribution factor is a factor that states which quality the mesh should be generated with. The target element size is a function of: (PRM, 2015):

$$l_e = r_e 0.06 \sqrt{(x_{max} - x_{min})^2 + (y_{max} - y_{min})^2} \quad (4.1)$$

where

r_e Relative element size factor, the values for different element distributions can be seen in the reference manual for *Plaxis 2D* (PRM, 2015).

l_e Average element size

After this automatically generated mesh, it is possible for the user to do local refinement of the mesh around points of interest or regions that are considered to be difficult to calculate correctly due to large stress concentrations caused by corners or edges of structural elements. *Plaxis* automatically makes the structural elements compatible with the soil elements (PRM, 2015).

4.3 Plate elements

In *Plaxis* plates are used to model slender geotechnical structures with a substantial bending stiffness and normal stiffness. In order to model these correctly the most important parameters are bending stiffness, EI , the axial stiffness, EA , and the thickness of the element, d_{eq} (PRM, 2015).

The 6-node soil elements are compatible with the 3-node plate elements and in analogy the 15-node soil elements are compatible with the 5-node plate elements as seen in Figure 4.3. In two-dimensional modelling these nodes have three degrees of freedom per node, one rotational and two translational. The Gaussian stress points seen in the plate elements below are used to calculate bending moment and axial forces, for the case with the 5-node plate element there are four pairs of stress points (PRM, 2015).

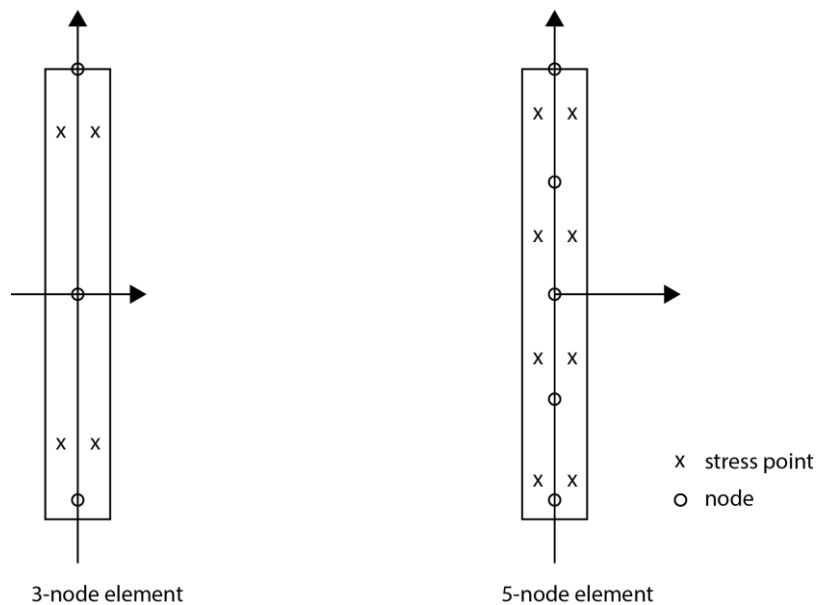


Figure 4.3 - Position of nodes and stress points in embedded beam row elements (PRM, 2015).

4.4 Interfaces and interface elements

The interfaces in *Plaxis 2D* are applied to plates or geogrids to enable accurate modelling of the interaction between the soil and structures. They can e.g. simulate the contact zone between a plate and soil, where the shearing is intense. An interface is usually assigned to both sides of the plate element (PRM, 2015).

When 15-node soil elements are used, the interface element consists of 5 pair of nodes with three translational degrees of freedom in every node (u_x, u_y, u_z). The three degrees of freedom enable the node pair to have different displacements relative to one another. Figure 4.4 shows the interface elements, in this figure the interface elements look similar to the plate elements. However the difference is that the interface elements consist of pairs of nodes, where the node coordinates are equal to one another. Hereby the thickness of the elements is zero. In the point where the interfaces end, the node pair is collapsed to a single node. These elements are numerically integrated using six Gauss points (PRM, 2015).

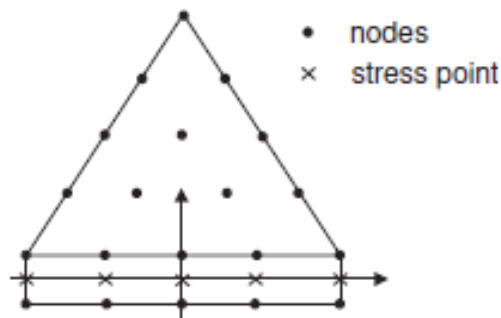


Figure 4.4 - Distribution of nodes and stress point sin 6-node beam elements and their connection to soil elements (PRM, 2015).

4.5 Fixed-end anchors

Fixed end anchors are modelled as point elements in *Plaxis 2D*. They have an axial stiffness but no bending stiffness. These are used to model the shoring supporting the retaining structure in one of the excavations (PSM, 2015).

4.6 Boundary conditions

Plaxis offers a number of different ways to set the boundary conditions for each phase. *Plaxis 2D* automatically assigns general boundary conditions to the geometry model. In *Plaxis* the vertical model boundaries are fixed in the x -direction, which means that $u_x = 0$ (no deformation) and free to move in the y -direction. It also automatically fixes the bottom boundary in all direction, i.e. $u_x = 0$, and $u_y = 0$. In contrast the boundary of the ground is set as free to move in all directions to enable modelling of soil movements. *Plaxis* provides the option to turn off or change these boundary conditions, but by doing so boundary conditions need to be set manually (PRM, 2015).

During the modelling in *Plaxis* it is of importance to ensure that the selected geometry boundaries do not affect the critical slip surface and the factor of safety in the model. Therefore it has been ensured that both the depth of the soil layer and the length of the

surface boundary outside the excavation pits (on both sides) are sufficient so that the slip surface is not affected by the outer boundaries.

In order to perform a *Fully coupled flow-deformation analysis* correctly the groundwater flow boundaries and hydraulic conditions need to be set. *Plaxis 2D* enables the user to determine which of the outer geometry boundaries that is open or closed in the model condition window. By default *Plaxis* sets the bottom boundary to closed and the three other boundaries to open, the definition of a closed boundary is that it does not allow groundwater flow across the boundary. Besides the default conditions the two vertical geometry boundaries are also set to closed in this work. In a *Fully coupled flow-deformation analysis* these boundaries are very important, since these control where the pore water may flow and therefore these properties influence the total pore pressures. These hydraulic boundary conditions always override the ones that are specified in the model conditions (PRM, 2015).

Plaxis also provides the possibility to enter hydraulic boundary conditions manually in several other ways; one is to define a groundwater head boundary condition to one of the other geometry boundaries. When this is done *Plaxis* will automatically generate external water pressures. During the deformation analysis *Plaxis* will work with the external water pressures as traction loads which are taken into consideration with the weight of the soil and the pore pressures (PRM, 2015). In this work a user defined groundwater head is applied to the outer bottom boundary of the model. *Plaxis* treats the time dependency of these hydraulic conditions in two different ways, either constant or time dependent. Here this will be treated as constants, which infers that a uniform value and the groundwater head may be specified as, h_{ref} . In the original case this will be assigned as $h_{ref} = -8$ m below the ground surface.

Plaxis also provides the possibility to model precipitation and evapotranspiration in the form of a precipitation boundary condition. The precipitation is automatically applied to all surfaces that symbolize the ground surface. There are three parameters that define the precipitation, the recharge, q [m/day] where a negative recharge symbolizes evapotranspiration, the maximum, ψ_{max} [m] and the minimum pore pressure head, ψ_{min} [m]. The two later parameters control the maximum infiltration and evapotranspiration. If the precipitation causes a resulting pore pressure head that reaches $y + \psi_{max}$, the discharge changes into the corresponding head to simulate run off. In analogy the minimum pore pressure head will, when the evapotranspiration reaches $y + \psi_{min}$ cause the evaporation to stay at a constant value of $y + \psi_{min}$. Here a tabulated value of the recharge value have been used, see Appendix A and values for minimum and maximum pore pressure head have been prescribed to $\psi_{min} = -0.15$ and $\psi_{max} = 1.0$.

Unlike horizontal surfaces, where q is applied as recharge to the boundary, the precipitation is applied perpendicular to inclined surface boundaries and the magnitude of the recharge is $q\cos\alpha$.

The boundary conditions between the retaining wall and the soil are modelled using interfaces, explained in Section 4.4. In situations where groundwater flow needs to be analysed the interface elements are especially important. When the elements are switched off, no flow occurs from one side to the other. The interface element then represents an impermeable boundary. This property is used during the modelling of the reinforced retaining wall in *Plaxis*. If the elements are switched on, there is a total coupling of the pore pressure degrees of freedom (PSM, 2015). The interfaces are also used model the strength reduction caused by the interaction between the soil and the retaining structure (PRM, 2015).

4.7 Drainage

In *Plaxis* there are several ways to model the drainage situation in the soil, drained or undrained behaviour. One of the most important parameters during an FE-analysis of soil is the pore pressure, since this significantly influences the time-dependent behaviour of the soil. The pore pressures are generated in correspondence to the drainage types. In this work *Plaxis 2D* is used to generate the pore pressures.

The Clay material is assumed to have a drained behaviour. This is based on a comparison of a drained and an undrained analysis in *Plaxis 2D*. The drained situation is suited for long-term situations and the undrained situation is suited for short-term situations without the time dependent development of pore pressures. In this drainage type excess pore pressures are a consequence of stress changes and the undrained analysis can be divided into three cases A, B and C (PRM, 2015). The drainage type *Undrained A* is chosen based on, that this model uses effective parameters to model the undrained behaviour and that it is assumed that the shear strength of the clays does not increase with the depth, which suits this model perfectly. The comparison for two identical excavation pits shows that the drained analysis provides a lower factor of safety and to avoid overestimating the factor of safety, the drained analysis is used in the rest of the FE-analysis.

The drained analysis is only available for the plastic calculations and the safety analysis. During the *Fully coupled flow-deformation analysis* the behaviour of the soil is determined by the saturated permeability and therefore the drainage type is disregarded in this calculation type. The saturated permeability is in this case a direct input parameter chosen in the flow parameters tab sheet (see Section 4.12) (PRM, 2015). *Plaxis 2D* provides a number of predefined hydraulic models, as *van Genuchten* or *Approximate van Genuchten*. Here the hydraulic model, *van Genuchten model* is used and the author used the international soil classification system *USDA* (predefined in *Plaxis 2D*) and the *van Genuchten* parameters for Clay.

Due to the fact that the *Fully coupled flow-deformation analysis* is used to model most of the phases in this master's dissertation, the selection of the drainage type will not have a significant impact on the results. But since there is a possibility that it will, the drainage type with the biggest influence was used.

4.8 Initial stress generation

The initial stresses in soil are affected by the water conditions, the weight of the soil and the history of the formation of the soil. *Plaxis* offers two different ways to generate the initial stresses, the K_0 -procedure and *Gravity loading*. In this master's dissertation the K_0 -procedure is used, which is a direct input procedure in *Plaxis 2D*. K_0 provides the initial ratio between horizontal effective stress and vertical effective stress, σ'_h/σ'_v but does not consider external loads. The K_0 -procedure is especially suited to generate the initial stresses for horizontal surfaces (PRM, 2015)

4.9 Safety calculations

Plaxis 2D uses a c/φ reduction to make a safety analysis which for the *Mohr-Coulomb material model* mean that the safety calculation reduces the strength parameters $\tan \varphi$ and c successively until failure occurs. This is done according to Equation 4.2 as

$$\sum M_{sf} = \frac{\tan \varphi_{input}}{\tan \varphi_{reduced}} = \frac{c_{input}}{c_{reduced}} \quad (4.2)$$

The strength reduction performed in *Plaxis* introduces out-of-balance forces in the model. The out-of-balance forces will in turn result in additional deformations (that does not have a physical meaning). However, the probable failure mechanism of the model is determined by the incremental displacements and/or the incremental shear strains during the last step of the calculations (PK, 2015).

The safety calculations are performed using the *load advancement number of steps procedure* in *Plaxis 2D*. In the first step the multiplier $\sum M_{sf}$ is set to 1.0 and M_{sf} specifies the increment of strength reduction during this step (PRM, 2015).

As the soil strength is gradually reduced until failure occurs, the factor of safety corresponds to the strength reduction factor. The failure is recognized by the small reduction in strength which leads to large change in displacements or strains (PK, 2015).

The safety calculation can be summarized as (PRM, 2015)

$$FS = \frac{\text{available strength}}{\text{strength at failure}} = \text{value of } \sum M_{sf} \text{ at failure} \quad (4.3)$$

It is important to note that the value of $\sum M_{sf}$ needs to have become steady in the end of the safety calculation, otherwise the factor of safety will not be a representable value, see Figure 4.5 (PK, 2015).

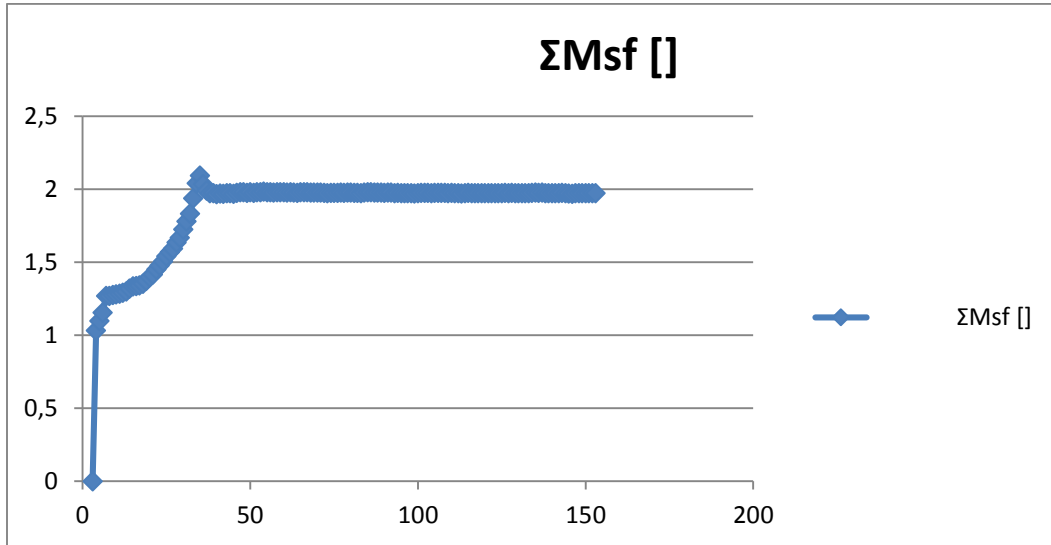


Figure 4.5 - A stable value of ΣM_{sf} is obtained and the resultant factor of safety is therefore representable.

4.10 Fully coupled flow-deformation

The significance of the *Fully coupled flow-deformation analysis* (FCFD) is that it is used to calculate deformations simultaneously with pore pressures caused by time dependent changes in the hydraulic conditions. During the FCFD analysis, the total pore pressures (the sum of steady state and excess pore pressures) are calculated (see Section 4.11). In order to correspond with the previously described calculations types, p_{steady} is calculated based on the the hydraulic conditions at the end of the calculation phases. This enables the excess pore pressures to be calculated from the total pore pressures. Because of this unsaturated soil behaviour and suction can be considered in a *Fully coupled flow-deformation analysis* (PRM, 2015)

4.11 Pore pressures

In general *Plaxis 2D* is used for effective stress analysis, where the sum of the effective stresses, σ' and the active pore pressure p_{active} results in the total stresses, σ , formulated as:

$$\sigma = \sigma' + p_{active} \quad (4.4)$$

The active pore pressure can in turn be divided into the product of the effective saturation, S_{eff} and the pore water pressure, p_{water} as

$$p_{active} = S_{eff}p_{water} = S_{eff}(p_{steady} + p_{excess}) \quad (4.5)$$

As seen above, the pore water pressure can be divided into steady state pore pressure, p_{steady} and excess pore pressure, p_{excess} . The steady state pore pressures represent the stable pore pressure state, which shall not change during a deformation analysis. There are several ways to generate these pore pressures, by selecting different pore pressure calculation types in the phases window. In the *Fully coupled flow-deformation analysis* the

pore water pressure and the displacements are calculated simultaneously and therefore the steady state pore water pressures are a result of a preliminary steady-state groundwater flow calculation. This calculation type uses the hydraulic boundary condition in the end of the calculation phase (PRM, 2015).

Stress changes in undrained materials, which result in deformations lead to the generation of excess pore pressures. However, excess pore pressure can occur in any material (excluding non-porous) during a FCFD analysis. Here the ruling parameter is the permeability (PRM, 2015).

In situations when the degree of saturation differs from unity (unsaturated soil) the pore water pressure is not equal to the active pore pressure. In these cases selection of a soil water retention curve, which relates the positive pore water stress (suction) to the degree of saturation, is needed. *Plaxis* carries a number of predefined data sets to model the flow of water in the unsaturated zone, see section 4.12 (PRM, 2015).

4.12 Predefined data sets

In *Plaxis* there are a number of predefined data sets to model the soil water retention curve, which is used to model the unsaturated flow of groundwater. This curve is generated with standardized soil classification systems, which in *Plaxis* are named as *USDA*, *Hypres*, *Standard* and *Staring*. In this master's dissertation *the van Genuchten hydraulic function* is used to model the SWRC. For the idealized geometries, clay from the *USDA* classification system is used. During the modelling of the "real life" case, the soil type Boulder Clay in the *Staring* classification system is used to model the Clay Till's hydraulic properties and the transition zone and bedrock is modeled with the *Standard* classification system and *Course* as soil type.

4.13 Suction

In *Plaxis 2D* there is an option to either ignore or allow suction during the FE-analysis. This option inflicts several properties on the pore pressures in the soil and regardless if ignore suction is used or not, this option is used in all phases during modelling in *Plaxis*. The initial stress generation, plastic calculation, *Fully coupled flow-deformation* and the safety calculation all supports this option.

4.13.1 Ignore suction

When this option is used the soil is considered fully saturated below and completely dry (ideally unsaturated) above the phreatic level. In the plastic calculation step the phreatic level is defined manually by the user but during the *Fully coupled flow-deformation analysis* it is generated as a calculation result from *Plaxis*. Ignore suction means that the positive steady state pore stresses will be set to zero (suction will be ignored) but excess pore pressure (positive and negative) both under and over the phreatic level, will be taken into account.

- In drained materials the effective saturation will be set to, $S_{eff} = 1$. This will reject any previous value.

- The steady-state pore pressure on or below the phreatic level is set as:

$$P_{steady} \leq 0, S = 1, S_{res} = 0, S_{sat} = 1 > S_{eff} = 1$$

Ignore suction will not affect stresses and related quantities that has previously been defined in the FE-analysis (except for the above mentioned). For the *Fully coupled flow-deformation analysis* the situation is different. As mentioned previously, the phreatic level is based on p_{water} instead of p_{steady} . During this type of analysis S_{eff} will not overrule the previous value.

4.13.2 Allow suction

This option allows suction to be included in the active pore pressure and pore water pressure. Now the soil saturation depends on the soil water retention curve, SWRC. In analogy with the ignore suction option, stresses and previous quantities still apply.

4.14 Material models

To be able to model geotechnical problems correctly a suitable material model must be used in *Plaxis*. There are a number of predefined material models that best suit various types of soil and the user is also given the possibility to create a user-defined model. The following section contains the material models used in this master's dissertation.

4.14.1 Mohr-Coulombs material model – linear elastic perfectly plastic

Since *the Mohr-Coulomb (MC) model* has a clear physical interpretation of the material parameters and is generally accepted, it is an advantage to use this during modelling.

The model is said to be linear elastic perfectly plastic, where perfectly plastic means that the model has a fixed yield surface. Which in practice mean that the model has a yield surface fully defined by model parameters and not affected by plastic straining (PMMM, 2015).

The parameters (and their units) used in *Plaxis 2D*, are shown below:

E	Young's modulus	[kN/m ²]
ν	Poisson's ratio	[-]
c	cohesion	[kN/m ²]
φ	Friction angle	[°]
ψ	Dilatancy angle	[°]
σ_t	Tension cut-off and tensile strength	[kN/m ²]

For the case where the axes are formulated in form of principal stresses, *Plaxis* uses six yield functions to define the yield condition, seen below. A hexagonal cone in the principal stress space, which can be seen in Figure 4.6, is generated when $f_{ii} = 0$ (PMMM, 2015).

$$f_{1a} = \frac{1}{2}(\sigma'_2 - \sigma'_3) + \frac{1}{2}(\sigma'_2 + \sigma'_3)\sin\varphi - c \cos\varphi \leq 0 \quad (4.6)$$

$$f_{1b} = \frac{1}{2}(\sigma'_3 - \sigma'_2) + \frac{1}{2}(\sigma'_3 + \sigma'_2)\sin\varphi - c \cos\varphi \leq 0 \quad (4.7)$$

$$f_{2a} = \frac{1}{2}(\sigma'_3 - \sigma'_1) + \frac{1}{2}(\sigma'_3 + \sigma'_1)\sin\varphi - c \cos\varphi \leq 0 \quad (4.8)$$

$$f_{2b} = \frac{1}{2}(\sigma'_1 - \sigma'_3) + \frac{1}{2}(\sigma'_1 + \sigma'_3)\sin\varphi - c \cos\varphi \leq 0 \quad (4.9)$$

$$f_{3a} = \frac{1}{2}(\sigma'_1 - \sigma'_2) + \frac{1}{2}(\sigma'_1 + \sigma'_2)\sin\varphi - c \cos\varphi \leq 0 \quad (4.10)$$

$$f_{3b} = \frac{1}{2}(\sigma'_2 - \sigma'_1) + \frac{1}{2}(\sigma'_2 + \sigma'_1)\sin\varphi - c \cos\varphi \leq 0 \quad (4.11)$$

There are also six plastic potential functions defined for the MC-model in *Plaxis*.

$$g_{1a} = \frac{1}{2}(\sigma'_2 - \sigma'_3) + \frac{1}{2}(\sigma'_2 + \sigma'_3)\sin\psi \quad (4.12)$$

$$g_{1b} = \frac{1}{2}(\sigma'_3 - \sigma'_2) + \frac{1}{2}(\sigma'_3 + \sigma'_2)\sin\psi \quad (4.13)$$

$$g_{2a} = \frac{1}{2}(\sigma'_3 - \sigma'_1) + \frac{1}{2}(\sigma'_3 + \sigma'_1)\sin\psi \quad (4.14)$$

$$g_{2b} = \frac{1}{2}(\sigma'_1 - \sigma'_3) + \frac{1}{2}(\sigma'_1 + \sigma'_3)\sin\psi \quad (4.15)$$

$$g_{3a} = \frac{1}{2}(\sigma'_1 - \sigma'_2) + \frac{1}{2}(\sigma'_1 + \sigma'_2)\sin\psi \quad (4.16)$$

$$g_{3b} = \frac{1}{2}(\sigma'_2 - \sigma'_1) + \frac{1}{2}(\sigma'_2 + \sigma'_1)\sin\psi \quad (4.17)$$

where the dilatancy angle, ψ is needed to model positive volumetric strain increments, something that is very important for dense soils (PMMM, 2015).

Depending on whether the failure criterion is linear or non-linear the failure surface varies. For the case with principal stresses, linear functions presents as planes and non-linear presents as curvilinear surfaces, the case for the linear failure criterion is showed below (Labuz & Zang, 2012).

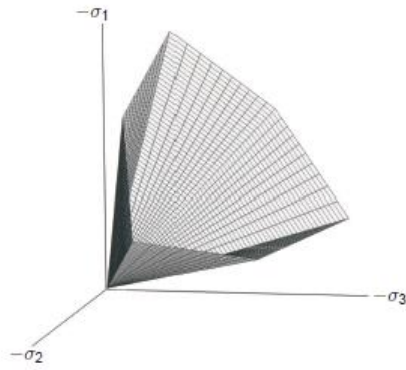


Figure 4.6 - Failure surface in principal stress space for cohesion less soil after (PMMM, 2015).

4.14.2 Groundwater flow – transient flow

The theory is presented here for the three-dimensional case regardless that two-dimensional modelling is performed in this master’s dissertation. There are two different ways to model the groundwater flow, *steady state-* and *transient groundwater flow* in *Plaxis*. In this master’s dissertation *transient groundwater flow* is used and the theory for it is presented below.

In *Plaxis* flow in a soil, a porous medium is described by Darcy’s law, seen below

$$q = \frac{k}{\rho_w g} (\nabla p_w + \rho_w g) \quad (5.13)$$

where

$$\nabla = \begin{bmatrix} \frac{\partial}{\partial x} \\ \frac{\partial}{\partial y} \\ \frac{\partial}{\partial z} \end{bmatrix} \quad (5.14)$$

q	Specific discharge
k	Coefficient of permeability
g	Gravitational acceleration vector
ρ_w	Density of water
∇p_w	Gradient of water pore pressure

The gravitational acceleration vector is used since the flow is unaffected by the gradient of water pore pressure in the vertical direction and is formulated as

$$g = \begin{bmatrix} 0 \\ -g \\ 0 \end{bmatrix} \quad (5.15)$$

The coefficient of permeability, k in unsaturated soil has two components, k_{sat} the permeability when the soil is saturated and k_{rel} the relative permeability. The relative permeability gives the relation of the permeability at a certain time to the permeability when the soil is fully saturated. The coefficient of permeability can be seen below (PSM, 2015):

$$k = k_{rel}k_{sat} \quad (5.16)$$

where

$$k_{sat} = \begin{bmatrix} k_x^{sat} & 0 & 0 \\ 0 & k_y^{sat} & 0 \\ 0 & 0 & k_z^{sat} \end{bmatrix} \quad (5.17)$$

The formulation of the relative permeability is described under Section 4.14.3

4.14.3 Hydraulic Models – van Genuchten

The theory for *the van Genuchten model* is described earlier and in this chapter only *the van Genuchten* theory used in *Plaxis* is treated. In *Plaxis* the VG equation relates the saturation to the soils pressure head, ϕ_p . The VG equation is formulated as (PMMM, 2015)

$$S(\phi_p) = S_{res} + (S_{sat} - S_{res})[1 + (g_a|\phi_p|)^{g_n}]^{g_c} \quad (5.18)$$

where

$$\phi_p = -\frac{p_w}{\gamma_w}$$

p_w	Suction pore stress
γ_w	Unit weight of the pore fluid
S_{res}	Describes residual saturation
S_{sat}	Describes the fully saturated state, the default value is 1.0.
g_a	Fitting parameter that describes the air entry value of the soil. [m ⁻¹]
g_n	Fitting parameter that describes the rate of water extraction from the soil after the air entry value has been passed.
g_c	Fitting parameter, that is used to convert the van Genuchten equation into a two parameter equation.

In analogy with the earlier stated theory regarding *the van Genuchten model*, *Plaxis* uses the equation $g_c = \frac{1-g_c}{g_n}$ to transform the VG model from a three parameter to a two parameter equation. The transformation means that *Plaxis* provides realistic results for suction in the lower and intermediate range. The saturation remains at the residual value for high suction values (PMMM, 2015).

As stated previously *Plaxis* uses the coefficient of permeability to model transient groundwater flow. This coefficient is connected to the saturation of a soil through the

effective saturation, S_{eff} . Under fully saturated conditions air is often still present (small values) in the saturated soil and under these conditions S_{sat} is reduced from one. In this case the effective saturation can be formulated as (PMMM, 2015):

$$S_{eff} = \frac{S - S_{res}}{S_{sat} - S_{res}} \quad (5.20)$$

Plaxis uses the following formulation for the relative permeability in the VG model:

$$k_{rel}(S) = \max \left[(S_{eff})^{g_l} \left(1 - \left[1 - S_{eff}^{\frac{g_n}{g_n-1}} \right]^{\frac{g_n-1}{g_n}} \right)^2, 10^{-4} \right] \quad (5.21)$$

where

g_l Fitting parameter that relates the relative permeability related to the suction pore pressure. Has to be measured for a specific material.

The degree of saturation with respect to suction pore pressure can be derived as (used to calculate the diffusivity)

$$\frac{\partial S(p_w)}{\partial p_w} = (S_{sat} - S_{res}) \left[\frac{1-g_n}{g_n} \right] \left[g_n \left(\frac{g_a}{\gamma_w} \right)^{g_n} p_w^{(g_n-1)} \right] \left[1 + \left(g_a \frac{p_w}{\gamma_w} \right)^{g_n} \right]^{\frac{1-2g_n}{g_n}} \quad (5.22)$$

5. Idealized cases

In order to evaluate the effect of suction two idealized cases have been studied. One sloped excavation pit and one excavation pit with a reinforced retaining structure (sheet-pile with shoring), the cases have identical soil material parameters to facilitate a smooth comparison. The main focus has been on evaluating what influence suction will have on the factor of safety in total stability calculations. Therefore these two cases have been modelled in *Plaxis 2D*, with the option *Ignore suction* both activated and deactivated, allowing for a comparison between the two.

Since there are several parameters, which affect suction, three parameters have been selected and studied during the FE-analysis. The choice is based on their significance for the suction phenomenon. Two idealized excavation pits, with the same phreatic level, soil parameters, retaining structure and shoring have been investigated. The groundwater level, the soil water retention curve, precipitation and evapotranspiration have then been varied. These variations are performed in stages separate from one another in order to avoid variation of multiple input parameters at the same time to enable identification of the influence from different parameters. The goal is to make a comparison for the factor of safety (FS) for the situations where suction is considered or not considered, to see which period of the year that yields the highest FS and which parameter that has the strongest influence on the FS. In this case, it is desirable to achieve a total stability failure mechanism during the safety calculations in *Plaxis*.

5.1 Idealized geometries

The geometry of both the idealized cases is symmetric; therefore the possibility to model half the geometry around the symmetry line in the middle of the excavation pit exists. However, in this case the model has been created for the entire geometry due to the fact that the calculations are not that time consuming and the results are more easily interpreted. *Plaxis* uses triangular elements and therefore this will result in a minor asymmetry in the mesh. However, this is considered to be of small magnitude and is therefore ignored. The generated mesh can be seen in Appendix B.

In this section the geometries, hydraulic conditions, mesh, material models and parameters for the soil, retaining structure and fixed-end-anchor are presented. The results from *Plaxis 2D* are presented after the assumptions and input parameters.

Sloped excavation pit

The height of the slope is 5 m and has a lateral length of 7.5 m which is equal to an inclination of 1:1.5. Both the idealized cases have a length of 20 meters at the bottom of the excavations. In analogy with Chapter 4, the length and depth of the surrounding soil has been increased sufficiently, in order to avoid that the global geometry boundaries affect the results of the FE-analysis. The shape and geometry of the sloped excavation pit can be seen in Figure 5.1.

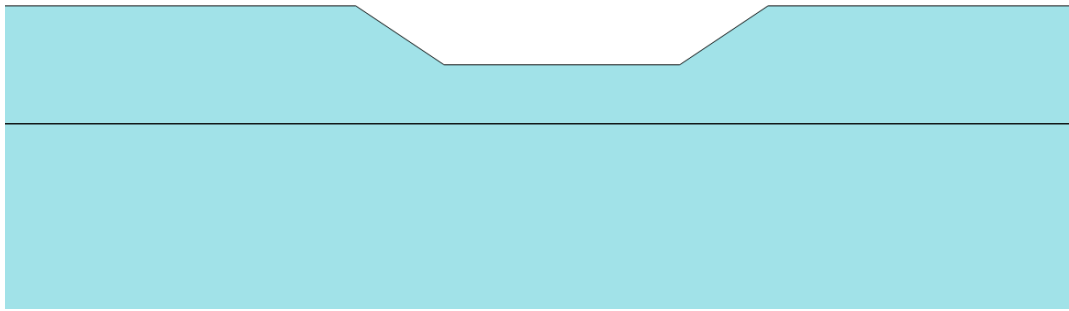


Figure 5.1 - The idealized geometry for the sloped excavation pit, in *Plaxis*.

Reinforced excavation pit

To enable a comparison between the idealized geometries, the length and height of the reinforced excavation pit is identical to the sloped excavation pit. The height of the retaining structure is 6.5 meters and the shoring is placed one meter below the ground surface.

The sheet-pile has been analytically calculated using characteristic values (without partial coefficients) to ensure that the chosen retaining structure can withstand the active earth pressures. The total stability has also been numerically calculated in *Plaxis 2D* (without precipitation), to ensure that the structure can support the generated loads and provide a reasonable factor of safety before the *Fully coupled flow-deformation analysis* is made. In similarity with the procedure used for the sloped excavation pit, the geometry for the excavation pit with the reinforced retaining structure is shown in Figure 5.2.

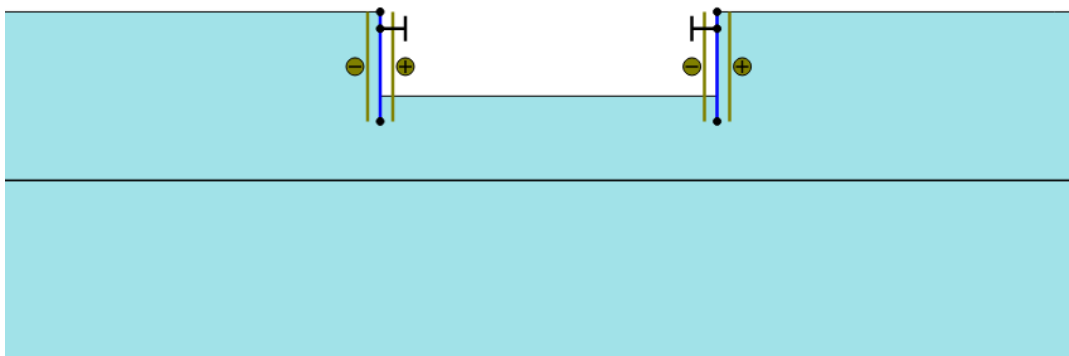


Figure 5.2 – The idealized geometry for the excavation pit with a reinforced retaining structure.

5.2 Hydraulic conditions

Matric suction only exists in unsaturated soils, therefore the water level is set to be three meters under the bottom of the excavation (8m under the ground surface), i.e. a hydraulic head boundary condition, h_{ref} is imposed to the bottom boundary of the global geometry, seen in Figure 5.3. The drainage type used in *Plaxis 2D* is *Drained*, however this is only valid for the initial stress generation and plastic calculation procedures. As mentioned

previously the drainage type is ignored during the *Fully coupled flow deformation analysis*, instead the pore pressures are generated during the coupled analysis.

In this situation the hydraulic function *van Genuchten* is used to model the flow in unsaturated soil. This is done according to Section 4.14.3, where the standardized soil system *USDA* is used and the soil is set as *Clay*.

Last but not least, the precipitation and evapotranspiration are set as a precipitation boundary condition to the boundaries representing the ground surface. The precipitation input values are presented in Section 5.5.

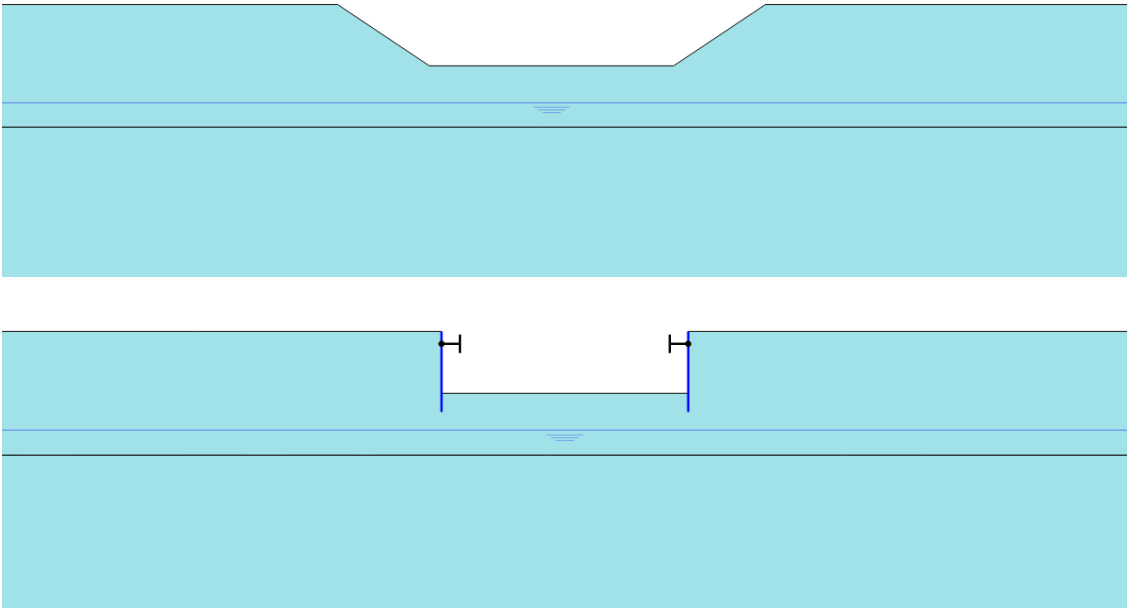


Figure 5.3 - Hydraulic conditions for the idealized geometries.

5.3 Parameters

During the FE-analyses the *Mohr-Coulomb material model* and the *van Genuchten function* was used to model the behaviour of the soil and the soil water retention curve. In Table 5.1, below the values of the material input parameters in *Plaxis 2D* is presented.

Table 5.1 - Soil and material parameters for the idealized excavation pits.

Input parameters			
Geometry			
Height of excavation	h_e	5	m
Height of retaining structure	h_r	6.5	m
Height of slope	h_s	5	m
Lateral length of slope	l	7.5	m
Clay			
Unit weight of saturated soil	γ_{sat}	17	kN/m ³
Unit weight of unsaturated soil	γ_{unsat}	17	kN/m ³
Friction angle	φ	30	°
Cohesion	c'	25	kPa
Young's Modulus	E	12000	kPa
Poisson's ratio	ν	0.3	-
Initializing K	K_0	0.5	-
Plate			
Thickness	t	0.006	m
Thickness (cross section)	h	0.22	m
Elasticity modulus	E	$210 \cdot 10^6$	kPa
Moment of inertia	I	$6600 \cdot 10^{-8}$	m ⁴ /m
Area (cross section)	A	0.0101	m ² /m
Unit weight of steel	γ_{steel}	78.5	kN/m ³
Anchor			
Modulus of elasticity	E	$210 \cdot 10^6$	kPa
Area	A	0.002124	m ² /m
Anchor spacing	$L_{spacing}$	4	m

5.4 Mesh

The global geometries are divided into two parts by a line created 10 meters under the ground surface in order to enable refinement of the upper part of the mesh where the excavation pits are located. This is seen in Figure 5.1 and 5.2 illustrated as a black line. Other areas of interest, as the surface boundaries where the precipitation is generated are also refined and the mesh is generated in correspondence with Chapter 4. The quality of the mesh and the generated elements can be seen in Appendix B.

5.5 Variables

Precipitation and evapotranspiration

With the aim of using accurate information regarding the precipitation, values have been collected from the Swedish Meteorological and Hydrological Institute, SMHI. In order to create a model, which is as accurate as possible, the amount of precipitation during a period of 24 hours has been used, incorporated into phases of one month in *Plaxis* and calculated for every month during a year. The meteorological station *Malmö A*, has been used to collect these values (SMHI, 2015) and to enable evaluation of to if suction, increases or decreases during certain parts of the year, values for three consecutive years, 2012, 2013 and 2014 are used.

In this situation, when suction is to be considered, it is more valuable to use the precise values of every day during one year than the mean values. This takes both the total precipitation and the extreme values of both evapotranspiration and precipitation into account. The usage of mean values will result in precipitation without larger variations and extreme values, which are needed to evaluate suction.

It has been more complicated to obtain accurate data, regarding the evapotranspiration. This is both a result of no existing measuring stations for evapotranspiration in Sweden at present time and that the equations for calculating the potential evapotranspiration are quite bad. Therefore these values have been collected from Bergström (1993), where Penman's equation has been used to calculate the potential evapotranspiration (mean value) during the period 1961-1978. In the FE-analysis the values for each month has been divided equally over every day of the month and subtracted from the amount of precipitation in *Plaxis* to simulate the evapotranspiration. These values can be seen in Table 5.2 (Bergström, 1993). The values for the precipitation and evapotranspiration can be seen in Appendix A.

Table 5.2 - Mean values [mm] for the potential evapotranspiration, calculated with Penman's equation (Bergström, 1993)

Station	J	F	M	A	M	J	J	A	S	O	N	D
Malmö	9	15	22	64	108	132	130	104	62	28	12	5

Groundwater level

To evaluate the effect of the groundwater level's impact on suction and the factor of safety, the precipitation for the month with the highest and lowest factor of safety is used (from the reinforced retaining structure) during this FE-analysis, which resulted in May and December 2012. This is based on the assumption that this will best represent the extreme values of the drying and wetting season. The groundwater level is then altered for the idealized geometries, the magnitude of the fluctuation is not meant to represent the natural groundwater fluctuation during a year but merely give an indication of how the FS will change if the groundwater level is moved. The values can be seen in Table 5.3. Due to the fact that suction only occurs in the unsaturated zone, the groundwater level is assumed to be below the bottom of the excavation pits at all times.

Table 5.3 - Variation in phreatic level, -8 m represent the original groundwater level.

Number	Groundwater level, below surface [m]
1	-6
2	-7
3	-8
4	-9
5	-10

Soil water retention curve

Clayey soils with different soil water retention curves have been analysed in likeness with the case where the groundwater level was varied (still May and December 2012). During which the permeability in both the *x*- and the *y*-direction have been kept equal to one another. Variation of the SWRC involves variation of several parameters as the permeability, air-entry value, residual and saturated water content and so on. Therefore this evaluation is done to show the significance of the SWRC for suction and the factor of safety and not in order to show in which magnitude this varies. The predefined *van Genuchten functions* for a series of clayey soils have been used in *Plaxis 2D* for the soil classification system *USDA*, listed in Table 5.4. In Appendix D the height of the potential head, linked to the residual saturation or the relative hydraulic conductivity can be seen for these soils.

Table 5.4 – Permeability in both *x*- and *y*-direction for different types of soil.

Type of Soil	Permeability
Silty Clay	0.0048
Clay	0.0475
Silty Clay Loam	0.1676
Sandy Clay	0.2877
Sandy Clay Loam	0.3145
Clay Loam	0.6238

5.6 Results

The results for the idealized excavations pit are presented in this section. In analogy with Section 5.5 the results are divided into three parts, after which of the parameters that was varied.

5.6.1 Precipitation

The resulting factor of safety for the case when precipitation and evapotranspiration where varied are presented in Table 5.5 and 5.6. The left column represents the factor of safety when suction is considered and the right column represents the factor of safety when suction is ignored (IS).

Table 5.5 - Factor of safety for the sloped excavation pit during 2012, 2013 and 2014 (IS – ignore suction).

Month	Factor of Safety					
	Sloped excavation pit					
	2012	2012-IS	2013	2013-IS	2014	2014-IS
January	1.76	1.30	1.39	1.28	2.04	1.28
February	2.25	1.28	2.99	1.27	1.70	1.28
March	3.05	1.28	3.04	1.28	1.84	1.29
April	2.17	1.27	3.14	1.28	1.66	1.26
May	3.14	1.28	3.14	1.28	1.45	1.27
June	3.10	1.29	1.76	1.28	2.99	1.30
July	1.77	1.24	3.12	1.24	1.81	1.25
August	3.14	1.28	3.13	1.28	1.04	1.10
September	2.02	1.28	1.42	1.28	2.89	1.28
October	1.94	1.29	1.41	1.30	1.62	1.30
November	1.89	1.28	1.80	1.32	3.01	1.27
December	1.38	1.33	1.38	1.28	1.55	1.27

Table 5.6 - Factor of safety for the excavation pit with a retaining structure during 2012, 2013 and 2014 (IS – ignore suction).

Month	Factor of Safety					
	Reinforced retaining structure					
	2012	2012-IS	2013	2013-IS	2014	2014-IS
January	2.07	1.48	2.00	1.49	2.13	1.48
February	2.37	1.47	2.41	1.48	2.15	1.50
March	2.49	1.48	2.48	1.48	2.59	1.48
April	2.20	1.48	2.57	1.48	2.57	1.48
May	2.59	1.48	2.19	1.48	2.14	1.49
June	2.58	1.48	1.98	1.48	2.10	1.48
July	2.33	1.48	2.56	1.48	2.12	1.48
August	2.57	1.47	2.58	1.49	1.65	1.37
September	2.20	1.48	2.08	1.48	2.58	1.48
October	2.14	1.48	2.06	1.48	2.04	1.48
November	2.10	1.48	2.07	1.47	2.40	1.49
December	1.97	1.48	1.98	1.48	1.90	1.48

Each year is visualized in the following diagrams. This shows, with the exception of August 2014, that the FS is higher for every month when suction is considered compared to when it is ignored. It can also clearly be seen that the fluctuation and amplitude of the sloped excavation pit is larger when related to the excavation pit with sheet-pile and shoring (if suction is considered). With the exception of spring 2014 these curves also follows one another, if the FS increases for the excavation pit with the retaining structure increases the FS for the sloped excavation pit will also increase. As seen in Figure 5.4, 5.5 and 5.6, the difference in FS between the two idealized geometries is of less magnitude when suction is ignored.

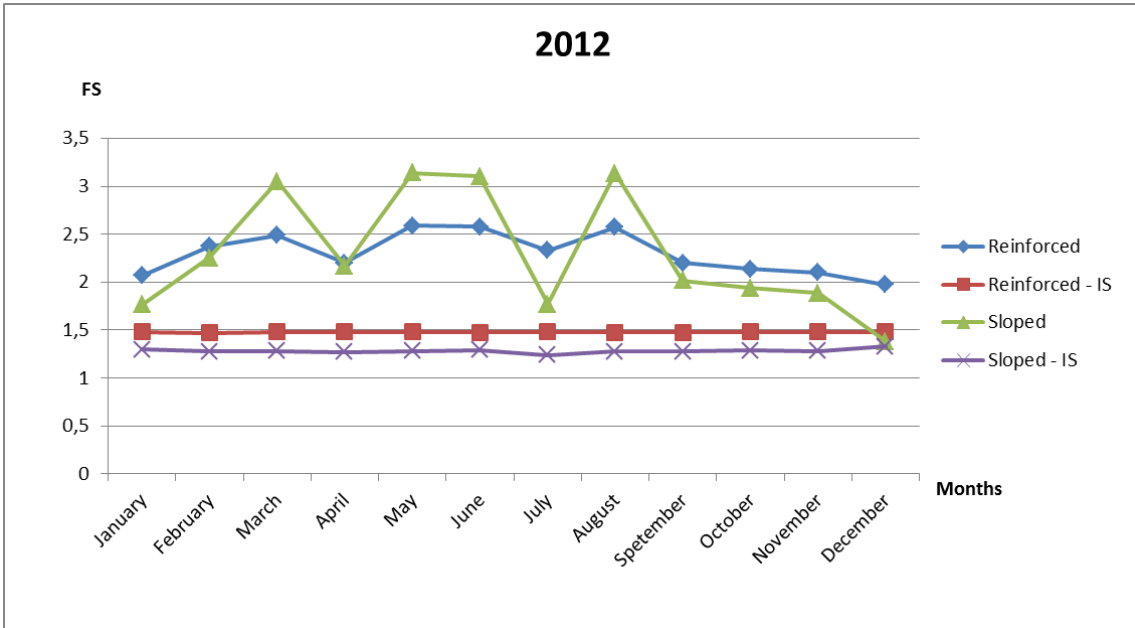


Figure 5.4 - The factor of safety plotted against time in months during 2012 (IS – ignore suction).

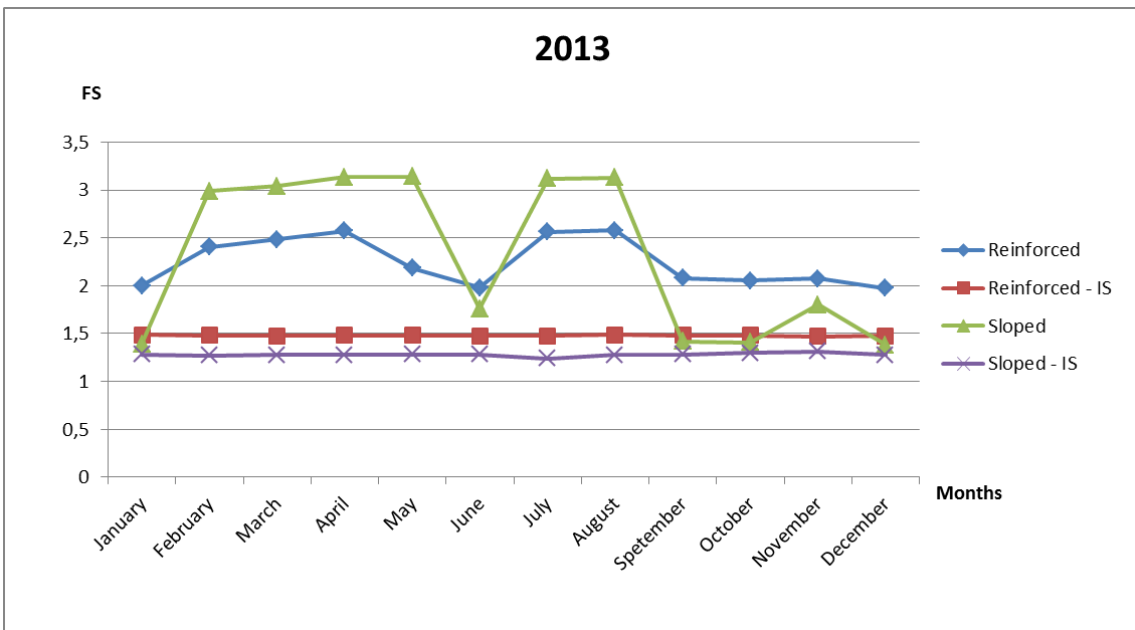


Figure 5.5 - The factor of safety plotted against time in months during 2013 (IS – ignore suction).

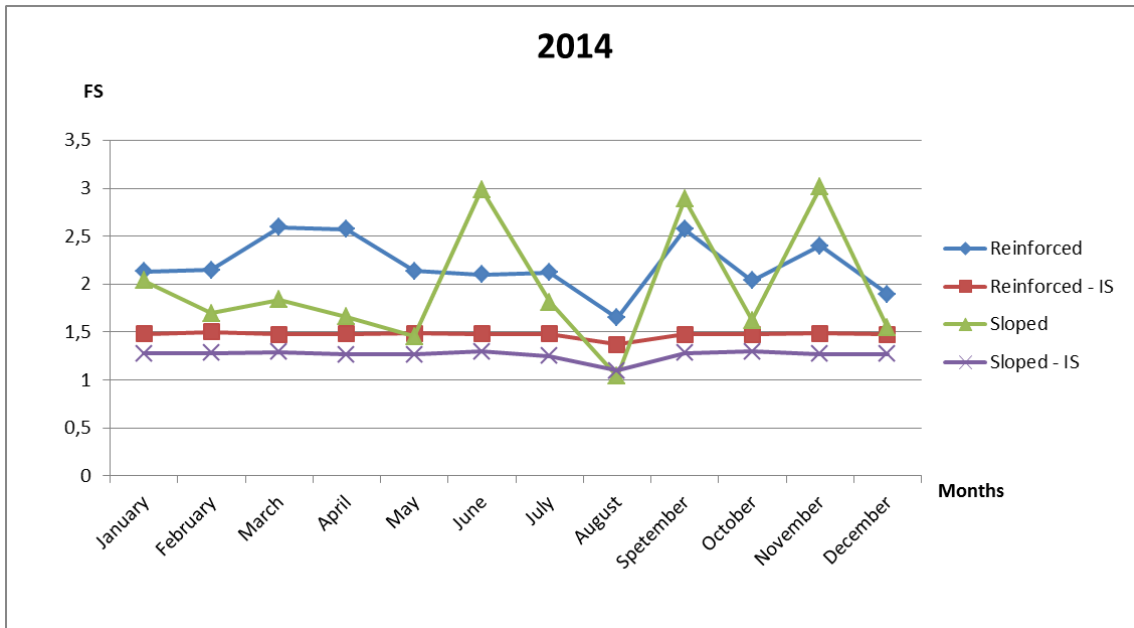


Figure 5.6 - The factor of safety plotted against time in months during 2014 (IS – ignore suction).

A comparison between the factor of safety (%) when suction is ignored and considered can be seen in Table 5.7 and 5.8. The mean- and minimum values for these years are shown to the right. In every case the factor of safety is higher, in percentage, if suction is considered (except August 2014).

Table 5.7 - Increase of FS [%] for the sloped excavation pit.

	ΔFS [%] - Sloped Excavation Pit				
	2012	2013	2014	Mean Value	Min. Value
January	36.0	8.7	59.7	34.8	8.7
February	76.1	135.4	32.2	81.2	32.2
March	138.0	138.4	42.6	106.3	42.6
April	71.0	145.3	31.2	82.5	31.2
May	145.1	145.2	14.8	101.7	14.8
June	140.6	37.1	130.4	102.7	37.1
July	42.8	151.9	45.4	80.0	42.8
August	145.2	144.8	-5.5	94.8	-5.5
September	57.8	10.8	125.8	64.8	10.8
October	50.6	8.5	24.8	28.0	8.5
November	47.4	36.9	136.8	73.7	36.9
December	3.8	8.2	21.5	11.2	3.8

Table 5.8 - Increase of FS [%] for the supported excavation pit.

	ΔFS [%] - Retaining Structure				
	2012	2013	2014	Mean Value	Min. Value
January	39.8	34.7	44.0	39.5	34.7
February	61.1	62.2	42.7	55.3	42.7
March	67.8	68.3	75.7	70.6	67.8
April	48.7	73.6	73.9	65.4	48.7
May	74.7	47.4	43.6	55.2	43.6
June	74.7	33.8	41.7	50.1	33.8
July	57.5	73.5	43.3	58.1	43.3
August	74.6	73.5	20.0	56.0	20.0
September	49.3	40.6	74.3	54.7	40.6
October	44.2	38.9	38.1	40.4	38.1
November	42.0	41.0	61.5	48.2	41.0
December	33.0	33.7	28.3	31.6	28.3

This can also be seen in Figure 5.7 and 5.8, it shows that the mean value of the sloped excavation pit is generally higher but that the minimum value of the idealized case is generally lower.

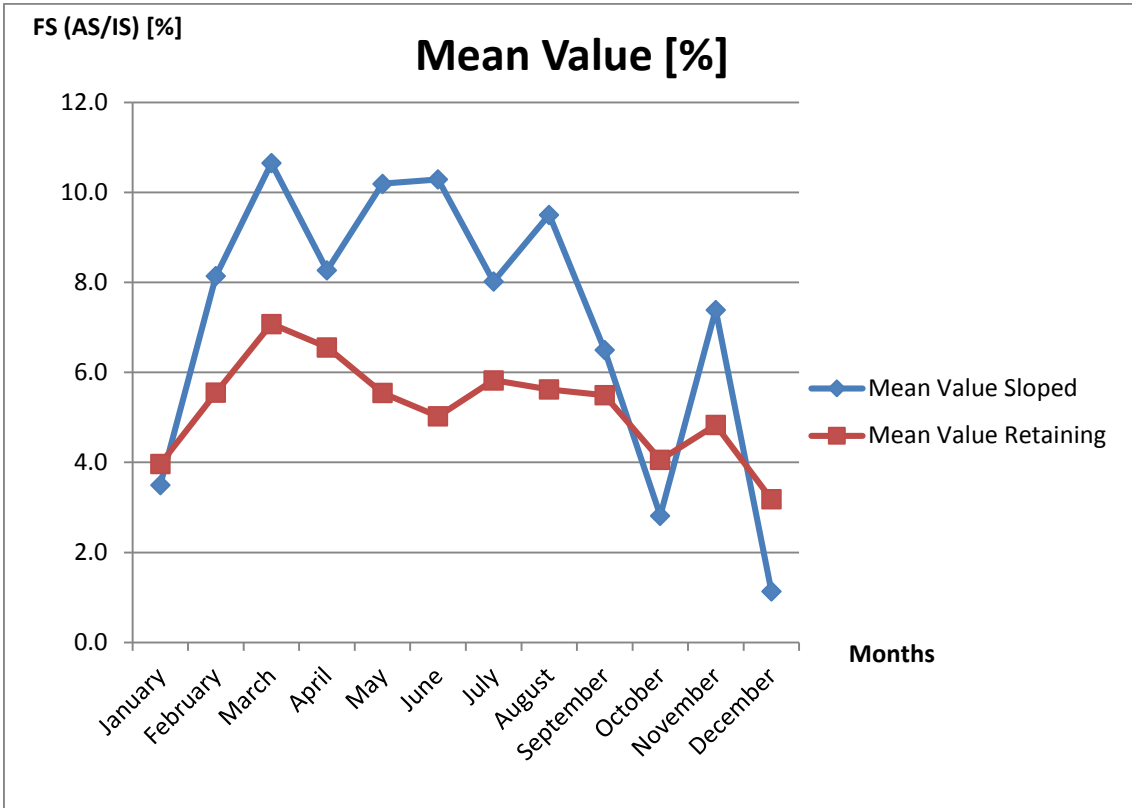


Figure 5.7 - The increase in FS expressed in mean value.

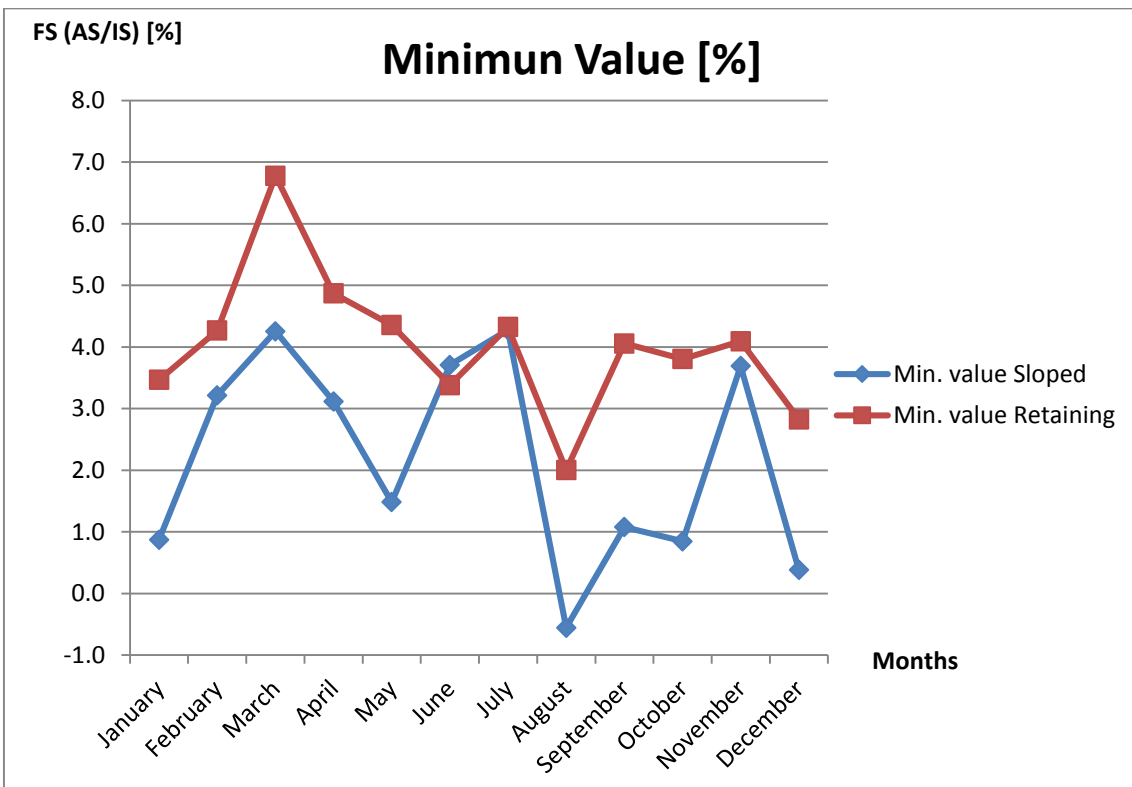


Figure 5.8 - The increase in FS expressed in the minimum value over a period of three years.

5.6.2 Groundwater

The results for the case when the groundwater level was varied are hereby presented. Table 5.9 and 5.10, show that the FS increases when the groundwater level is moved away from the ground surface and decreases when the phreatic level is moved towards the ground surface. This is valid for the cases when suction is considered, with the exception for the month of December for the sloped excavation pit.

Table 5.9 - Calculated factor of safety, for the sloped excavation pit, for the situation where the phreatic level was varied.

Factor of Safety - Sloped Excavation Pit				
Type of soil	Maj 2012 - AS	Maj 2012 - IS	Dec 2012 - AS	Dec 2012 - IS
Silty Clay	3.17	1.29	1.13	1.24
Clay	3.14	1.28	1.38	1.33
Silty Clay Loam	2.90	1.29	2.60	1.27
Sandy Clay	2.68	1.28	2.04	1.26
Sandy Clay Loam	1.92	1.28	1.81	1.28
Clay Loam	2.59	1.28	2.48	1.28

Table 5.10 - Calculated factor of safety, for the supported excavation pit, for the situation where the phreatic level was varied. This table is for the supported excavation pit.

Factor of Safety - Retaining Structure				
Type of soil	Maj 2012 - AS	Maj 2012 - IS	Dec 2012 - AS	Dec 2012 - IS
Silty Clay	2.62	1.48	1.92	1.47
Clay	2.59	1.48	1.97	1.48
Silty Clay Loam	2.37	1.48	2.17	1.49
Sandy Clay	2.21	1.48	2.00	1.49
Sandy Clay Loam	1.78	1.48	1.73	1.48
Clay Loam	2.16	1.48	2.05	1.48

Table 5.9 and 5.10 are visualized in Figure 5.9 and 5.10.

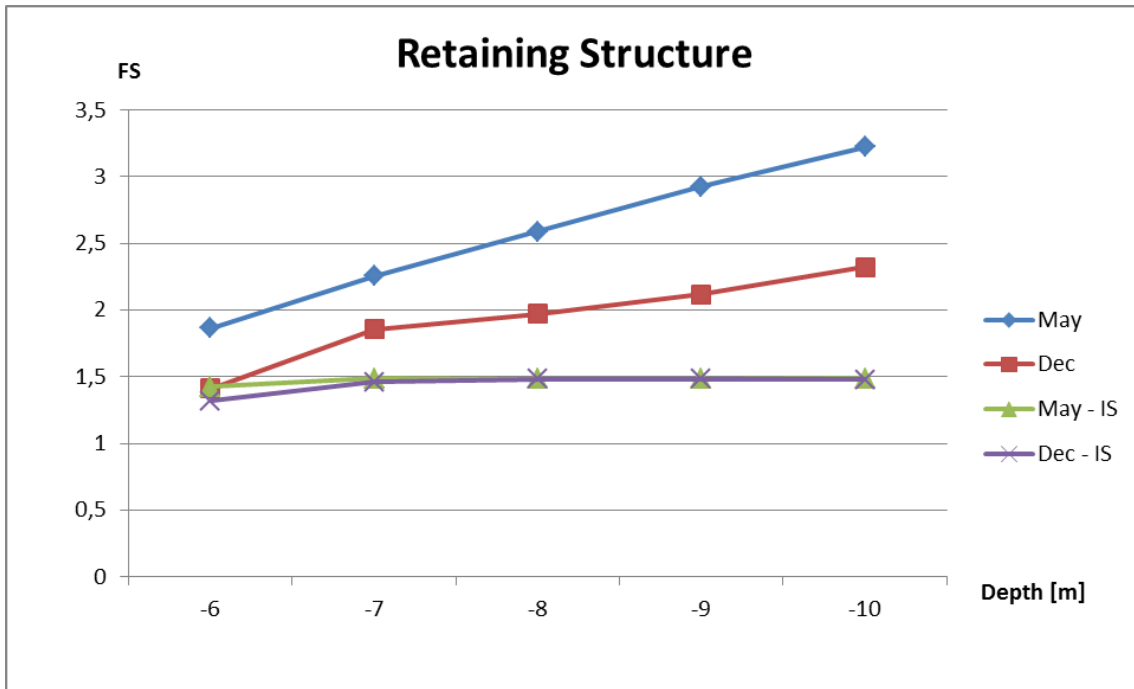


Figure 5.9 - FS plotted against groundwater level (in m below surface).

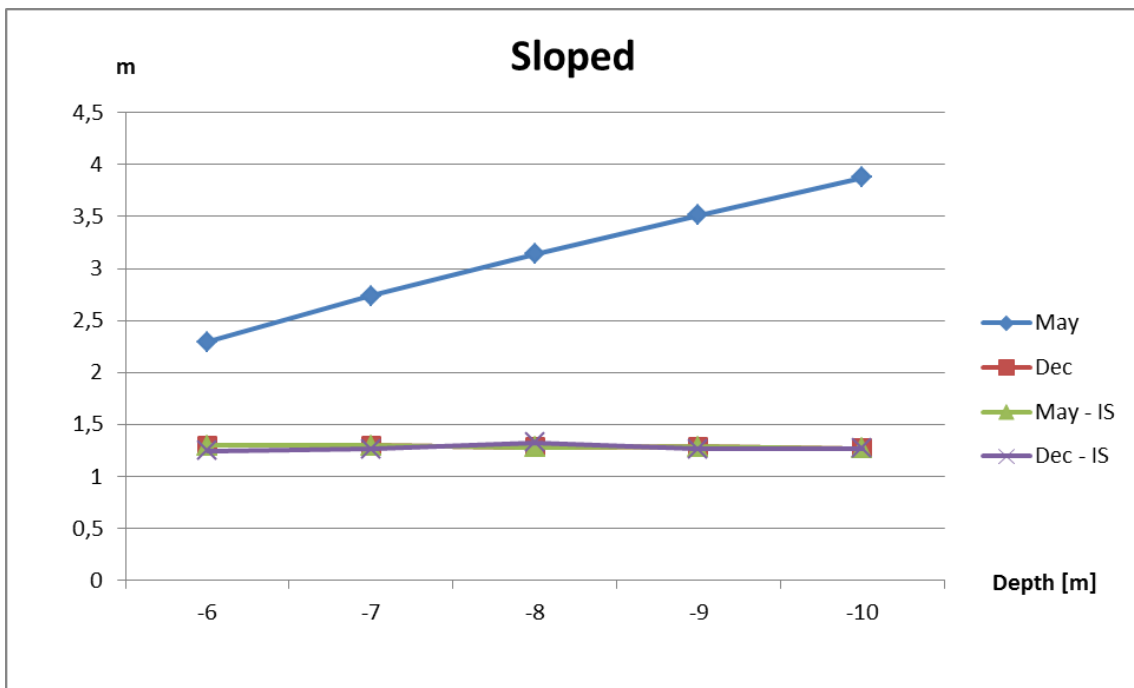


Figure 5.10 - FS plotted against groundwater level (in m below surface).

5.6.3 Soil water retention curve

The results of the FS for different soil water characteristic curves are presented in Table 5.11 and 5.12.

Table 5.11 - Factor of safety for the sloped geometry. The SWRC was varied.

Factor of Safety - Sloped Excavation Pit				
Type of soil	Maj 2012 - AS	Maj 2012 - IS	Dec 2012 - AS	Dec 2012 - IS
Silty Clay	3.174	1.285	1.131	1.238
Clay	3.14	1.281	1.376	1.33
Silty Clay Loam	2.896	1.285	2.596	1.266
Sandy Clay	2.681	1.284	2.043	1.261
Sandy Clay Loam	1.922	1.281	1.812	1.275
Clay Loam	2.593	1.279	2.481	1.28

Table 5.12 – Factor of safety for the sloped geometry. The SWRC was varied.

Factor of Safety - Retaining Structure				
Type of soil	Maj 2012 - AS	Maj 2012 - IS	Dec 2012 - AS	Dec 2012 - IS
Silty Clay	2.621	1.48	1.916	1.474
Clay	2.589	1.482	1.973	1.484
Silty Clay Loam	2.368	1.479	2.174	1.486
Sandy Clay	2.212	1.479	2.001	1.486
Sandy Clay Loam	1.779	1.48	1.729	1.481
Clay Loam	2.159	1.48	2.045	1.479

This is visualized in Figure 5.11 and 5.12, where it can be seen that the variation of these parameters does not provide equally clear cut results as the others. However, it is noticeable that the obtained value of the factor of safety is generally lower when suction is ignored.

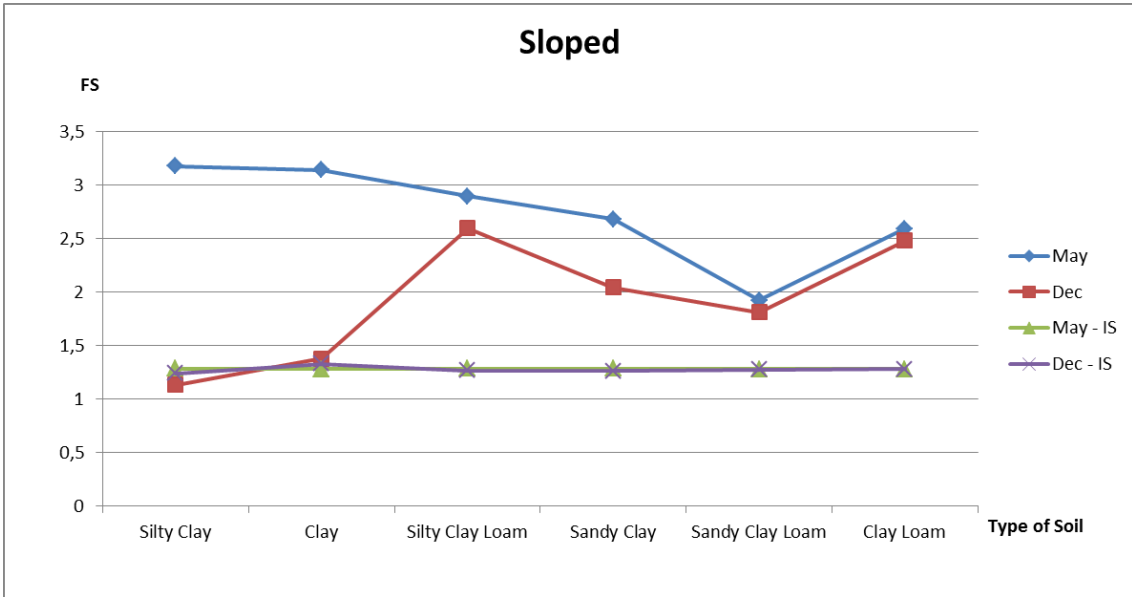


Figure 5.11 - FS plotted against soil type and used soil water retention curve. Sloped Excavation pit.

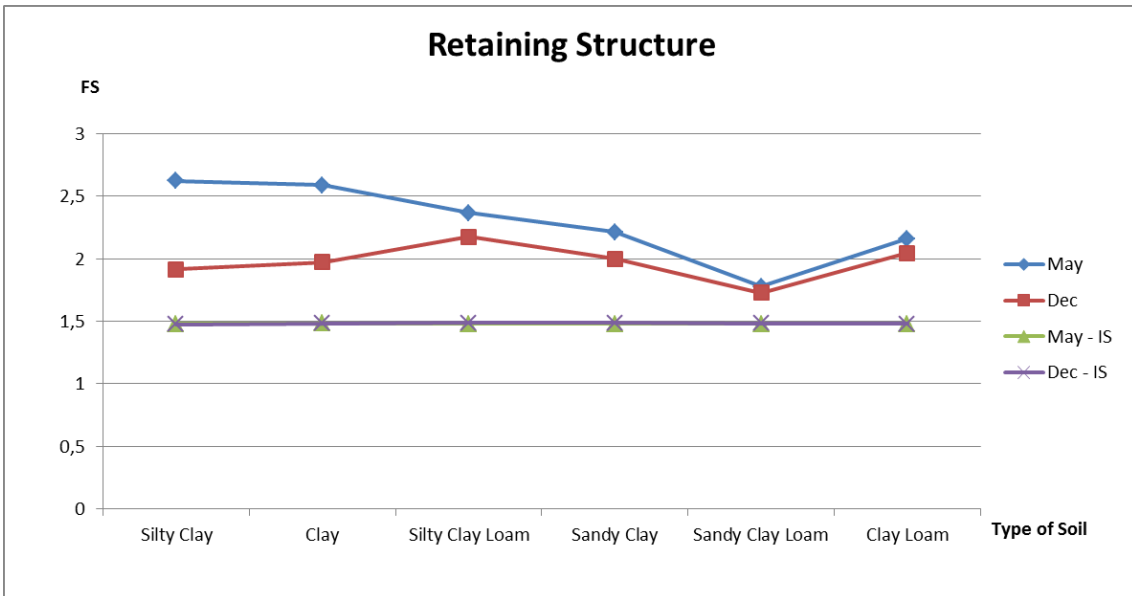


Figure 5.12 - FS plotted against soil type and used soil water retention curve. Sloped Excavation pit.

5.6.4 Failure mechanism

The idealized geometries exhibit a total stability failure mechanism in all the modelled cases which can be seen in Appendix C for both the sloped excavation pit and the excavation pit with a reinforced retaining structure.

6. Case study - ESS

The European Spallation Source (ESS) is a massive research facility that is being built in the outskirts of Lund. In this chapter the geometry, parameters and hydraulic conditions for the ESS-site is presented. This excavation pit is created with a reinforced retaining structure, i.e. sheet-pile with a shoring. Since this is a “real life” case the soil profile differs from the idealized cases and is described under Section 6.1. In analogy with the idealized geometries this has been modelled in *Plaxis 2D*, with the option *Ignore suction* both activated and deactivated, allowing for a comparison between the two.

6.1 Idealized geometry

This geometry has been created in similarity with the previous described, idealized geometries. It is meant to resemble the excavation for the Target building at the ESS-site. An important notice should be made, that the parameters and measurements used, differs from the actual building site. This is due to that the parameters have been evaluated from idealized data that is not connected to a specific point at the ESS-site. Furthermore, certain simplifications have been made during this master’s dissertation to enable the FE-analysis. Among other things, the dolerite dykes, which are present at the site, are not taken into consideration in this work. The different soil types used and the parameters for each layer are presented in Table 6.1.

Unlike the idealized geometry, this model is created around the symmetry line in the middle of the excavation, in order to simplify the FE-analysis. The geometry, retaining structure and the soil layers can be seen in Figure 6.1.

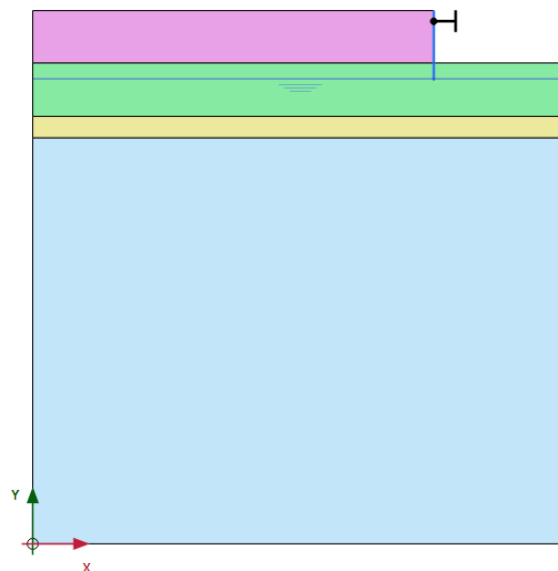


Figure 6.1 - Global geometry and soil layers for the target excavation pit at the ESS-site.

Table 6.1 - Type of soil and drainage type for the sloped excavation pit.

Level [m]	Type of soil	Drainage type
49.9-45	Upper Clay Till	Undrained A
45-40	Lower Clay Till	Undrained A
40-38	Transistion Zone	Drained
38-0	Bedrock - Clay shale	Drained
43	Groundwater Level	-

6.2 Hydraulic conditions

The hydraulic conditions for this situation have been created in correspondence with the conditions made for the idealized geometries. The difference is that the precipitation and evaporation has only been used for the year 2012 and that the groundwater head is located 7 meters below the ground surface.

The *van Genuchten function* for the soil classification system, *Staring* and *Standard* has been used. Here the *Staring* classification system and the Boulder Clay type of soil have been used to simulate the SWRC for the upper and lower clay till. For the transition zone and the bedrock, the *Standard* soil classification system and coarse soil has been used to model the SWRC. Selection of SWRC for the bedrock and transition zone is of less importance since these are located below the phreatic level.

6.3 Parameters

The *Mohr-Coulomb material model* is used during the FE-analysis, with the predefined *van Genuchten functions* for the *Staring* and *Standard* soil classification system. The dolerite dykes present at the ESS-site are not taken into consideration in this work. The Hoek-Brown material model parameters have been recalculated using the software; known as *RocLab* in order to be converted to *Mohr-Coulomb* parameters. The soil parameters used are presented in Table 6.2, 6.3, 6.4 and 6.5 while the parameters for the retaining structure and anchor are presented in Table 6.6.

The Clay Till has been divided into two parts, Upper- and Lower Clay Till. This is two idealized zones and the partition is due to that the soil has deviant properties from each other.

Table 6.2 – Soil parameters for the upper clay till.

Soil parameters			
Upper Clay Till	Variable	Value	Unit
Unit weight of saturated soil	γ_{sat}	19.6	kN/m ³
Unit weight of unsaturated soil	γ_{unsat}	19.6	kN/m ³
Friction angle	ϕ	32.5	°
Cohesion	c	200	kPa
Effective cohesion	c'	20	kPa
Young's Modulus	E	380000	kPa
Poisson's ratio	ν	0.4	-
Initializing K	K_0	0.4627	-
Void ratio	e_{void}	0.4	-

Table 6.3 – Soil parameters for the lower clay till.

Soil parameters			
Lower Clay Till	Variable	Value	Unit
Unit weight of saturated soil	γ_{sat}	20.6	kN/m ³
Unit weight of unsaturated soil	γ_{unsat}	20.6	kN/m ³
Friction angle	ϕ	32.5	°
Cohesion	c	300	kPa
Effective cohesion	c'	25	kPa
Young's Modulus	E	360000	kPa
Poisson's ratio	ν	0.4	-
Initializing K	K_0	0,4627	-
Void ratio	e_{void}	0.4	-

Table 6.4 – Soil parameters for the transition zone.

Soil parameters			
Transition Zone	Variable	Value	Unit
Unit weight of saturated soil	γ_{sat}	20.6	kN/m ³
Unit weight of unsaturated soil	γ_{unsat}	20.6	kN/m ³
Friction angle	ϕ	37	°
Effective cohesion	c'	2	kPa
Young's Modulus	E	480000	kPa
Poisson's ratio	ν	0.4	kPa
Initializing K	K_0	0.3982	-
Void ratio	e_{void}	0.4	-

Table 6.5 – Soil parameters for the bedrock.

Soil parameters			
Bedrock – Clay Shale	Variable	Value	Unit
Unit weight of saturated rock	γ_{sat}	26.2	kN/m ³
Unit weight of unsaturated rock	γ_{unsat}	26.2	kN/m ³
Friction angle	ϕ	30.52	°
Cohesion	c	1.992	kPa
Young's Modulus	E	4608000	kPa
Poisson's ratio	ν	0.22	kPa
Initializing K	K_0	0.4922	-
Void ratio	e_{void}	0.06	-
Compression strength	σ_c	40000	-
Geological Investigation Strength	GIS	50	-

Table 6.6 – Parameters for the plate and anchor.

Parameters			
Plate	Variable	Value	Unit
Thickness	t	0.006	m
Thickness (cross section)	h	0.22	m
Elasticity Modulus	E_{steel}	210*10 ⁶	kPa
Area (cross section)	A	0.0101	m ² /m
Moment of inertia	I	6.6*10 ⁻⁵	m ² /m
Unit weight steel	γ	78.5	kN/m ³
Anchor			
Elasticity Modulus	E_{steel}	210*10 ⁶	kPa
Area (cross section)	A	0.002124	m ²
Anchor Spacing	$L_{spacing}$	4	m

6.4 Mesh

The mesh for the global geometry is generated in correspondence with Chapter 4 and the length and depth of the global geometry have been sufficiently increased in order to avoid the geometry to affect the results. The quality of the mesh and the generated elements can be seen in Appendix B.

6.5 Results

The results for “real life” case are presented in this chapter. The factor of safety for when suction is considered or not considered is presented in Table 6.7.

Table 6.7 – The factor of safety for the excavation at the ESS –site (IS – Ignore suction)

Month	Factor of Safety	
	2012	2012-IS
January	2.67	2.51
February	2.65	2.49
March	2.73	2.50
April	2.72	2.54
May	2.71	2.49
June	2.75	2.56
July	2.71	2.48
August	2.71	2.50
September	2.70	2.51
October	2.67	2.47
November	2.69	2.46
December	2.79	2.54

In Figure 6.2 the results are visualized and it can be seen that the factor of safety has a higher value if suction is taken into account in the modelling. This also shows that the two curves follow the same pattern.

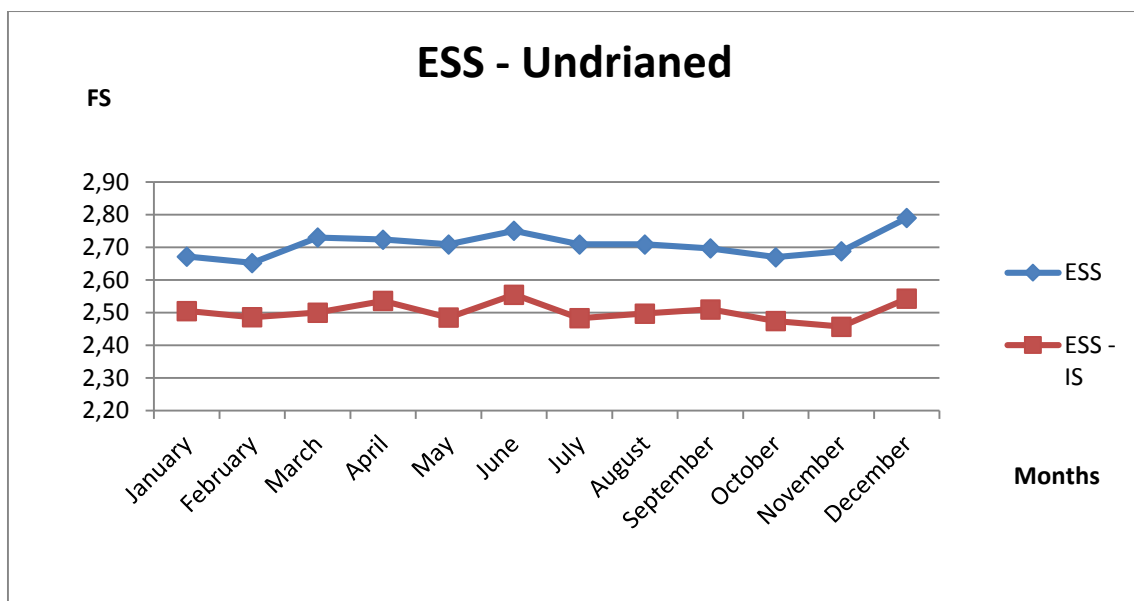


Figure 6.2 – The factor of safety for the ESS-site (IS – Ignore suction).

The difference in factor of safety between the case when suction is included and when it is not included can be seen in Table 6.8 and is visualized in Figure 6.3.

Table 6.8 – Increase of FS [%] for the excavation pit at the ESS-site.

	ESS - Δ FS [%]
Month	2012
January	6.67
February	6.68
March	9.20
April	7.41
May	9.01
June	7.67
July	9.10
August	8.49
September	7.45
October	7.92
November	9.40
December	9.71

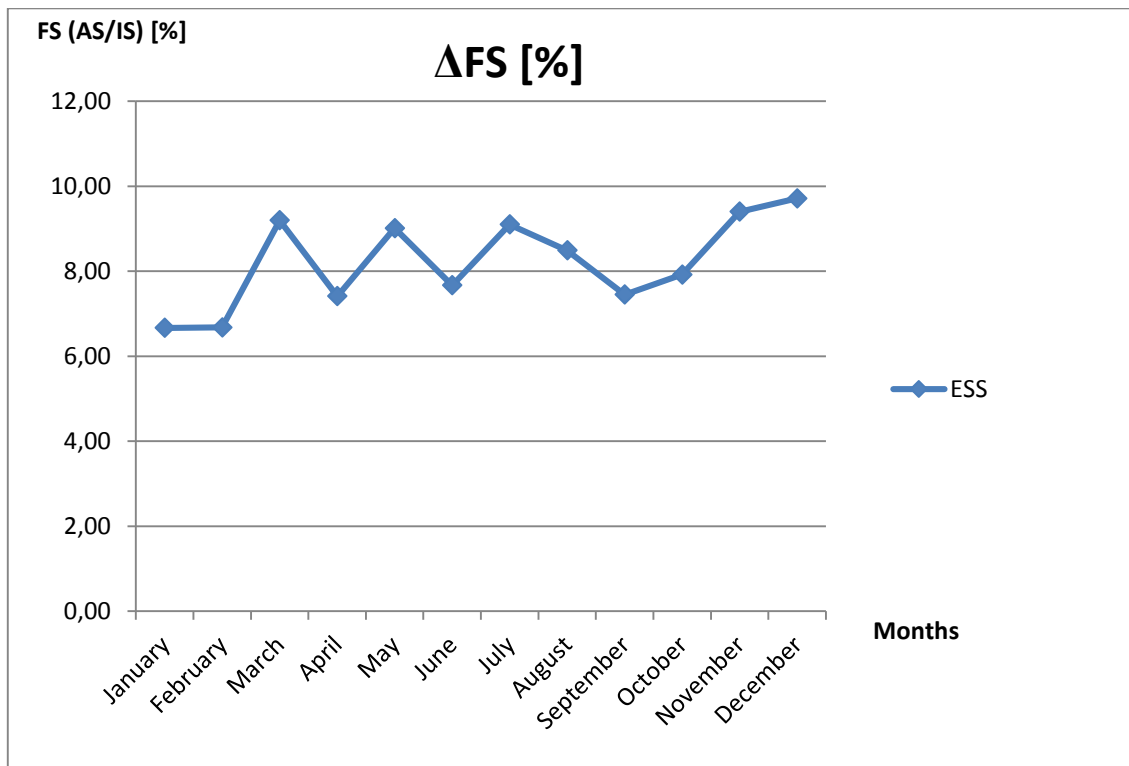


Figure 6.3 – The increase in factor of safety [%].

7. Discussion and conclusions

In this chapter the conclusions drawn from the results are presented and related to the objective stated in Section 1.2. This is followed by suggestions to further work.

7.1 Discussion and conclusions

Throughout this master's dissertation it has been seen that suction, when included in the calculations, in many cases may increase the factor of safety and the total stability. This has a huge potential for geotechnical engineers, since retaining structures may be constructed more slender, both sloped and sheet-piled excavation pits that can not reach a satisfactory FS can possibly achieve an adequate FS if suction is included into the numerical calculations.

As mentioned previously in this master's dissertation, suction is dependent on a lot of input parameters, as the specific SWRC for the soil, water content, precipitation etc. These parameters are needed in order to create a suitable model of the reality. Fitting parameters for the *van Genuchten function*, takes a lot of time, is difficult to evaluate and is expensive to analyse in laboratories. One way to get around this is to develop the FE-analysis further, using predefined SWRC's from the grain size distribution of the soil. This would open the possibility for FE-analyses of suction without actual knowledge of the real *van Genuchten* parameters. Since this is a major simplification of the reality, this should of course be done with great caution since a heavy rainfall can severely decrease the magnitude of suction and may result in a complete loss of suction and potential failure of the structure.

In general, the sloped geometry shows a higher fluctuation and amplitude than the curve for the excavation pit with the reinforced retaining structure. This is most likely due to the lack of retaining structure and due to the fact that the sloped excavation pit has two additional sloped boundaries. The additional boundaries are exposed to precipitation and evapotranspiration, which enables the soil to dry out or become wet faster than the case with the retaining structure. This result was quite expected due to the design of the excavation pits.

For all of the calculated years, the function for these two idealized geometries shows the same kind of pattern, if one of them increases the other increases too. The months of February, March and April of 2014 are exceptions from this. During these months the FS for the sloped excavation does not increase as much as expected, the geometry has been rebuilt and the months have been recalculated in *Plaxis* a number of times without any changes in the result. Why these months differ from the rest, is therefore hard to explain.

It can clearly be seen that the factor of safety varies over the months. It is hard to state an exact period of time when it is best to excavate. If attention is directed towards the diagrams in the result section, it can be clearly seen that the factor of safety is highest during the spring and summer. It is important to note that the FS for a specific month may still fluctuate between the years. As expected the months with the lowest amount of precipitation and highest evapotranspiration produces an increase in total stability. To be able to state which period of the year that is best for performing excavations, further tests

must be done. The connection may be easier to see if the FE-analysis is performed over a period of perhaps 15 - 20 years.

For August of 2014, there is a large amount of total precipitation and the last two days have a high maximum value of precipitation. During this period the FS actually decreases for the idealized geometries. For the sloped excavation pit the value becomes lower than if suction is ignored. The resulting value seems very reasonable due to the table of precipitation and it leads to another important conclusion, heavy rainfall might lead to a decrease in suction, factor of safety and therefore lead to a failure of excavations even if suction is ignored during the calculations. Sloped geometries are especially exposed for this danger. In general excavation pits with retaining structures are showing less impact of heavy rainfalls, however they are still affected. As mentioned previously there are a number of articles, which show that several cases of slope failures are a result from loss of suction due to an extra heavy rainfall.

It is also worth mentioning that the case where the soil and SWRC where varied, there are several parameters as, grain size distribution, the air-entry level, permeability in both x - and y -direction etc. which are affected. Once again it can be observed that both of the idealized geometries follow the same pattern. The variations for the sloped excavation pit between May and December are larger and for the retaining structure the curves for these two months follows the same pattern from one another. For the month of May the factor of safety is larger. The factor of safety for the sloped excavation varies more than the other case. It is hard to single out one parameter, which can cause this kind of variation, where the FS can increase and then decrease. But it is thought to be a consequence of the grain size distribution and permeability, which in turn affects the soil water retention curve.

It can be clearly seen that the phreatic level affects the unsaturated zone, suction and therefore the factor of safety. As the groundwater level moves closer to the ground surface the FS decreases and vice versa. Once again the two idealized geometries follow the same pattern, with the exception for the month of December for the sloped excavation pit. During this month the factor of safety when suction is allowed lies close to the value when suction is ignored. This is believed to be due to the amount of precipitation during this month and the previously stated reasons as lack of retaining structure and additional boundaries. Overall the results for the idealized cases seem reasonable and deemed to be correct.

The results of the case study for the ESS-case are similar to the results of the idealized excavation pits. If suction is considered, this results in a higher factor of safety than if suction is not considered. The difference between this case study and the idealized cases is that the calculations for the situation where suction is not considered results in a varying factor of safety for the ESS-case. Here, the FS follow the same pattern as if suction is considered, but with a lower value. This was not the case for the idealized excavation pits (not to the same degree, anyway). The difference is most likely due to the fact that multiple soil layers and different soil water retention curves where used compared to the

idealized cases. The upper and lower clay till were also modelled as *Unsaturated A*, which may affect the results. All together these results seem reasonable.

It is worth pointing out that it is important to know how the FE-software works and how the calculations are made otherwise the results of the calculations might be completely wrong without this being noted. But then again, *Plaxis* are responsible for that the calculations are performed according to the specifications given in their manuals. Since there is no information about if it is the maximum value or total precipitation that influences the factor of safety the most during the calculations, *Plaxis* calculations has to be trusted to be correct. In *Plaxis Reference Manual* (2015) it is stated that in general a heavy rainfall, during a short period of time will be of less significance than a lesser rainfall during a longer period.

The approach taken in this master's dissertation, the procedure, creation of boundary conditions and phases has its origin in an internal report from *Plaxis* (Galavi, 2010). According to this document they have used a very simple case to verify the *Fully coupled flow-deformation analysis* and therefore a similar approach is used to create the finite element model in this work. The procedure has to be deemed to be correct and a valid approach of these types of calculations.

There are a number of sources for error. During this work the evapotranspiration is assumed to be equal during 24 hours, when it is in fact close to zero during the night and reaches its maximum value during the day. This might affect the results of the FE-analysis even though this might be the case; this is assumed to be of minor magnitude since there are a lot of other factors which affect the discharge. The two most important parameters are assumed to be permeability and grain size distribution; these are limiting the evaporation from the soil. A similar reasoning is made for the precipitation where the total amount of rainfall is spread out during 24 hours.

During this work the thermal flow is not incorporated, which is in fact an important aspect that determines the amount of evapotranspiration. This could be taken into account, although Penman's formula takes the mean temperature, wind speed, air pressure and solar radiation into account to some extent. In the winter some of the precipitation falls as snow or hail. This will lead to an accumulation of snow, i.e. no infiltration into the ground and when this melts it will increase the infiltration in comparison with the situation without melting snow. This is considered an important factor, since this affects the magnitude of suction in the soil. In reality the factor of safety could be higher during the winter and lower during the spring when snow melts (not taking frozen ground into account).

It is worth mentioning that *Plaxis*, in their reference manual states that the option, allow suction should be used with caution, since it can lead to an overestimation of the FS. However during these calculations with precipitation and evapotranspiration it is deemed correct to use it.

Another factor which is hard to predict is the future precipitation and evapotranspiration, especially the precipitation since potential evapotranspiration is calculated in the same way

anyways. This is a factor that is interesting and important to take into account. It is fairly easy to check old values of the precipitation but way harder to predict the future, if not impossible. Further attention needs to be paid to this in order to make accurate finite element analyses.

The suction phenomenon is a complex matter, which can be of significant important for future geotechnical investigations. Therefore this will be interesting to see how this subject develops and how the view on the finite element method evolves.

7.2 Future work

Throughout this master's dissertation the importance of modelling the precipitation and evapotranspiration correctly has been well noted. An especially problematic part of this is to predict the future discharge of water from and to the soil. Further work may therefore consist of evaluating the best way to use old, previous registered data for the precipitation, for example from SMHI that has been historically confirmed. A more accurate way to predict the rainfall and evapotranspiration from statistical evaluation would result in a more accurate model of suction and the factor of safety.

Until now the precipitation has only been dealt with. It would also be of significant interest to find a better way to predict and model the evapotranspiration. This is of almost equal importance as the precipitation for the magnitude of suction. Today's equations for predicting the potential evapotranspiration needs to be improved.

Another important element, which affects the water content in soil, is heat and thermal flow. During this work, one of the limitations is to neglect the thermal flow, thus neglecting the influence of sunny days to the evapotranspiration. The occurrence of winds on the surface is also neglected. This affects in which rate the evapotranspiration can be transported from the surface and allow for more vaporization.

During this master's dissertation, the depth of the excavation pits has been assumed to 5 meters. To understand more about how suction affects the total stability, the depth of the excavation in relation to the contribution of suction to the factor of safety for both sloped excavation pits and excavation pits with retaining structures are other suggestions for future work.

Here mostly cohesion soils are considered, however the suction phenomenon may be as important for friction soils. There are a number of previous reports and articles as *Matrix suction in silt and sand slopes* (Öberg-Högsta, 1997) which is in this vicinity of subjects. However, this needs further investigation.

Plaxis is one of the most used finite element software in geotechnical engineering. On the account of this other software should be compared to *Plaxis*, in order to evaluate which one that most accurately can predict the phenomenon studied. It is clear that taking suction into account may have a huge potential in future geotechnical finite element analyses.

8. Bibliography

- Bergström, S., 1993. Sveriges Hydrologi - Grundläggande hydrologiska förhållanden. SMHI/Svenska Hydrologiska rådet.
- Blatz, J. A., Ferriera, N. J. & Graham, J., 2004. Effects of near Surface Environmental conditions on instability of an unsaturated soil slope. *Canadian Geotechnical Journal* 41, pp. 1111-1126.
- Fredlund, D. G., 2006. Unsaturated Soil Mechanics in Engineering Practice. *Journal of Geotechnical and Geoenvironmental Engineering*, Issue March, pp. 286-321.
- Fredlund, D. & Rahardjo, H., 1993. *Soil Mechanics for Unsaturated Soils*. 605 Third Avenue, New York, NY: John Wiley and Sons inc.
- Frydman, S. & Baker, R., 2014. Matric Suction and Shear Strength of unsaturated Clay. *Unsaturated Soils - research and applications*, pp. Taylor and Francis Group, London.
- Galavi, V., 2010. *Plaxis - Internal Report*. [Online]
Available at: http://kb.plaxis.nl/sites/kb.plaxis.nl/files/kb-publications/Galavi_Groundwater_flow_and_Coupled_analysis.pdf
[Accessed 20 04 2015].
- Hultén, C. et al., 2005. *Släntstabilitet i Jord - underlag för att förutse och förebygga naturolyckor i Sverige vid förändrat klimat*. [Online]
Available at: <http://www.swedgeo.se/upload/Publikationer/Varia/pdf/SGI-V560-1.pdf>
[Accessed 18 03 2015].
- Labuz, J. F. & Zang, A., 2012. Mohr-Coulomb Failure Criterion. *Rock Mechanics And Rock Engineering Volume. 45, issue 6*, pp. 975-979.
- Lu, N. & Likos, W. J., 2004. *Unsaturated Soil Mechanics*. Hoboken, New Jersey: John Wiley & Sons.
- Öberg-Högsta, A.-L., 1997. *Matrix suction in silt and sand slopes: significance and practical use in stability analysis*. Göteborg: Chalmers Tekniska Högskola.
- Ottosen, N. & Petersson, H., 1992. *Introduction to the Finite Element Method*. Essex, England: Pearson Education Limited, Edinburgh Gate, Harlow, Essex CM20 2JE, England.
- Ottosen, N. S. & Ristinmaa, M., 2005. *The Mechanics of Constitutive Modelling, first edition*. The boulevard, Langford Kidlington, Oxford OX5 1GB: Elsevier Ltd.
- PK, 2015. *Plaxis Knowledgebase*. [Online]
Available at: <http://kb.plaxis.nl/tips-and-tricks/safety-analysis-and-displacements>
[Accessed 05 05 2015].
- PMMM, 2015. *Plaxis Material Model Manual*. [Online]
Available at: <http://www.plaxis.nl/files/files/2D-3-Material-Models.pdf>
[Accessed 19 03 2015].

PRM, 2015. *Plaxis Reference Manual*. [Online]

Available at: <http://www.plaxis.nl/files/files/2DAnniversaryEdition-2-Reference.pdf>
[Accessed 02 03 2015].

PSM, 2015. *Plaxis Scientific Manual*. [Online]

Available at: <http://www.plaxis.nl/files/files/2D-4-Scientific.pdf>
[Accessed 19 03 2015].

SMHI, 2015. *SMHI - Öppna data*. [Online]

Available at: <http://opendata-catalog.smhi.se/explore/>
[Accessed 20 04 2015].

TVRL, 2015. *Teknisk Vattenresurslära - Kompletterande Material*. [Online]

Available at: http://www.tvrl.lth.se/fileadmin/tvrl/files/vvr145/Kompletterande_materialf4.pdf
[Accessed 10 05 2015].

van Genuchten, M. T., 1980. A Closed-form Equation for Predicting the Hydraulic Conductivity of Unsaturated Soils. *Soil Science Society of America Journal*, Volume 44, no.5, Issue September-October.

Zhou, Y. D., Than, L. G., Kwong, A. K. & Tang, X. W., 2010. Mechanisms of drying induced rebound movements in a soil slope in Sai KunG, Hong Kong. *Engineering Geology*, pp. 86-94.

Appendix

A - Values for precipitation

Year:2014 Day	Month																							
	January		February		March		April		May		June		July		August		September		October		November		December	
	Prec.	Evapo.	Prec.	Evapo.	Prec.	Evapo.	Prec.	Evapo.	Prec.	Evapo.	Prec.	Evapo.	Prec.	Evapo.	Prec.	Evapo.	Prec.	Evapo.	Prec.	Evapo.	Prec.	Evapo.	Prec.	Evapo.
1	0.0	0.29	1.9	0.54	0.0	0.71	0.0	2.13	0.0	3.48	0.0	4.4	0.2	4.19	0	3.35	0	2.07	1.1	0.9	0.1	0.4	0	0.16
2	6.0	0.29	0.0	0.54	0.0	0.71	0.1	2.13	0.0	3.48	0.1	4.4	1.2	4.19	7.6	3.35	0.2	2.07	0.4	0.9	1	0.4	0	0.16
3	2.3	0.29	0.0	0.54	0.0	0.71	0.0	2.13	0.0	3.48	5.5	4.4	0.6	4.19	17.8	3.35	0	2.07	0	0.9	0.5	0.4	0	0.16
4	0.0	0.29	0.0	0.54	0.0	0.71	0.0	2.13	0.0	3.48	0.3	4.4	0	4.19	7.8	3.35	0	2.07	0	0.9	6.5	0.4	0	0.16
5	0.7	0.29	0.0	0.54	0.0	0.71	0.3	2.13	0.0	3.48	1.6	4.4	0	4.19	0	3.35	0	2.07	0	0.9	2	0.4	7.2	0.16
6	6.4	0.29	0.5	0.54	0.0	0.71	3.6	2.13	0.5	3.48	0.0	4.4	0	4.19	0	3.35	0	2.07	0	0.9	0.7	0.4	0.4	0.16
7	0.1	0.29	7.9	0.54	0.4	0.71	0.2	2.13	9.0	3.48	0.0	4.4	27.8	4.19	4.2	3.35	2.5	2.07	11.2	0.9	0.9	0.4	15.7	0.16
8	0.9	0.29	10.6	0.54	0.0	0.71	2.5	2.13	2.6	3.48	0.0	4.4	1.8	4.19	0	3.35	0	2.07	1.1	0.9	0	0.4	0.9	0.16
9	12.0	0.29	1.6	0.54	0.0	0.71	0.3	2.13	5.7	3.48	0.0	4.4	0	4.19	7	3.35	12	2.07	0.7	0.9	0.3	0.4	0.2	0.16
10	4.6	0.29	0.0	0.54	0.0	0.71	0.1	2.13	9.2	3.48	0.0	4.4	0	4.19	2.5	3.35	2	2.07	0	0.9	0.2	0.4	6.7	0.16
11	8.1	0.29	2.4	0.54	0.0	0.71	0.4	2.13	0.8	3.48	4.0	4.4	0	4.19	0	3.35	0	2.07	0.6	0.9	0	0.4	1.3	0.16
12	0.1	0.29	2.0	0.54	0.0	0.71	1.8	2.13	8.8	3.48	0.1	4.4	11.7	4.19	0.3	3.35	0	2.07	0.3	0.9	0	0.4	14	0.16
13	1.2	0.29	8.0	0.54	0.0	0.71	4.9	2.13	2.7	3.48	0.6	4.4	1.1	4.19	0	3.35	9.1	2.07	22.9	0.9	0	0.4	0	0.16
14	0.0	0.29	2.3	0.54	0.9	0.71	1.8	2.13	0.4	3.48	0.0	4.4	17.1	4.19	0	3.35	0	2.07	2.1	0.9	0	0.4	0	0.16
15	0.0	0.29	0.5	0.54	0.3	0.71	0.0	2.13	0.0	3.48	0.0	4.4	0	4.19	0	3.35	0	2.07	6.9	0.9	0	0.4	6	0.16
16	5.2	0.29	0.2	0.54	6.4	0.71	0.0	2.13	0.0	3.48	0.0	4.4	0	4.19	0.5	3.35	0.2	2.07	14.9	0.9	0.9	0.4	1.7	0.16
17	1.5	0.29	0.0	0.54	1.1	0.71	9.1	2.13	0.0	3.48	0.0	4.4	0	4.19	11.4	3.35	0	2.07	12.3	0.9	0.1	0.4	0.3	0.16
18	0.6	0.29	0.8	0.54	0.7	0.71	0.0	2.13	10.4	3.48	0.0	4.4	0	4.19	15.3	3.35	0	2.07	0	0.9	0.2	0.4	20.1	0.16
19	0.0	0.29	2.9	0.54	0.3	0.71	0.0	2.13	0.0	3.48	10.1	4.4	0	4.19	0.1	3.35	0	2.07	28.6	0.9	0.2	0.4	4	0.16
20	0.0	0.29	1.6	0.54	0.0	0.71	0.0	2.13	0.0	3.48	0.2	4.4	0	4.19	0	3.35	0	2.07	0	0.9	0.1	0.4	13.7	0.16
21	0.0	0.29	4.2	0.54	6.9	0.71	0.0	2.13	0.0	3.48	1.4	4.4	0	4.19	0.3	3.35	8	2.07	9.1	0.9	0.7	0.4	25.1	0.16
22	0.0	0.29	0.3	0.54	3.6	0.71	0.0	2.13	0.0	3.48	1.1	4.4	0	4.19	4.1	3.35	0.2	2.07	0.4	0.9	2.8	0.4	11.8	0.16
23	0.0	0.29	0.0	0.54	0.0	0.71	0.3	2.13	2.2	3.48	3.2	4.4	0	4.19	0	3.35	1.2	2.07	0	0.9	0.2	0.4	3.7	0.16
24	0.0	0.29	0.0	0.54	0.0	0.71	0.0	2.13	0.0	3.48	10.5	4.4	0	4.19	0.8	3.35	4.2	2.07	2.1	0.9	10	0.4	13.6	0.16
25	0.2	0.29	0.0	0.54	6.9	0.71	0.0	2.13	0.0	3.48	6.4	4.4	0	4.19	0	3.35	1.1	2.07	1.1	0.9	0	0.4	3.7	0.16
26	0.2	0.29	0.3	0.54	0.0	0.71	0.0	2.13	0.0	3.48	0.0	4.4	0	4.19	1.3	3.35	0.5	2.07	0	0.9	0	0.4	0.2	0.16
27	4.3	0.29	0.6	0.54	0.0	0.71	0.0	2.13	0.0	3.48	5.9	4.4	0	4.19	0	3.35	0	2.07	0	0.9	0	0.4	1.4	0.16
28	0.6	0.29	8.1	0.54	0.0	0.71	0.0	2.13	0.0	3.48	0.0	4.4	0	4.19	0	3.35	0	2.07	0	0.9	0.1	0.4	0.2	0.16
29	0.5	0.29			0.0	0.71	0.0	2.13	0.0	3.48	3.8	4.4	1	4.19	6.2	3.35	0	2.07	0.5	0.9	0	0.4	0.3	0.16
30	0.2	0.29			0.0	0.71	0.0	2.13	0.0	3.48	0.0	4.4	8.6	4.19	5.4	3.35	3.7	2.07	0.1	0.9	0	0.4	0	0.16
31	1.1	0.29			0.0	0.71	0.0	2.13	0.0	3.48	0.0	4.4	0	4.19	53.4	3.35			0.9	0.9	0	0.4	0	0.16

Evapo.=Evapotranspiration [mm]
Preci.=Precipitation [mm]

Year:2013	Month																							
	January		February		March		April		May		June		July		August		September		October		November		December	
	Prec.	Evapo.	Prec.	Evapo.	Prec.	Evapo.	Prec.	Evapo.	Prec.	Evapo.	Prec.	Evapo.	Prec.	Evapo.	Prec.	Evapo.	Prec.	Evapo.	Prec.	Evapo.	Prec.	Evapo.	Prec.	Evapo.
1	1.8	0.29	0.6	0.54	0	0.71	0	2.13	0	3.48	22.3	4.4	0	4.19	0	3.35	0.9	2.07	0	0.9	2.9	0.4	0.1	0.16
2	5.8	0.29	0	0.54	0	0.71	0	2.13	0	3.48	0	4.4	0	4.19	0	3.35	3.1	2.07	0	0.9	7.4	0.4	0	0.16
3	0	0.29	1.3	0.54	0	0.71	0	2.13	0	3.48	0	4.4	0.6	4.19	0	3.35	0	2.07	0	0.9	3.9	0.4	0.4	0.16
4	0.4	0.29	6.1	0.54	0	0.71	0	2.13	0	3.48	0	4.4	0	4.19	0	3.35	0	2.07	1.5	0.9	10.4	0.4	2.1	0.16
5	0	0.29	3.2	0.54	0	0.71	0	2.13	0	3.48	0	4.4	0	4.19	0	3.35	0	2.07	0	0.9	0	0.4	5.4	0.16
6	1.1	0.29	0.6	0.54	0	0.71	0	2.13	0	3.48	0	4.4	0	4.19	0	3.35	0	2.07	0	0.9	0.1	0.4	5.6	0.16
7	5	0.29	0.8	0.54	0	0.71	2.7	2.13	6.2	3.48	0	4.4	0	4.19	0	3.35	0	2.07	0	0.9	1.2	0.4	0.9	0.16
8	0.3	0.29	0.9	0.54	0	0.71	0	2.13	0	3.48	0	4.4	0	4.19	3.5	3.35	0	2.07	0	0.9	3.4	0.4	10.8	0.16
9	13.4	0.29	1	0.54	0.1	0.71	0	2.13	0.1	3.48	0	4.4	0	4.19	0	3.35	4.3	2.07	2.3	0.9	9.3	0.4	1.1	0.16
10	0.3	0.29	0.2	0.54	0.1	0.71	0	2.13	0	3.48	0	4.4	0	4.19	1.4	3.35	21.1	2.07	0.6	0.9	17.1	0.4	0.4	0.16
11	0	0.29	1.5	0.54	0	0.71	1.7	2.13	0.2	3.48	0	4.4	0	4.19	2.8	3.35	4.2	2.07	0	0.9	0.1	0.4	0	0.16
12	0	0.29	0.5	0.54	0	0.71	0.2	2.13	0.1	3.48	0.4	4.4	0	4.19	2.8	3.35	0	2.07	0.7	0.9	8.6	0.4	0.4	0.16
13	0.2	0.29	0	0.54	0	0.71	1.6	2.13	2.4	3.48	18.9	4.4	0	4.19	1.6	3.35	0	2.07	16.7	0.9	0	0.4	7.6	0.16
14	2.6	0.29	0	0.54	0	0.71	0	2.13	0.1	3.48	0	4.4	0	4.19	9.2	3.35	5	2.07	0	0.9	0	0.4	0.1	0.16
15	2.4	0.29	0	0.54	0	0.71	4	2.13	0	3.48	14.5	4.4	0	4.19	0.7	3.35	4.5	2.07	0	0.9	0	0.4	1.8	0.16
16	0	0.29	0	0.54	0	0.71	1	2.13	0	3.48	2.6	4.4	0	4.19	0.1	3.35	2.2	2.07	0	0.9	0	0.4	1.4	0.16
17	0	0.29	1.1	0.54	0	0.71	4	2.13	0	3.48	0	4.4	0	4.19	0.1	3.35	0.1	2.07	4.2	0.9	0	0.4	3.5	0.16
18	0	0.29	11.5	0.54	0.9	0.71	0	2.13	0	3.48	0	4.4	0	4.19	2.5	3.35	10.1	2.07	0	0.9	0.6	0.4	0.1	0.16
19	0.1	0.29	0	0.54	3.9	0.71	0	2.13	11.6	3.48	9.2	4.4	0	4.19	0	3.35	0.2	2.07	7.3	0.9	1.4	0.4	2	0.16
20	0	0.29	0	0.54	2.7	0.71	0	2.13	0	3.48	0.1	4.4	0	4.19	0	3.35	0	2.07	5.2	0.9	0.8	0.4	0.7	0.16
21	1.2	0.29	0	0.54	0.3	0.71	0	2.13	2.3	3.48	0	4.4	0	4.19	0.2	3.35	0	2.07	18	0.9	0	0.4	2.9	0.16
22	0	0.29	0	0.54	0.1	0.71	0	2.13	7.1	3.48	0.8	4.4	0	4.19	0	3.35	0.2	2.07	0	0.9	0.3	0.4	0.8	0.16
23	0	0.29	0	0.54	0	0.71	0	2.13	0	3.48	1.4	4.4	0	4.19	0	3.35	0	2.07	0.3	0.9	0.1	0.4	3.7	0.16
24	0	0.29	0.6	0.54	0	0.71	0.2	2.13	5.2	3.48	0	4.4	0	4.19	0	3.35	0	2.07	0.8	0.9	0	0.4	1.7	0.16
25	0	0.29	0	0.54	0	0.71	2.8	2.13	0.3	3.48	8.8	4.4	0	4.19	0	3.35	0	2.07	1.8	0.9	0	0.4	0	0.16
26	1.2	0.29	0	0.54	0	0.71	1.2	2.13	2.2	3.48	1.1	4.4	0	4.19	0	3.35	0.3	2.07	0	0.9	0.9	0.4	2.6	0.16
27	5	0.29	0	0.54	0	0.71	0	2.13	0.2	3.48	2.1	4.4	1.3	4.19	0	3.35	0	2.07	1.7	0.9	0	0.4	7.1	0.16
28	4.1	0.29	0	0.54	0	0.71	0	2.13	0	3.48	4.6	4.4	0.2	4.19	0	3.35	0	2.07	3.7	0.9	0	0.4	4	0.16
29	10.8	0.29			0.3	0.71	0	2.13	1.5	3.48	8	4.4	0.9	4.19	0	3.35	0	2.07	5.7	0.9	7.2	0.4	0	0.16
30	4.8	0.29			0	0.71	0	2.13	0	3.48	0.7	4.4	24.5	4.19	1	3.35	0.2	2.07	0	0.9	0	0.4	0.1	0.16
31	0.2	0.29			0	0.71			0	3.48	0.3	4.19	0.8			3.35			6.2	0.9			0	0.16

Evapo.=Evapotranspiration [mm]
Preci.=Precipitation [mm]

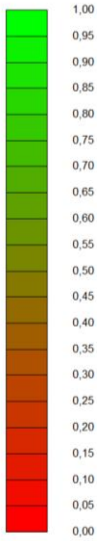
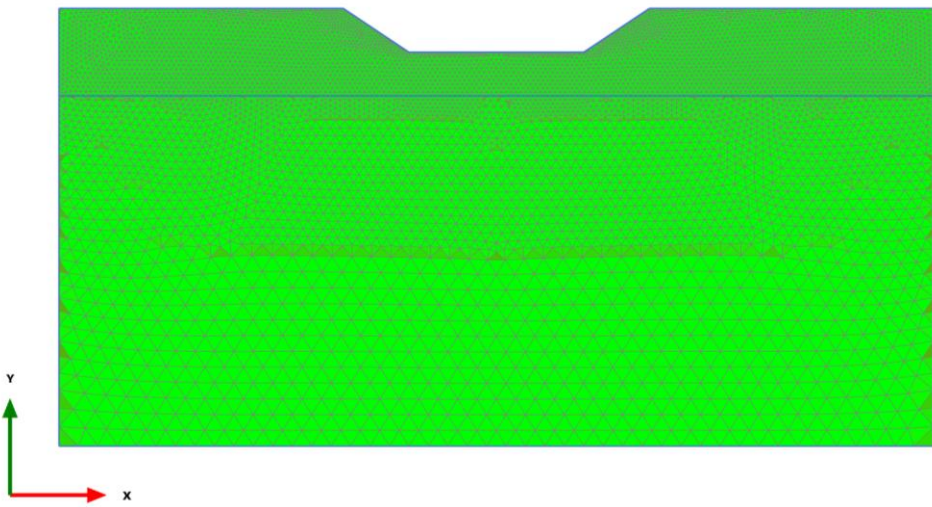
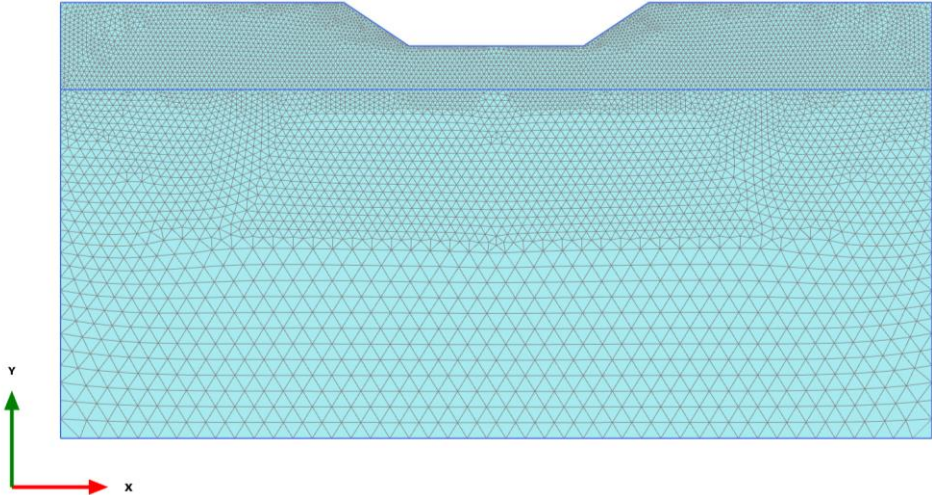
Year, 2012	Month																							
	January		February		March		April		May		June		July		August		September		October		November		December	
	Prec.	Evapo.	Prec.	Evapo.	Prec.	Evapo.	Prec.	Evapo.	Prec.	Evapo.	Prec.	Evapo.	Prec.	Evapo.	Prec.	Evapo.	Prec.	Evapo.	Prec.	Evapo.	Prec.	Evapo.	Prec.	Evapo.
1	23.6	0.29	0.1	0.54	0	0.71	2.9	2.13	0	3.48	5.1	4.4	0.2	4.19	0	3.35	0	2.07	0	0.9	5.3	0.4	2.4	0.16
2	0	0.29	0.1	0.54	0	0.71	0	2.13	0	3.48	2.7	4.4	0	4.19	0.2	3.35	0.1	2.07	1.2	0.9	0.8	0.4	3.2	0.16
3	11.7	0.29	0	0.54	0	0.71	0	2.13	0	3.48	0	4.4	0	4.19	0	3.35	0	2.07	8.3	0.9	5.4	0.4	1.5	0.16
4	6.5	0.29	0	0.54	0	0.71	0	2.13	0	3.48	0	4.4	0	4.19	0	3.35	0	2.07	1	0.9	3.4	0.4	1.1	0.16
5	10.7	0.29	0	0.54	0	0.71	0	2.13	0	3.48	0	4.4	0.1	4.19	0	3.35	0	2.07	7.7	0.9	6.3	0.4	2.6	0.16
6	0.7	0.29	0	0.54	0	0.71	5.1	2.13	0	3.48	1.2	4.4	0.4	4.19	2	3.35	0.3	2.07	5.1	0.9	2.2	0.4	2.2	0.16
7	4.6	0.29	0	0.54	2.9	0.71	0.4	2.13	0	3.48	0	4.4	3	4.19	4.3	3.35	0	2.07	0	0.9	0.9	0.4	0.1	0.16
8	0.4	0.29	0	0.54	1.7	0.71	0	2.13	0	3.48	2.3	4.4	0.2	4.19	0.1	3.35	0	2.07	0.4	0.9	1.5	0.4	0	0.16
9	6.7	0.29	0	0.54	2.1	0.71	1.8	2.13	0	3.48	0	4.4	0	4.19	0	3.35	0	2.07	6.6	0.9	0	0.4	3.9	0.16
10	0	0.29	0	0.54	1.7	0.71	3.6	2.13	10.9	3.48	0.3	4.4	3.4	4.19	0	3.35	0.8	2.07	4.3	0.9	3.6	0.4	2	0.16
11	0.5	0.29	0.7	0.54	0	0.71	1.3	2.13	0	3.48	0	4.4	13.9	4.19	0	3.35	2.8	2.07	0	0.9	0	0.4	0	0.16
12	1.9	0.29	2.8	0.54	0	0.71	0	2.13	1.9	3.48	0	4.4	1	4.19	0	3.35	0.4	2.07	5.6	0.9	0.1	0.4	0	0.16
13	0	0.29	0	0.54	0	0.71	0.2	2.13	0	3.48	0	4.4	1.5	4.19	0	3.35	0	2.07	2.4	0.9	0.7	0.4	0	0.16
14	0	0.29	2.4	0.54	0.1	0.71	0.2	2.13	0	3.48	0	4.4	2.5	4.19	0	3.35	1.5	2.07	11.8	0.9	0.1	0.4	5.6	0.16
15	0.2	0.29	0	0.54	0	0.71	0	2.13	0.9	3.48	1	4.4	0	4.19	0	3.35	0	2.07	3.9	0.9	0	0.4	2.2	0.16
16	0	0.29	5.2	0.54	0	0.71	0	2.13	0.7	3.48	6.9	4.4	4.4	4.19	0.2	3.35	0	2.07	1.4	0.9	0	0.4	2.5	0.16
17	0	0.29	0.1	0.54	0	0.71	0	2.13	0.4	3.48	0.7	4.4	0.4	4.19	0	3.35	0.7	2.07	0.1	0.9	0	0.4	4	0.16
18	5.6	0.29	7	0.54	0.6	0.71	0	2.13	0	3.48	1.6	4.4	10.8	4.19	0.2	3.35	0.2	2.07	0	0.9	0.6	0.4	0.3	0.16
19	8.4	0.29	0	0.54	0	0.71	0	2.13	0.5	3.48	0	4.4	1.8	4.19	0.3	3.35	0.3	2.07	0	0.9	0	0.4	0	0.16
20	0.9	0.29	2.6	0.54	0	0.71	0	2.13	0	3.48	0	4.4	0	4.19	0	3.35	0.4	2.07	0	0.9	0	0.4	0.4	0.16
21	11.1	0.29	0.2	0.54	0	0.71	0	2.13	0	3.48	0	4.4	0	4.19	2.1	3.35	4.3	2.07	0	0.9	0	0.4	0	0.16
22	2	0.29	4.6	0.54	0	0.71	1.7	2.13	0	3.48	4.8	4.4	0	4.19	2.8	3.35	5.6	2.07	0.6	0.9	0	0.4	0	0.16
23	0	0.29	0.2	0.54	0	0.71	0	2.13	0	3.48	0.2	4.4	0	4.19	0	3.35	0	2.07	0	0.9	2.7	0.4	3.9	0.16
24	0	0.29	0	0.54	0	0.71	5.2	2.13	0	3.48	19.8	4.4	0	4.19	0.2	3.35	10.3	2.07	0.2	0.9	0	0.4	4	0.16
25	0	0.29	0	0.54	0	0.71	7.7	2.13	0	3.48	3	4.4	0	4.19	1.5	3.35	2.3	2.07	0.7	0.9	13.3	0.4	3.3	0.16
26	0	0.29	0	0.54	0	0.71	0.7	2.13	0.2	3.48	0	4.4	0	4.19	2.3	3.35	3	2.07	0	0.9	1	0.4	2.6	0.16
27	0	0.29	5.5	0.54	0	0.71	0	2.13	0	3.48	0	4.4	0	4.19	0	3.35	8.8	2.07	0	0.9	0.2	0.4	3.8	0.16
28	0	0.29	0.3	0.54	0	0.71	0.6	2.13	0	3.48	0	4.4	0	4.19	1.8	3.35	0.1	2.07	0	0.9	0.2	0.4	5.8	0.16
29	0	0.29	0	0.54	0	0.71	0	2.13	0.4	3.48	11.1	4.4	1.4	4.19	7.6	3.35	2.1	2.07	8.3	0.9	0	0.4	0.1	0.16
30	0	0.29			1.1	0.71	0	2.13	0.1	3.48	0.1	4.4	12.8	4.19	10	3.35	0.1	2.07	0	0.9	1.2	0.4	4.3	0.16
31	0	0.29			0	0.71			0	3.48			4.1	4.19	0.1	3.35			0	0.9			6.1	0.16

Evapo.=Evapotranspiration [mm]
Preci.=Precipitation [mm]

Appendix B – Finite element mesh

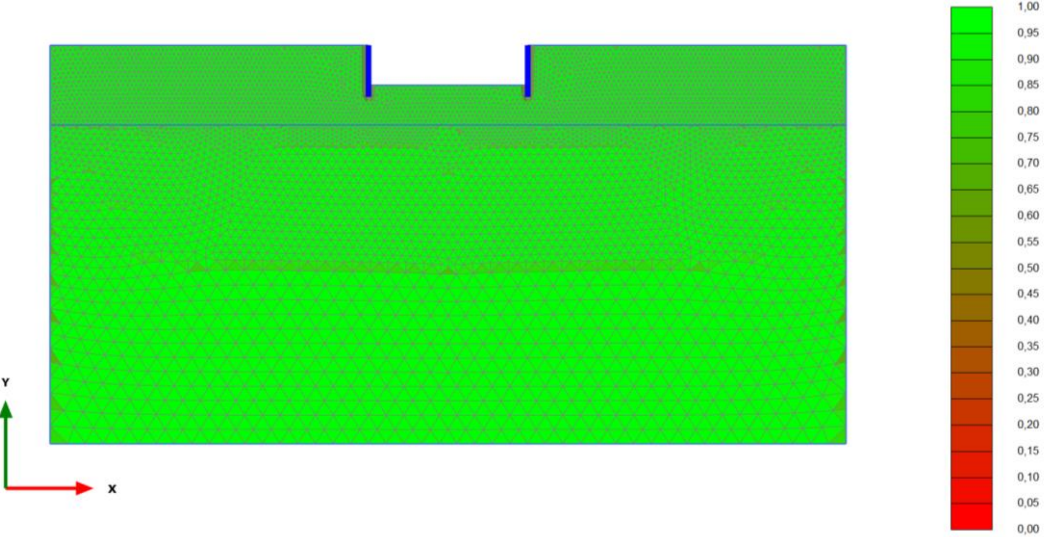
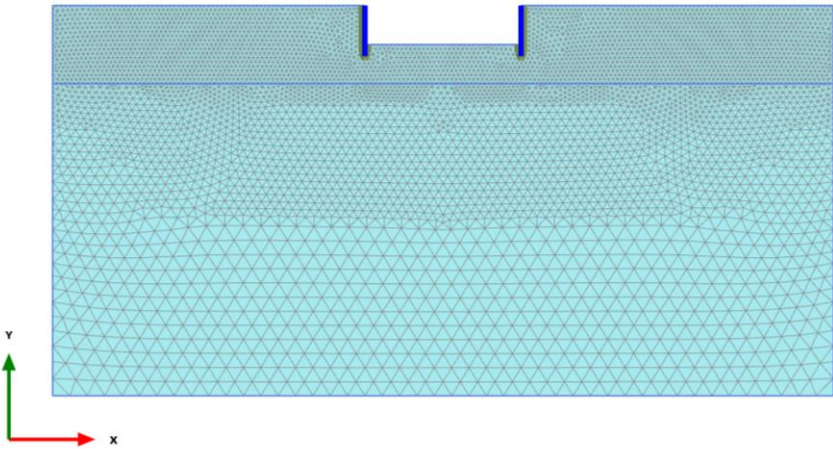
The generated mesh (blue figure) and the mesh quality (green figure) are showed below. First the mesh for the sloped excavation pit is generated, the excavation pit with the retaining structure and last the mesh for the excavation pit at the ESS-site is generated.

Sloped Excavation pit



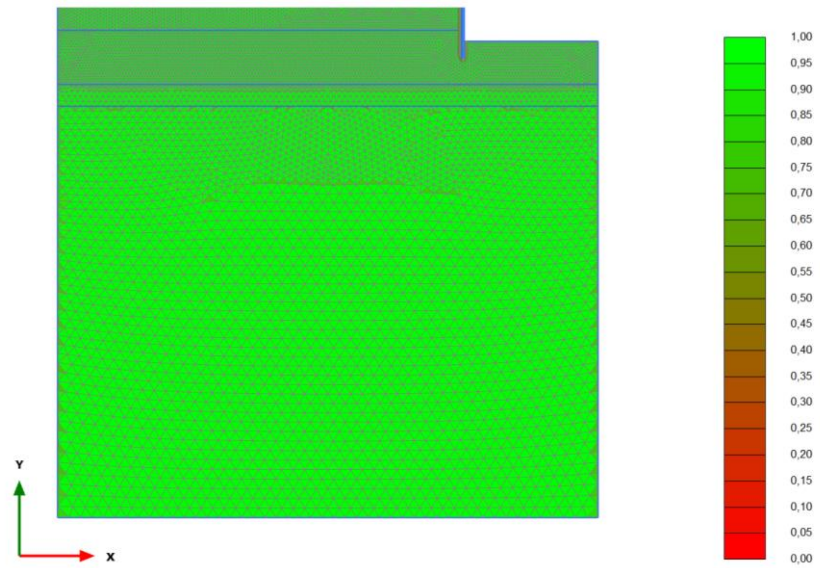
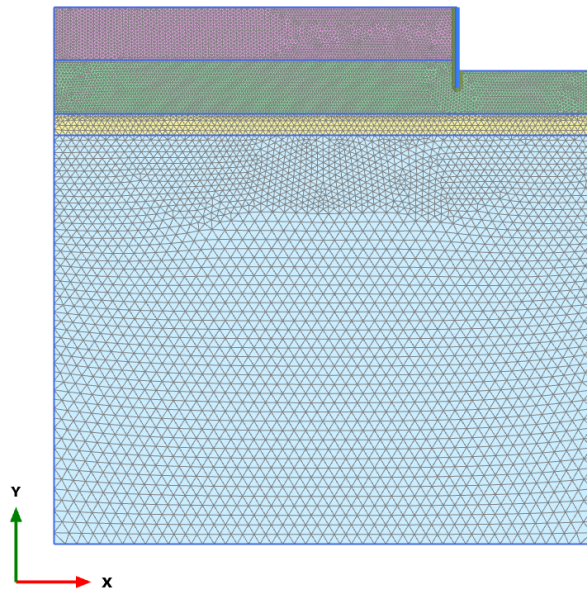
Quality
Maximum value = 1,000 (Element 2306)
Minimum value = 0,5296 (Element 12774)

Excavation pit with reinforced retaining structure



Quality
Maximum value = 1,000 (Element 10261)
Minimum value = 0,5296 (Element 11248)

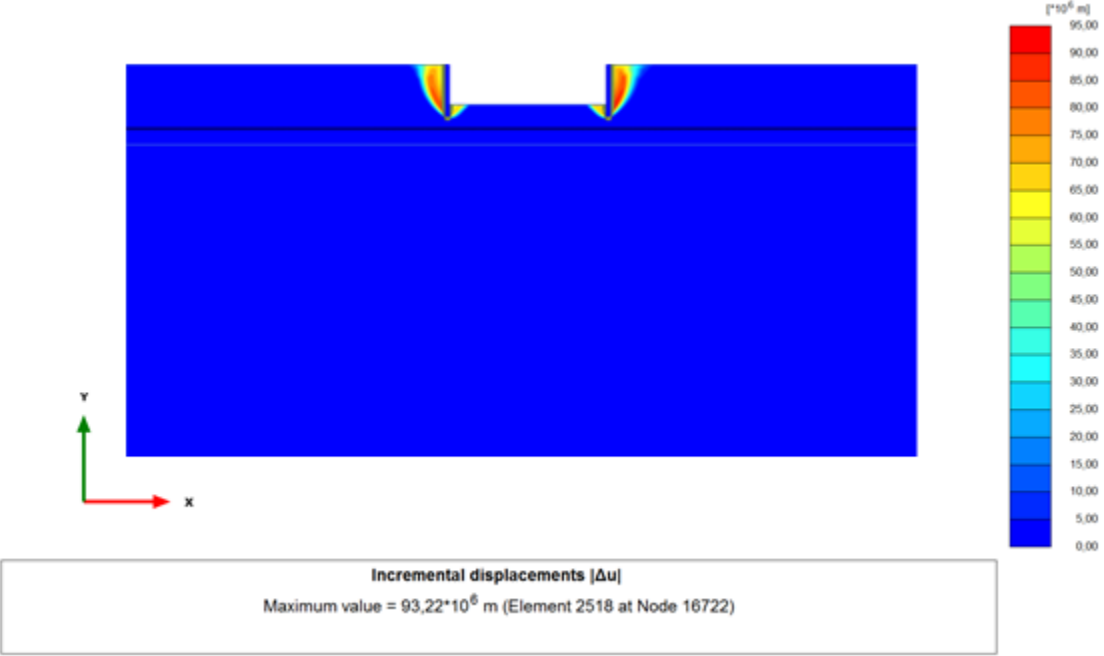
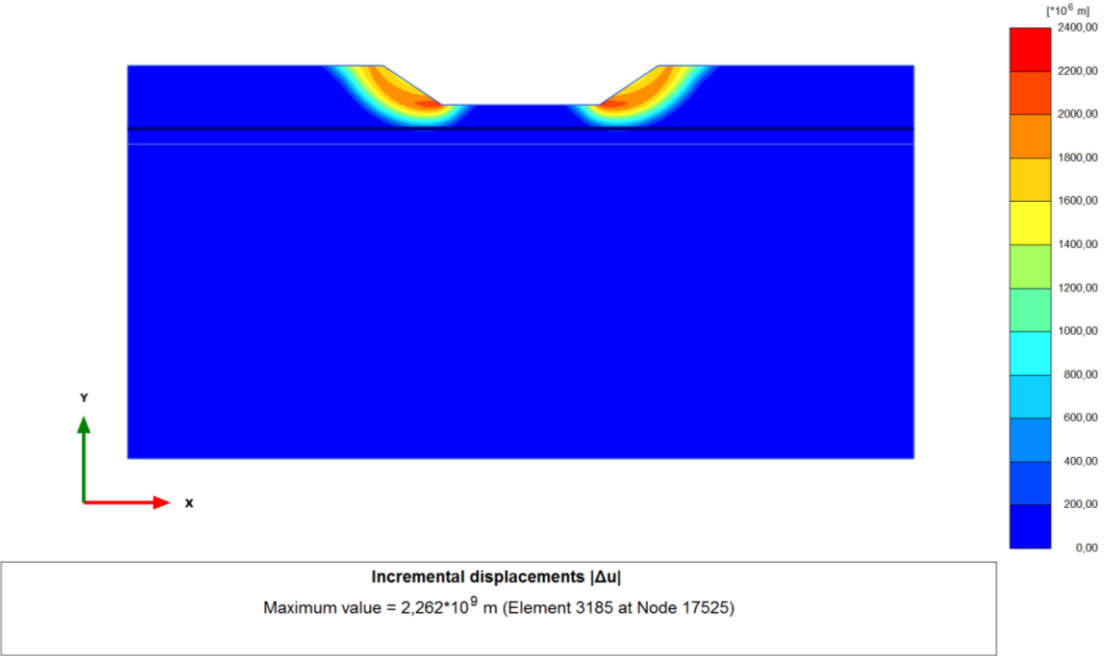
ESS excavation pit

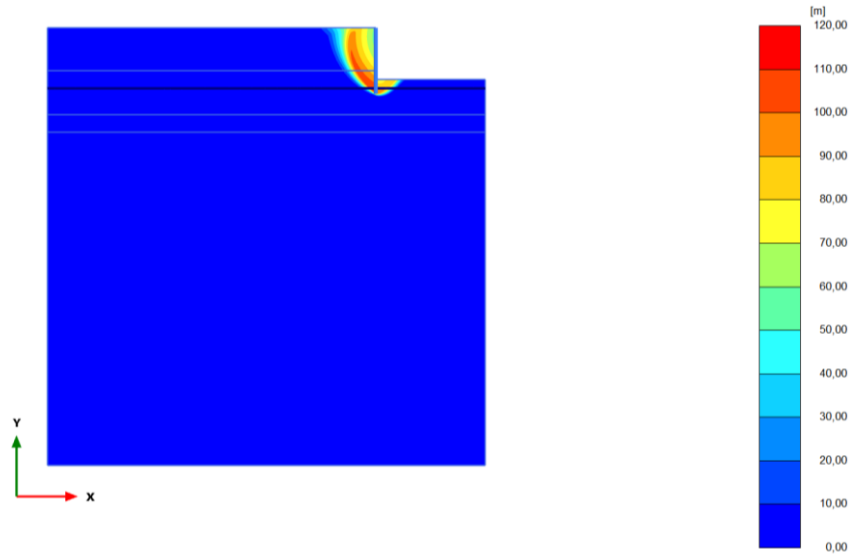


Quality
Maximum value = 1,000 (Element 553)
Minimum value = 0,5790 (Element 18276)

Appendix C - Failure Mechanism

The failure mechanism for the idealized geometries and the ESS-model can be seen below (total stability failure mechanism).

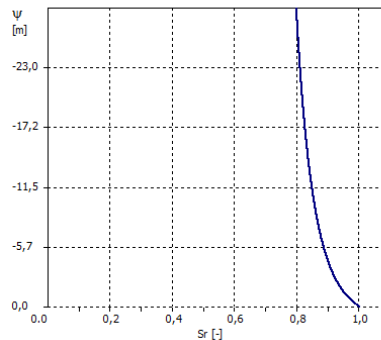
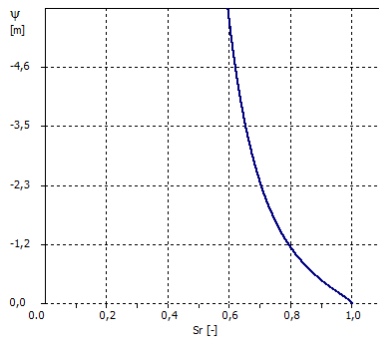
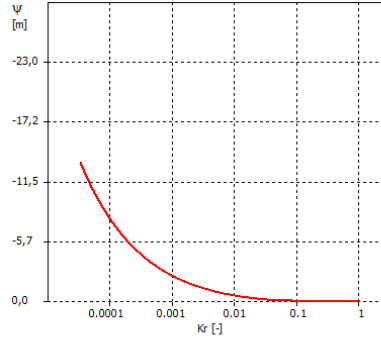
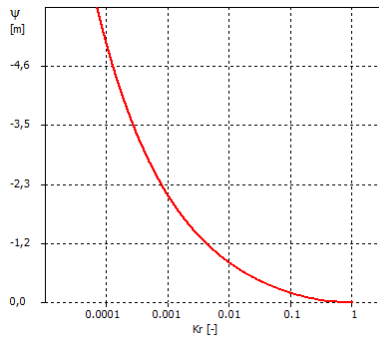




Incremental displacements $|\Delta u|$
Maximum value = 115,6 m (Element 1228 at Node 6062)

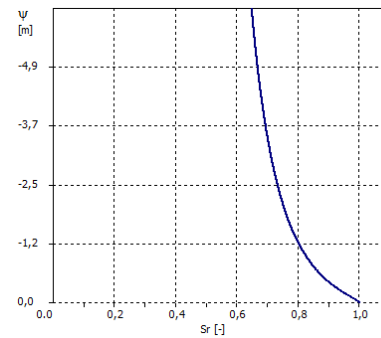
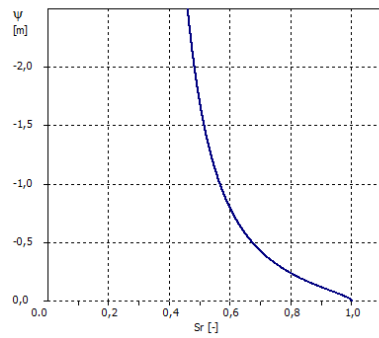
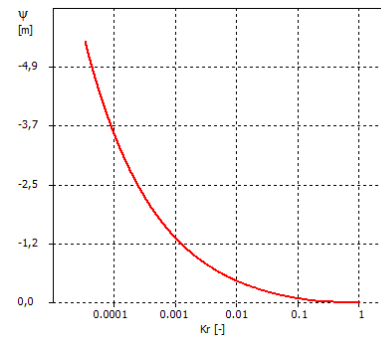
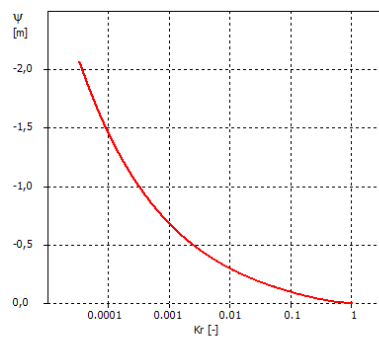
D - SWRC Curves

The height of the potential head plotted against the residual saturation or relative hydraulic conductivity can be seen below for the different soil types used in the idealized cases.



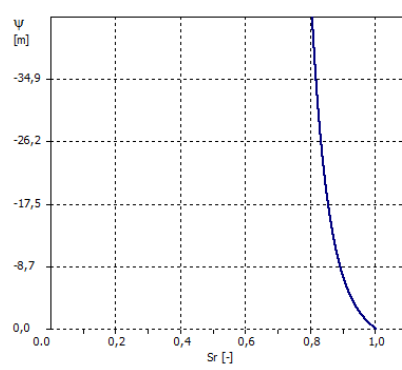
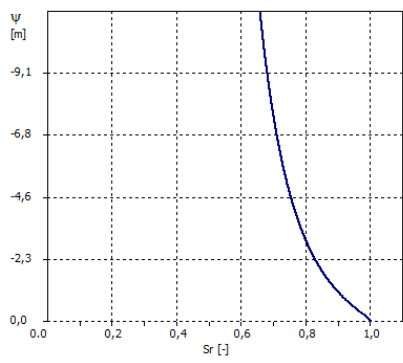
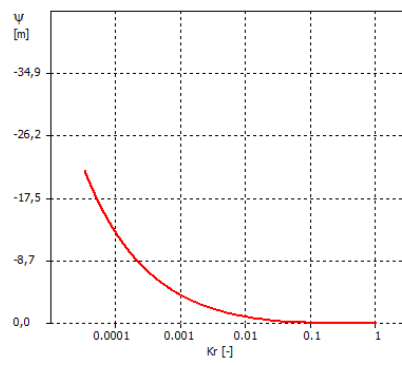
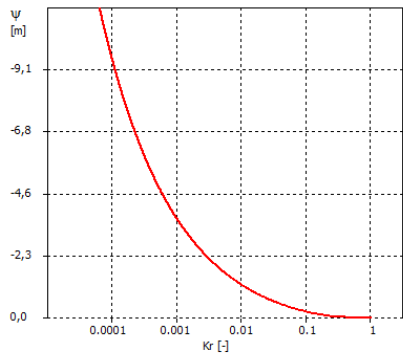
Clay Loam

Clay



Sandy Clay Loam

Sandy Clay



Silty Clay Loam

Silty Clay